CHAPTER

Wavelet Bases

7

One can construct wavelets ψ such that the dilated and translated family

$$\left\{\psi_{j,n}(t) = \frac{1}{\sqrt{2^j}}\,\psi\left(\frac{t-2^j n}{2^j}\right)\right\}_{(j,n)\in\mathbb{Z}^2}$$

is an orthonormal basis of $\mathbf{L^2}(\mathbb{R})$. Behind this simple statement lie very different points of view that open a fruitful exchange between harmonic analysis and discrete signal processing.

Orthogonal wavelets dilated by 2^j carry signal variations at the resolution 2^{-j}. The construction of these bases can be related to multiresolution signal approximations. Following this link leads us to an unexpected equivalence between wavelet bases and conjugate mirror filters used in discrete multirate filter banks. These filter banks implement a fast orthogonal wavelet transform that requires only $O(N)$ operations for signals of size N. The design of conjugate mirror filters also gives new classes of wavelet orthogonal bases including regular wavelets of compact support. In several dimensions, wavelet bases of $\mathbf{L^2}(\mathbb{R}^d)$ are constructed with separable products of functions of one variable. Wavelet bases are also adapted to bounded domains and surfaces with lifting algorithms.

7.1 ORTHOGONAL WAVELET BASES

Our search for orthogonal wavelets begins with multiresolution approximations. For $f \in \mathbf{L^2}(\mathbb{R})$, the partial sum of wavelet coefficients $\sum_{n=-\infty}^{+\infty} \langle f, \psi_{j,n}\rangle\, \psi_{j,n}$ can indeed be interpreted as the difference between two approximations of f at the resolutions 2^{-j+1} and 2^{-j}. Multiresolution approximations compute the approximation of signals at various resolutions with orthogonal projections on different spaces $\{\mathbf{V}_j\}_{j\in\mathbb{Z}}$. Section 7.1.3 proves that multiresolution approximations are entirely characterized by a particular discrete filter that governs the loss of information across resolutions. These discrete filters provide a simple procedure for designing and synthesizing orthogonal wavelet bases.

7.1.1 Multiresolution Approximations

Adapting the signal resolution allows one to process only the relevant details for a particular task. In computer vision, Burt and Adelson [126] introduced a multiresolution pyramid that can be used to process a low-resolution image first and then selectively increase the resolution when necessary. This section formalizes multiresolution approximations, which set the ground for the construction of orthogonal wavelets.

The approximation of a function f at a resolution 2^{-j} is specified by a discrete grid of samples that provides local averages of f over neighborhoods of size proportional to 2^j. Thus, a multiresolution approximation is composed of embedded grids of approximation. More formally, the approximation of a function at a resolution 2^{-j} is defined as an orthogonal projection on a space $\mathbf{V}_j \subset \mathbf{L^2}(\mathbb{R})$. The space $\mathbf{V}_j$ regroups all possible approximations at the resolution 2^{-j}. The orthogonal projection of f is the function $f_j \in \mathbf{V}_j$ that minimizes $\|f - f_j\|$. The following definition, introduced by Mallat [362] and Meyer [44], specifies the mathematical properties of multiresolution spaces. To avoid confusion, let us emphasize that a scale parameter 2^j is the inverse of the resolution 2^{-j}.

Definition 7.1: *Multiresolutions.* A sequence $\{\mathbf{V}_j\}_{j\in\mathbb{Z}}$ of closed subspaces of $\mathbf{L^2}(\mathbb{R})$ is a multiresolution approximation if the following six properties are satisfied:

$$\forall (j,k) \in \mathbb{Z}^2, \quad f(t) \in \mathbf{V}_j \Leftrightarrow f(t - 2^j k) \in \mathbf{V}_j, \tag{7.1}$$

$$\forall j \in \mathbb{Z}, \quad \mathbf{V}_{j+1} \subset \mathbf{V}_j, \tag{7.2}$$

$$\forall j \in \mathbb{Z}, \quad f(t) \in \mathbf{V}_j \Leftrightarrow f\left(\frac{t}{2}\right) \in \mathbf{V}_{j+1}, \tag{7.3}$$

$$\lim_{j \to +\infty} \mathbf{V}_j = \bigcap_{j=-\infty}^{+\infty} \mathbf{V}_j = \{0\}, \tag{7.4}$$

$$\lim_{j \to -\infty} \mathbf{V}_j = \text{Closure}\left(\bigcup_{j=-\infty}^{+\infty} \mathbf{V}_j \right) = \mathbf{L^2}(\mathbb{R}), \tag{7.5}$$

and there exists θ such that $\{\theta(t-n)\}_{n\in\mathbb{Z}}$ is a Riesz basis of $\mathbf{V}_0$.

Let us give an intuitive explanation of these mathematical properties. Property (7.1) means that $\mathbf{V}_j$ is invariant by any translation proportional to the scale 2^j. As we shall see later, this space can be assimilated to a uniform grid with intervals 2^j, which characterizes the signal approximation at the resolution 2^{-j}. The inclusion (7.2) is a causality property that proves that an approximation at a resolution 2^{-j} contains all the necessary information to compute an approximation at a coarser resolution 2^{-j-1}. Dilating functions in $\mathbf{V}_j$ by 2 enlarges the details by 2 and (7.3) guarantees that it defines an approximation at a coarser resolution 2^{-j-1}. When the resolution 2^{-j} goes to 0 (7.4) implies that we lose all the details of f and

$$\lim_{j \to +\infty} \|P_{\mathbf{V}_j} f\| = 0. \tag{7.6}$$

On the other hand, when the resolution 2^{-j} goes $+\infty$, property (7.5) imposes that the signal approximation converges to the original signal:

$$\lim_{j \to -\infty} \|f - P_{\mathbf{V}_j} f\| = 0. \tag{7.7}$$

When the resolution 2^{-j} increases, the decay rate of the approximation error $\|f - P_{\mathbf{V}_j} f\|$ depends on the regularity of f. In Section 9.1.3 we relate this error to the uniform Lipschitz regularity of f.

The existence of a Riesz basis $\{\theta(t-n)\}_{n\in\mathbb{Z}}$ of $\mathbf{V}_0$ provides a discretization theorem as explained in Section 3.1.3. The function θ can be interpreted as a unit resolution cell; Section 5.1.1 gives the definition of a Riesz basis. It is a family of linearly independent functions such that there exist $B \geq A > 0$, which satisfy

$$\forall f \in \mathbf{V}_0, \quad A\|f\|^2 \leq \sum_{n=-\infty}^{+\infty} |\langle f(t), \theta(t-n)\rangle|^2 \leq B\|f\|^2. \tag{7.8}$$

This energy equivalence guarantees that signal expansions over $\{\theta(t-n)\}_{n\in\mathbb{Z}}$ are numerically stable. One may verify that the family $\{2^{-j/2}\theta(2^{-j}t-n)\}_{n\in\mathbb{Z}}$ is a Riesz basis of $\mathbf{V}_j$ with the same Riesz bounds A and B at all scales 2^j. Theorem 3.4 proves that $\{\theta(t-n)\}_{n\in\mathbb{Z}}$ is a Riesz basis if and only if

$$\forall \omega \in [-\pi, \pi], \quad A \leq \sum_{k=-\infty}^{+\infty} |\hat{\theta}(\omega + 2k\pi)|^2 \leq B. \tag{7.9}$$

EXAMPLE 7.1: Piecewise Constant Approximations

A simple multiresolution approximation is composed of piecewise constant functions. Space $\mathbf{V}_j$ is the set of all $g \in \mathbf{L}^2(\mathbb{R})$ such that $g(t)$ is constant for $t \in [n2^j, (n+1)2^j)$ and $n \in \mathbb{Z}$. The approximation at a resolution 2^{-j} of f is the closest piecewise constant function on intervals of size 2^j. The resolution cell can be chosen to be the box window $\theta = \mathbf{1}_{[0,1)}$. Clearly, $\mathbf{V}_j \subset \mathbf{V}_{j-1}$, since functions constant on intervals of size 2^j are also constant on intervals of size 2^{j-1}. The verification of the other multiresolution properties is left to the reader. It is often desirable to construct approximations that are smooth functions, in which case piecewise constant functions are not appropriate.

EXAMPLE 7.2: Shannon Approximations

Frequency band-limited functions also yield multiresolution approximations. Space $\mathbf{V}_j$ is defined as the set of functions with a Fourier transform support included in $[-2^{-j}\pi, 2^{-j}\pi]$. Theorem 3.5 provides an orthonormal basis $\{\theta(t-n)\}_{n\in\mathbb{Z}}$ of $\mathbf{V}_0$ defined by

$$\theta(t) = \frac{\sin \pi t}{\pi t}. \tag{7.10}$$

All other properties of multiresolution approximation are easily verified.

The approximation at the resolution 2^{-j} of $f \in \mathbf{L}^2(\mathbb{R})$ is the function $P_{\mathbf{V}_j} f \in \mathbf{V}_j$ that minimizes $\|P_{\mathbf{V}_j} f - f\|$. It is proved in (3.12) that its Fourier transform is obtained with a frequency filtering:

$$\widehat{P_{\mathbf{V}_j} f}(\omega) = \hat{f}(\omega)\, \mathbf{1}_{[-2^{-j}\pi, 2^{-j}\pi]}(\omega).$$

This Fourier transform is generally discontinuous at $\pm 2^{-j}\pi$, in which case $|P_{\mathbf{V}_j} f(t)|$ decays like $|t|^{-1}$ for large $|t|$, even though f might have a compact support.

EXAMPLE 7.3: Spline Approximations

Polynomial spline approximations construct smooth approximations with fast asymptotic decay. The space $\mathbf{V}_j$ of splines of degree $m \geq 0$ is the set of functions that are $m-1$ times continuously differentiable and equal to a polynomial of degree m on any interval $[n2^j, (n+1)2^j]$ for $n \in \mathbb{Z}$. When $m = 0$, it is a piecewise constant multiresolution approximation. When $m = 1$, functions in $\mathbf{V}_j$ are piecewise linear and continuous.

A Riesz basis of polynomial splines is constructed with *box splines*. A box spline θ of degree m is computed by convolving the box window $\mathbf{1}_{[0,1]}$ with itself $m+1$ times and centering at 0 or $1/2$. Its Fourier transform is

$$\hat{\theta}(\omega) = \left(\frac{\sin(\omega/2)}{\omega/2} \right)^{m+1} \exp\left(\frac{-i\varepsilon\omega}{2} \right). \tag{7.11}$$

If m is even, then $\varepsilon = 1$ and θ has a support centered at $t = 1/2$. If m is odd, then $\varepsilon = 0$ and $\theta(t)$ is symmetric about $t = 0$. Figure 7.1 displays a cubic box spline $m = 3$ and its Fourier transform. For all $m \geq 0$, one can prove that $\{\theta(t-n)\}_{n \in \mathbb{Z}}$ is a Riesz basis of $\mathbf{V}_0$ by verifying the condition (7.9). This is done with a closed-form expression for the series (7.19).

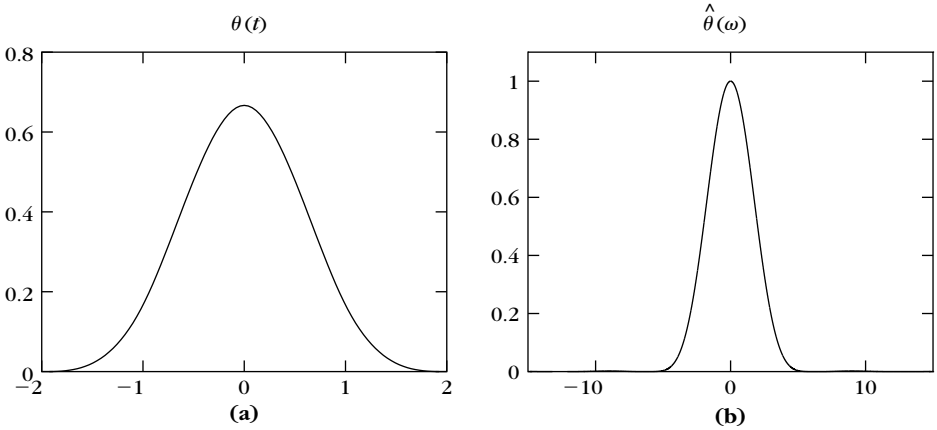

FIGURE 7.1

Cubic box spline θ **(a)** and its Fourier transform $\hat{\theta}$ **(b)**.

7.1.2 Scaling Function

The approximation of f at the resolution 2^{-j} is defined as the orthogonal projection $P_{\mathbf{V}_j} f$ on $\mathbf{V}_j$. To compute this projection, we must find an orthonormal basis of $\mathbf{V}_j$. Theorem 7.1 orthogonalizes the Riesz basis $\{\theta(t-n)\}_{n\in\mathbb{Z}}$ and constructs an orthogonal basis of each space $\mathbf{V}_j$ by dilating and translating a single function ϕ called a *scaling function*. To avoid confusing the resolution 2^{-j} and the scale 2^j, in the rest of this chapter the notion of resolution is dropped and $P_{\mathbf{V}_j} f$ is called an approximation at the scale 2^j.

Theorem 7.1. Let $\{\mathbf{V}_j\}_{j\in\mathbb{Z}}$ be a multiresolution approximation and ϕ be the scaling function having a Fourier transform

$$\hat{\phi}(\omega) = \frac{\hat{\theta}(\omega)}{\left(\sum_{k=-\infty}^{+\infty} |\hat{\theta}(\omega+2k\pi)|^2\right)^{1/2}}. \tag{7.12}$$

Let us denote

$$\phi_{j,n}(t) = \frac{1}{\sqrt{2^j}}\,\phi\left(\frac{t-n}{2^j}\right).$$

The family $\{\phi_{j,n}\}_{n\in\mathbb{Z}}$ is an orthonormal basis of $\mathbf{V}_j$ for all $j\in\mathbb{Z}$.

Proof. To construct an orthonormal basis, we look for a function $\phi\in\mathbf{V}_0$. Thus, it can be expanded in the basis $\{\theta(t-n)\}_{n\in\mathbb{Z}}$:

$$\phi(t) = \sum_{n=-\infty}^{+\infty} a[n]\,\theta(t-n),$$

which implies that

$$\hat{\phi}(\omega) = \hat{a}(\omega)\,\hat{\theta}(\omega),$$

where $\hat{a}$ is a 2π periodic Fourier series of finite energy. To compute $\hat{a}$ we express the orthogonality of $\{\phi(t-n)\}_{n\in\mathbb{Z}}$ in the Fourier domain. Let $\bar{\phi}(t) = \phi^*(-t)$. For any $(n,p)\in\mathbb{Z}^2$,

$$\begin{aligned}\langle \phi(t-n), \phi(t-p)\rangle &= \int_{-\infty}^{+\infty} \phi(t-n)\,\phi^*(t-p)\,dt \\ &= \phi \star \bar{\phi}(p-n).\end{aligned} \tag{7.13}$$

Thus, $\{\phi(t-n)\}_{n\in\mathbb{Z}}$ is orthonormal if and only if $\phi\star\bar{\phi}(n) = \delta[n]$. Computing the Fourier transform of this equality yields

$$\sum_{k=-\infty}^{+\infty} |\hat{\phi}(\omega+2k\pi)|^2 = 1. \tag{7.14}$$

Indeed, the Fourier transform of $\phi\star\bar{\phi}(t)$ is $|\hat{\phi}(\omega)|^2$, and we proved in (3.3) that sampling a function periodizes its Fourier transform. The property (7.14) is verified if we choose

$$\hat{a}(\omega) = \left(\sum_{k=-\infty}^{+\infty} |\hat{\theta}(\omega+2k\pi)|^2\right)^{-1/2}.$$

We saw in (7.9) that the denominator has a strictly positive lower bound, so $\hat{a}$ is a 2π periodic function of finite energy. ■

Approximation

The orthogonal projection of f over $\mathbf{V}_j$ is obtained with an expansion in the scaling orthogonal basis

$$P_{\mathbf{V}_j} f = \sum_{n=-\infty}^{+\infty} \langle f, \phi_{j,n} \rangle \, \phi_{j,n}. \tag{7.15}$$

The inner products

$$a_j[n] = \langle f, \phi_{j,n} \rangle \tag{7.16}$$

provide a discrete approximation at the scale 2^j. We can rewrite them as a convolution product:

$$a_j[n] = \int_{-\infty}^{+\infty} f(t) \, \frac{1}{\sqrt{2^j}} \, \phi\left(\frac{t - 2^j n}{2^j}\right) dt = f \star \bar{\phi}_j(2^j n), \tag{7.17}$$

with $\bar{\phi}_j(t) = \sqrt{2^{-j}}\phi(2^{-j}t)$. The energy of the Fourier transform $\hat{\phi}$ is typically concentrated in $[-\pi, \pi]$, as illustrated by Figure 7.2. As a consequence, the Fourier transform $\sqrt{2^j}\hat{\phi}^*(2^j\omega)$ of $\bar{\phi}_j(t)$ is mostly nonnegligible in $[-2^{-j}\pi, 2^{-j}\pi]$. The discrete approximation $a_j[n]$ is therefore a low-pass filtering of f sampled at intervals 2^j. Figure 7.3 gives a discrete multiresolution approximation at scales $2^{-9} \leqslant 2^j \leqslant 2^{-4}$.

EXAMPLE 7.4

For piecewise constant approximations and Shannon multiresolution approximations we have constructed Riesz bases $\{\theta(t-n)\}_{n\in\mathbb{Z}}$ that are orthonormal bases, thus $\phi = \theta$.

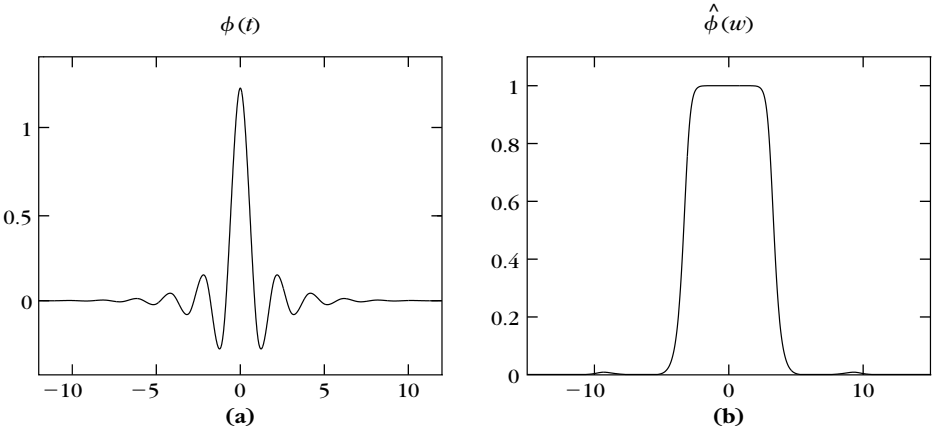

FIGURE 7.2

Cubic spline–scaling function ϕ **(a)** and its Fourier transform $\hat{\phi}$ computed with (7.18) **(b)**.

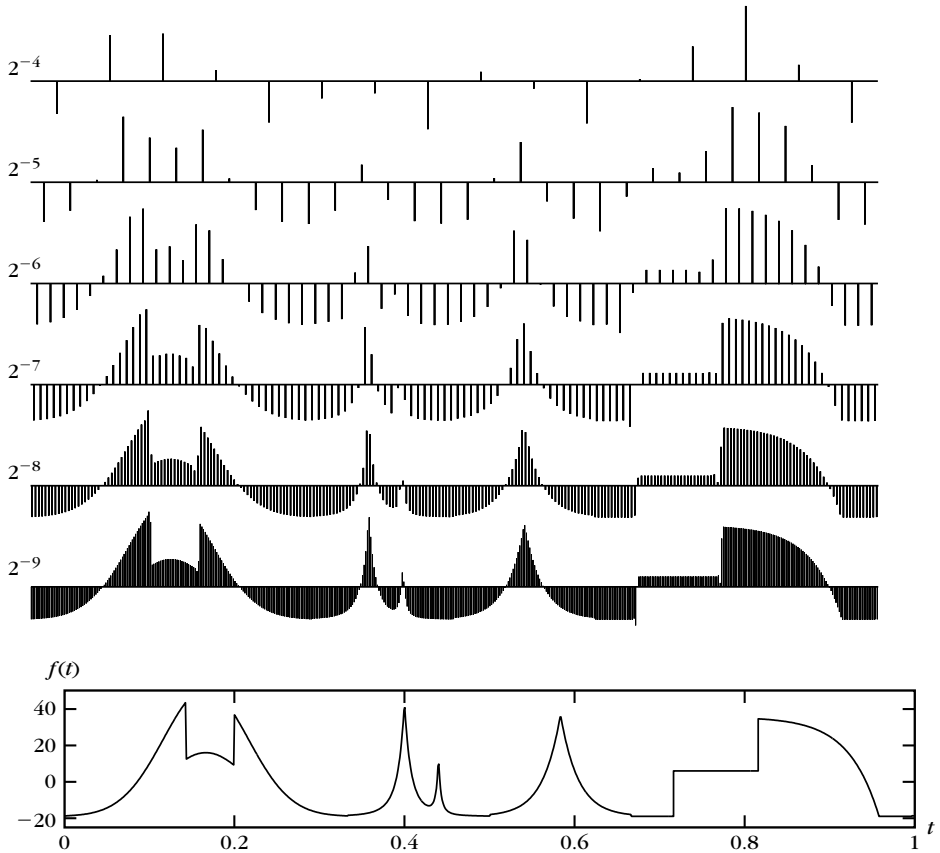

FIGURE 7.3

Discrete multiresolution approximations $a_j[n]$ at scales 2^j, computed with cubic splines.

EXAMPLE 7.5

Spline multiresolution approximations admit a Riesz basis constructed with a box spline θ of degree m, having a Fourier transform given by (7.11). Inserting this expression in (7.12) yields

$$\hat{\phi}(\omega) = \frac{\exp(-i\varepsilon\omega/2)}{\omega^{m+1}\sqrt{S_{2m+2}(\omega)}}, \tag{7.18}$$

with

$$S_n(\omega) = \sum_{k=-\infty}^{+\infty} \frac{1}{(\omega + 2k\pi)^n}, \tag{7.19}$$

and $\varepsilon = 1$ if m is even or $\varepsilon = 0$ if m is odd. A closed-form expression of $S_{2m+2}(\omega)$ is obtained by computing the derivative of order $2m$ of the identity

$$S_2(2\omega) = \sum_{k=-\infty}^{+\infty} \frac{1}{(2\omega + 2k\pi)^2} = \frac{1}{4\sin^2 \omega}.$$

linear splines, $m = 1$ and

$$S_4(2\omega) = \frac{1 + 2\cos^2 \omega}{48 \sin^4 \omega}, \tag{7.20}$$

which yields

$$\hat{\phi}(\omega) = \frac{4\sqrt{3}\sin^2(\omega/2)}{\omega^2 \sqrt{1 + 2\cos^2(\omega/2)}}. \tag{7.21}$$

The cubic spline–scaling function corresponds to $m = 3$, and $\hat{\phi}(\omega)$ is calculated with (7.18) by inserting

$$\begin{aligned} S_8(2\omega) = &\frac{5 + 30\cos^2 \omega + 30\sin^2 \omega \cos^2 \omega}{105\, 2^8 \sin^8 \omega} \\ &+ \frac{70\cos^4 \omega + 2\sin^4 \omega \cos^2 \omega + 2/3 \sin^6 \omega}{105\, 2^8 \sin^8 \omega}. \end{aligned} \tag{7.22}$$

This cubic spline–scaling function ϕ and its Fourier transform are displayed in Figure 7.2. It has an infinite support but decays exponentially.

7.1.3 Conjugate Mirror Filters

A multiresolution approximation is entirely characterized by the scaling function ϕ that generates an orthogonal basis of each space $\mathbf{V}_j$. We study the properties of ϕ, which guarantee that the spaces $\mathbf{V}_j$ satisfy all conditions of a multiresolution approximation. It is proved that any scaling function is specified by a discrete filter called a *conjugate mirror filter*.

Scaling Equation

The multiresolution causality property (7.2) imposes that $\mathbf{V}_j \subset \mathbf{V}_{j-1}$; in particular, $2^{-1/2}\phi(t/2) \in \mathbf{V}_1 \subset \mathbf{V}_0$. Since $\{\phi(t-n)\}_{n\in\mathbb{Z}}$ is an orthonormal basis of $\mathbf{V}_0$, we can decompose

$$\frac{1}{\sqrt{2}}\phi\left(\frac{t}{2}\right) = \sum_{n=-\infty}^{+\infty} h[n]\,\phi(t-n), \tag{7.23}$$

with

$$h[n] = \left\langle \frac{1}{\sqrt{2}}\phi\left(\frac{t}{2}\right), \phi(t-n) \right\rangle. \tag{7.24}$$

This scaling equation relates a dilation of ϕ by 2 to its integer translations. The sequence $h[n]$ will be interpreted as a discrete filter.

The Fourier transform of both sides of (7.23) yields

$$\hat{\phi}(2\omega) = \frac{1}{\sqrt{2}}\,\hat{h}(\omega)\,\hat{\phi}(\omega) \tag{7.25}$$

for $\hat{h}(\omega) = \sum_{n=-\infty}^{+\infty} h[n]\,\mathrm{e}^{-in\omega}$. Thus, it is tempting to express $\hat{\phi}(\omega)$ directly as a product of dilations of $\hat{h}(\omega)$. For any $p \geqslant 0$, (7.25) implies

$$\hat{\phi}(2^{-p+1}\omega) = \frac{1}{\sqrt{2}}\,\hat{h}(2^{-p}\omega)\,\hat{\phi}(2^{-p}\omega). \tag{7.26}$$

By substitution, we obtain

$$\hat{\phi}(\omega) = \left(\prod_{p=1}^{P} \frac{\hat{h}(2^{-p}\omega)}{\sqrt{2}}\right)\hat{\phi}(2^{-P}\omega). \tag{7.27}$$

If $\hat{\phi}(\omega)$ is continuous at $\omega = 0$, then $\lim_{P\to+\infty} \hat{\phi}(2^{-P}\omega) = \hat{\phi}(0)$, so

$$\hat{\phi}(\omega) = \prod_{p=1}^{+\infty} \frac{\hat{h}(2^{-p}\omega)}{\sqrt{2}}\,\hat{\phi}(0). \tag{7.28}$$

Theorem 7.2 [44, 362] gives necessary and sufficient conditions on $\hat{h}(\omega)$ to guarantee that this infinite product is the Fourier transform of a scaling function.

Theorem 7.2: *Mallat, Meyer.* Let $\phi \in \mathbf{L^2}(\mathbb{R})$ be an integrable scaling function. The Fourier series of $h[n] = \langle 2^{-1/2}\phi(t/2), \phi(t-n)\rangle$ satisfies

$$\forall \omega \in \mathbb{R}, \quad |\hat{h}(\omega)|^2 + |\hat{h}(\omega+\pi)|^2 = 2, \tag{7.29}$$

and

$$\hat{h}(0) = \sqrt{2}. \tag{7.30}$$

Conversely, if $\hat{h}(\omega)$ is 2π periodic and continuously differentiable in a neighborhood of $\omega = 0$, if it satisfies (7.29) and (7.30) and if

$$\inf_{\omega\in[-\pi/2,\pi/2]} |\hat{h}(\omega)| > 0, \tag{7.31}$$

then

$$\hat{\phi}(\omega) = \prod_{p=1}^{+\infty} \frac{\hat{h}(2^{-p}\omega)}{\sqrt{2}} \tag{7.32}$$

is the Fourier transform of a scaling function $\phi \in \mathbf{L^2}(\mathbb{R})$.

Proof. This theorem is a central result and its proof is long and technical. It is divided in several parts.

Proof of the necessary condition (7.29). The necessary condition is proved to be a consequence of the fact that $\{\phi(t-n)\}_{n\in\mathbb{Z}}$ is orthonormal. In the Fourier domain, (7.14)

gives an equivalent condition:

$$\forall \omega \in \mathbb{R}, \quad \sum_{k=-\infty}^{+\infty} |\hat{\phi}(\omega + 2k\pi)|^2 = 1. \tag{7.33}$$

Inserting $\hat{\phi}(\omega) = 2^{-1/2}\hat{h}(\omega/2)\,\hat{\phi}(\omega/2)$ yields

$$\sum_{k=-\infty}^{+\infty} \left|\hat{h}\left(\frac{\omega}{2} + k\pi\right)\right|^2 \left|\hat{\phi}\left(\frac{\omega}{2} + k\pi\right)\right|^2 = 2.$$

Since $\hat{h}(\omega)$ is 2π periodic, separating the even and odd integer terms gives

$$\left|\hat{h}\left(\frac{\omega}{2}\right)\right|^2 \sum_{p=-\infty}^{+\infty} \left|\hat{\phi}\left(\frac{\omega}{2} + 2p\pi\right)\right|^2 + \left|\hat{h}\left(\frac{\omega}{2} + \pi\right)\right|^2 \sum_{p=-\infty}^{+\infty} \left|\hat{\phi}\left(\frac{\omega}{2} + \pi + 2p\pi\right)\right|^2 = 2.$$

Inserting (7.33) for $\omega' = \omega/2$ and $\omega' = \omega/2 + \pi$ proves that

$$|\hat{h}(\omega')|^2 + |\hat{h}(\omega' + \pi)|^2 = 2.$$

Proof of the necessary condition (7.30). We prove that $\hat{h}(0) = \sqrt{2}$ by showing that $\hat{\phi}(0) \neq 0$. Indeed, we know that $\hat{\phi}(0) = 2^{-1/2}\,\hat{h}(0)\,\hat{\phi}(0)$. More precisely, we verify that $|\hat{\phi}(0)| = 1$ is a consequence of the completeness property (7.5) of multiresolution approximations.

The orthogonal projection of $f \in \mathbf{L^2}(\mathbb{R})$ on $\mathbf{V}_j$ is

$$P_{\mathbf{V}_j} f = \sum_{n=-\infty}^{+\infty} \langle f, \phi_{j,n} \rangle\, \phi_{j,n}. \tag{7.34}$$

Property (7.5) expressed in the time and Fourier domains with the Plancherel formula implies that

$$\lim_{j \to -\infty} \|f - P_{\mathbf{V}_j} f\|^2 = \lim_{j \to -\infty} 2\pi\, \|\hat{f} - \widehat{P_{\mathbf{V}_j} f}\|^2 = 0. \tag{7.35}$$

To compute the Fourier transform $\widehat{P_{\mathbf{V}_j} f}(\omega)$, we denote $\phi_j(t) = \sqrt{2^{-j}}\phi(2^{-j}t)$. Inserting the convolution expression (7.17) in (7.34) yields

$$P_{\mathbf{V}_j} f(t) = \sum_{n=-\infty}^{+\infty} f \star \bar{\phi}_j(2^j n)\, \phi_j(t - 2^j n) = \phi_j \star \sum_{n=-\infty}^{+\infty} f \star \bar{\phi}_j(2^j n)\, \delta(t - 2^j n).$$

The Fourier transform of $f \star \bar{\phi}_j(t)$ is $\sqrt{2^j}\hat{f}(\omega)\hat{\phi}^*(2^j\omega)$. A uniform sampling has a periodized Fourier transform calculated in (3.3), and thus,

$$\widehat{P_{\mathbf{V}_j} f}(\omega) = \hat{\phi}(2^j\omega) \sum_{k=-\infty}^{+\infty} \hat{f}\left(\omega - \frac{2k\pi}{2^j}\right) \hat{\phi}^*\left(2^j\left[\omega - \frac{2k\pi}{2^j}\right]\right). \tag{7.36}$$

Let us choose $\hat{f} = \mathbf{1}_{[-\pi,\pi]}$. For $j < 0$ and $\omega \in [-\pi, \pi]$, (7.36) gives $\widehat{P_{\mathbf{V}_j} f}(\omega) = |\hat{\phi}(2^j\omega)|^2$. The mean-square convergence (7.35) implies that

$$\lim_{j \to -\infty} \int_{-\pi}^{\pi} \left|1 - |\hat{\phi}(2^j\omega)|^2\right|^2 d\omega = 0.$$

Since ϕ is integrable, $\hat{\phi}(\omega)$ is continuous and thus $\lim_{j \to -\infty} |\hat{\phi}(2^j\omega)| = |\hat{\phi}(0)| = 1$.

We now prove that the function ϕ, having a Fourier transform given by (7.32), is a scaling function. This is divided in two intermediate results.

Proof that $\{\phi(t-n)\}_{n\in\mathbb{Z}}$ is orthonormal. Observe first that the infinite product (7.32) converges and that $|\hat{\phi}(\omega)| \leq 1$ because (7.29) implies that $|\hat{h}(\omega)| \leq \sqrt{2}$. The Parseval formula gives

$$\langle \phi(t), \phi(t-n)\rangle = \int_{-\infty}^{+\infty} \phi(t)\,\phi^*(t-n)\,dt = \frac{1}{2\pi}\int_{-\infty}^{+\infty} |\hat{\phi}(\omega)|^2\, e^{in\omega}\,d\omega.$$

Verifying that $\{\phi(t-n)\}_{n\in\mathbb{Z}}$ is orthonormal is equivalent to showing that

$$\int_{-\infty}^{+\infty} |\hat{\phi}(\omega)|^2\, e^{in\omega}\,d\omega = 2\pi\,\delta[n].$$

This result is obtained by considering the functions

$$\hat{\phi}_k(\omega) = \prod_{p=1}^{k} \frac{\hat{h}(2^{-p}\omega)}{\sqrt{2}}\,\mathbf{1}_{[-2^k\pi, 2^k\pi]}(\omega),$$

and computing the limit, as k increases to $+\infty$, of the integrals

$$I_k[n] = \int_{-\infty}^{+\infty} |\hat{\phi}_k(\omega)|^2\, e^{in\omega}\,d\omega = \int_{-2^k\pi}^{2^k\pi} \prod_{p=1}^{k} \frac{|\hat{h}(2^{-p}\omega)|^2}{2}\, e^{in\omega}\,d\omega.$$

First, let us show that $I_k[n] = 2\pi\delta[n]$ for all $k \geq 1$. To do this, we divide $I_k[n]$ into two integrals:

$$I_k[n] = \int_{-2^k\pi}^{0} \prod_{p=1}^{k} \frac{|\hat{h}(2^{-p}\omega)|^2}{2}\, e^{in\omega}\,d\omega + \int_{0}^{2^k\pi} \prod_{p=1}^{k} \frac{|\hat{h}(2^{-p}\omega)|^2}{2}\, e^{in\omega}\,d\omega.$$

Let us make the change of variable $\omega' = \omega + 2^k\pi$ in the first integral. Since $\hat{h}(\omega)$ is 2π periodic, when $p < k$, then $|\hat{h}(2^{-p}[\omega' - 2^k\pi])|^2 = |\hat{h}(2^{-p}\omega')|^2$. When $k = p$ the hypothesis (7.29) implies that

$$|\hat{h}(2^{-k}[\omega' - 2^k\pi])|^2 + |\hat{h}(2^{-k}\omega')|^2 = 2.$$

For $k > 1$, the two integrals of $I_k[n]$ become

$$I_k[n] = \int_{0}^{2^k\pi} \prod_{p=1}^{k-1} \frac{|\hat{h}(2^{-p}\omega)|^2}{2}\, e^{in\omega}\,d\omega. \tag{7.37}$$

Since $\prod_{p=1}^{k-1} |\hat{h}(2^{-p}\omega)|^2\, e^{in\omega}$ is $2^k\pi$ periodic we obtain $I_k[n] = I_{k-1}[n]$, and by induction $I_k[n] = I_1[n]$. Writing (7.37) for $k = 1$ gives

$$I_1[n] = \int_{0}^{2\pi} e^{in\omega}\,d\omega = 2\pi\,\delta[n],$$

which verifies that $I_k[n] = 2\pi\delta[n]$, for all $k \geq 1$.

We shall now prove that $\hat{\phi} \in \mathbf{L^2}(\mathbb{R})$. For all $\omega \in \mathbb{R}$,

$$\lim_{k \to \infty} |\hat{\phi}_k(\omega)|^2 = \prod_{p=1}^{\infty} \frac{|\hat{h}(2^{-p}\omega)|^2}{2} = |\hat{\phi}(\omega)|^2.$$

The Fatou lemma (A.1) on positive functions proves that

$$\int_{-\infty}^{+\infty} |\hat{\phi}(\omega)|^2 \, d\omega \leqslant \lim_{k \to \infty} \int_{-\infty}^{+\infty} |\hat{\phi}_k(\omega)|^2 \, d\omega = 2\pi, \tag{7.38}$$

because $I_k[0] = 2\pi$ for all $k \geqslant 1$. Since

$$|\hat{\phi}(\omega)|^2 \, \mathrm{e}^{in\omega} = \lim_{k \to \infty} |\hat{\phi}_k(\omega)|^2 \, \mathrm{e}^{in\omega},$$

we finally verify that

$$\int_{-\infty}^{+\infty} |\hat{\phi}(\omega)|^2 \, \mathrm{e}^{in\omega} \, d\omega = \lim_{k \to \infty} \int_{-\infty}^{+\infty} |\hat{\phi}_k(\omega)|^2 \, \mathrm{e}^{in\omega} \, d\omega = 2\pi \, \delta[n] \tag{7.39}$$

by applying the dominated convergence theorem (A.1). This requires verifying the upper-bound condition (A.1). This is done in our case by proving the existence of a constant C such that

$$\left| |\hat{\phi}_k(\omega)|^2 \, \mathrm{e}^{in\omega} \right| = |\hat{\phi}_k(\omega)|^2 \leqslant C \, |\hat{\phi}(\omega)|^2. \tag{7.40}$$

Indeed, we showed in (7.38) that $|\hat{\phi}(\omega)|^2$ is an integrable function.

The existence of $C > 0$ satisfying (7.40) is trivial for $|\omega| > 2^k \pi$ since $\hat{\phi}_k(\omega) = 0$. For $|\omega| \leqslant 2^k \pi$ since $\hat{\phi}(\omega) = 2^{-1/2} \, \hat{h}(\omega/2) \, \hat{\phi}(\omega/2)$, it follows that

$$|\hat{\phi}(\omega)|^2 = |\hat{\phi}_k(\omega)|^2 \, |\hat{\phi}(2^{-k}\omega)|^2.$$

Therefore, to prove (7.40) for $|\omega| \leqslant 2^k \pi$, it is sufficient to show that $|\hat{\phi}(\omega)|^2 \geqslant 1/C$ for $\omega \in [-\pi, \pi]$.

Let us first study the neighborhood of $\omega = 0$. Since $\hat{h}(\omega)$ is continuously differentiable in this neighborhood and since $|\hat{h}(\omega)|^2 \leqslant 2 = |\hat{h}(0)|^2$, the functions $|\hat{h}(\omega)|^2$ and $\log_{\mathrm{e}} |\hat{h}(\omega)|^2$ have derivatives that vanish at $\omega = 0$. It follows that there exists $\varepsilon > 0$ such that

$$\forall |\omega| \leqslant \varepsilon, \quad 0 \geqslant \log_{\mathrm{e}} \left(\frac{|\hat{h}(\omega)|^2}{2} \right) \geqslant -|\omega|.$$

Thus, for $|\omega| \leqslant \varepsilon$

$$|\hat{\phi}(\omega)|^2 = \exp\left[\sum_{p=1}^{+\infty} \log_{\mathrm{e}} \left(\frac{|\hat{h}(2^{-p}\omega)|^2}{2} \right) \right] \geqslant \mathrm{e}^{-|\omega|} \geqslant \mathrm{e}^{-\varepsilon}. \tag{7.41}$$

Now let us analyze the domain $|\omega| > \varepsilon$. To do this we take an integer l such that $2^{-l}\pi < \varepsilon$. Condition (7.31) proves that $K = \inf_{\omega \in [-\pi/2, \pi/2]} |\hat{h}(\omega)| > 0$, so if $|\omega| \leqslant \pi$,

$$|\hat{\phi}(\omega)|^2 = \prod_{p=1}^{l} \frac{|\hat{h}(2^{-p}\omega)|^2}{2} \left| \hat{\phi}\left(2^{-l}\omega\right) \right|^2 \geqslant \frac{K^{2l}}{2^l} \, \mathrm{e}^{-\varepsilon} = \frac{1}{C}.$$

This last result finishes the proof of inequality (7.40). Applying the dominated convergence theorem (A.1) proves (7.39) and that $\{\phi(t-n)\}_{n\in\mathbb{Z}}$ is orthonormal. A simple change of variable shows that $\{\phi_{j,n}\}_{j\in\mathbb{Z}}$ is orthonormal for all $j\in\mathbb{Z}$.

Proof that $\{\mathbf{V}_j\}_{j\in\mathbb{Z}}$ is a multiresolution approximation. To verify that ϕ is a scaling function, we must show that the spaces $\mathbf{V}_j$ generated by $\{\phi_{j,n}\}_{j\in\mathbb{Z}}$ define a multiresolution approximation. The multiresolution properties (7.1) and (7.3) are clearly true. The causality $\mathbf{V}_{j+1}\subset\mathbf{V}_j$ is verified by showing that for any $p\in\mathbb{Z}$,

$$\phi_{j+1,p}=\sum_{n=-\infty}^{+\infty} h[n-2p]\,\phi_{j,n}.$$

This equality is proved later in (7.107). Since all vectors of a basis of $\mathbf{V}_{j+1}$ can be decomposed in a basis of $\mathbf{V}_j$, it follows that $\mathbf{V}_{j+1}\subset\mathbf{V}_j$.

To prove the multiresolution property (7.4) we must show that any $f\in\mathbf{L}^2(\mathbb{R})$ satisfies

$$\lim_{j\to+\infty}\|P_{\mathbf{V}_j}f\|=0. \tag{7.42}$$

Since $\{\phi_{j,n}\}_{n\in\mathbb{Z}}$ is an orthonormal basis of $\mathbf{V}_j$,

$$\|P_{\mathbf{V}_j}f\|^2=\sum_{n=-\infty}^{+\infty}|\langle f,\phi_{j,n}\rangle|^2.$$

Suppose first that f is bounded by A and has a compact support included in $[2^J,2^J]$. The constants A and J may be arbitrarily large. It follows that

$$\begin{aligned}\sum_{n=-\infty}^{+\infty}|\langle f,\phi_{j,n}\rangle|^2&\leqslant 2^{-j}\left[\sum_{n=-\infty}^{+\infty}\int_{-2^J}^{2^J}|f(t)|\,|\phi(2^{-j}t-n)|\,dt\right]^2\\&\leqslant 2^{-j}A^2\left[\sum_{n=-\infty}^{+\infty}\int_{-2^J}^{2^J}|\phi(2^{-j}t-n)|\,dt\right]^2.\end{aligned}$$

Applying the Cauchy-Schwarz inequality to $1\times|\phi(2^{-j}t-n)|$ yields

$$\begin{aligned}\sum_{n=-\infty}^{+\infty}|\langle f,\phi_{j,n}\rangle|^2&\leqslant A^2\,2^{J+1}\sum_{n=-\infty}^{+\infty}\int_{-2^J}^{2^J}|\phi(2^{-j}t-n)|^2\,2^{-j}\,dt\\&\leqslant A^2 2^{J+1}\int_{S_j}|\phi(t)|^2\,dt=A^2\,2^{J+1}\int_{-\infty}^{+\infty}|\phi(t)|^2\,\mathbf{1}_{S_j}(t)\,dt,\end{aligned}$$

with $S_j=\cup_{n\in\mathbb{Z}}[n-2^{J-j},n+2^{J-j}]$ for $j>J$. For $t\notin\mathbb{Z}$, we obviously have $\mathbf{1}_{S_j}(t)\to 0$ for $j\to+\infty$. The dominated convergence theorem (A.1) applied to $|\phi(t)|^2\,\mathbf{1}_{S_j}(t)$ proves that the integral converges to 0 and thus,

$$\lim_{j\to+\infty}\sum_{n=-\infty}^{+\infty}|\langle f,\phi_{j,n}\rangle|^2=0.$$

Property (7.42) is extended to any $f\in\mathbf{L}^2(\mathbb{R})$ by using the density in $\mathbf{L}^2(\mathbb{R})$ of bounded function with a compact support, and Theorem A.5.

To prove the last multiresolution property (7.5) we must show that for any $f \in \mathbf{L}^2(\mathbb{R})$,

$$\lim_{j \to -\infty} \|f - P_{\mathbf{V}_j} f\|^2 = \lim_{j \to -\infty} \left(\|f\|^2 - \|P_{\mathbf{V}_j} f\|^2 \right) = 0. \tag{7.43}$$

We consider functions f that have a Fourier transform $\hat{f}$ that has a compact support included in $[-2^J \pi, 2^J \pi]$ for J large enough. We proved in (7.36) that the Fourier transform of $P_{\mathbf{V}_j} f$ is

$$\widehat{P_{\mathbf{V}_j} f}(\omega) = \hat{\phi}(2^j \omega) \sum_{k=-\infty}^{+\infty} \hat{f}\left(\omega - 2^{-j} 2k\pi\right) \hat{\phi}^*\left(2^j \left[\omega - 2^{-j} 2k\pi\right]\right).$$

If $j < -J$, then the supports of $\hat{f}(\omega - 2^{-j} 2k\pi)$ are disjoint for different k, so

$$\|P_{\mathbf{V}_j} f\|^2 = \frac{1}{2\pi} \int_{-\infty}^{+\infty} |\hat{f}(\omega)|^2 \, |\hat{\phi}(2^j \omega)|^4 \, d\omega \tag{7.44}$$

$$+ \frac{1}{2\pi} \int_{-\infty}^{+\infty} \sum_{\substack{k=-\infty \\ k \neq 0}}^{+\infty} |\hat{f}\left(\omega - 2^{-j} 2k\pi\right)|^2 \, |\hat{\phi}(2^j \omega)|^2 \, |\hat{\phi}\left(2^j \left[\omega - 2^{-j} 2k\pi\right]\right)|^2 \, d\omega.$$

We have already observed that $|\phi(\omega)| \leqslant 1$ and (7.41) proves that if ω is sufficiently small then $|\phi(\omega)| \geqslant e^{-|\omega|}$, so

$$\lim_{\omega \to 0} |\hat{\phi}(\omega)| = 1.$$

Since $|\hat{f}(\omega)|^2 |\hat{\phi}(2^j \omega)|^4 \leqslant |\hat{f}(\omega)|^2$ and $\lim_{j \to -\infty} |\hat{\phi}(2^j \omega)|^4 |\hat{f}(\omega)|^2 = |\hat{f}(\omega)|^2$, one can apply the dominated convergence theorem (A.1), to prove that

$$\lim_{j \to -\infty} \int_{-\infty}^{+\infty} |\hat{f}(\omega)|^2 \, |\hat{\phi}(2^j \omega)|^4 \, d\omega = \int_{-\infty}^{+\infty} |\hat{f}(\omega)|^2 \, d\omega = \|f\|^2. \tag{7.45}$$

The operator $P_{\mathbf{V}_j}$ is an orthogonal projector, so $\|P_{\mathbf{V}_j} f\| \leqslant \|f\|$. With (7.44) and (7.45), this implies that $\lim_{j \to -\infty} (\|f\|^2 - \|P_{\mathbf{V}_j} f\|^2) = 0$ and thus verifies (7.43). This property is extended to any $f \in \mathbf{L}^2(\mathbb{R})$ by using the density in $\mathbf{L}^2(\mathbb{R})$ of functions having compactly supported Fourier transforms and the result of Theorem A.5. ■

Discrete filters that have transfer functions that satisfy (7.29) are called *conjugate mirror filters*. As we shall see in Section 7.3, they play an important role in discrete signal processing; they make it possible to decompose discrete signals in separate frequency bands with filter banks. One difficulty of the proof is showing that the infinite cascade of convolutions that is represented in the Fourier domain by the product (7.32) does converge to a decent function in $\mathbf{L}^2(\mathbb{R})$. The sufficient condition (7.31) is not necessary to construct a scaling function, but it is always satisfied in practical designs of conjugate mirror filters. It cannot just be removed as shown by the example $\hat{h}(\omega) = \cos(3\omega/2)$, which satisfies all other conditions. In this case, a simple calculation shows that $\phi = 1/3 \, \mathbf{1}_{[-3/2, 3/2]}$. Clearly $\{\phi(t - n)\}_{n \in \mathbb{Z}}$ is not orthogonal, so ϕ is not a scaling function. However, the condition (7.31) may be replaced by a weaker but more technical necessary and sufficient condition proved by Cohen [16, 167].

EXAMPLE 7.6

For a Shannon multiresolution approximation, $\hat{\phi} = \mathbf{1}_{[-\pi,\pi]}$. Thus, we derive from (7.32) that

$$\forall \omega \in [-\pi, \pi], \quad \hat{h}(\omega) = \sqrt{2}\, \mathbf{1}_{[-\pi/2,\pi/2]}(\omega).$$

EXAMPLE 7.7

For piecewise constant approximations, $\phi = \mathbf{1}_{[0,1]}$. Since $h[n] = \langle 2^{-1/2}\phi(t/2), \phi(t-n)\rangle$, it follows that

$$h[n] = \begin{cases} 2^{-1/2} & \text{if } n = 0, 1 \\ 0 & \text{otherwise} \end{cases} \tag{7.46}$$

EXAMPLE 7.8

Polynomial splines of degree m correspond to a conjugate mirror filter $\hat{h}(\omega)$ that is calculated from $\hat{\phi}(\omega)$ with (7.25):

$$\hat{h}(\omega) = \sqrt{2}\, \frac{\hat{\phi}(2\omega)}{\hat{\phi}(\omega)}. \tag{7.47}$$

Inserting (7.18) yields

$$\hat{h}(\omega) = \exp\left(\frac{-i\varepsilon\omega}{2}\right) \sqrt{\frac{S_{2m+2}(\omega)}{2^{2m+1} S_{2m+2}(2\omega)}}, \tag{7.48}$$

where $\varepsilon = 0$ if m is odd and $\varepsilon = 1$ if m is even. For linear splines $m = 1$, so (7.20) implies that

$$\hat{h}(\omega) = \sqrt{2} \left[\frac{1 + 2\cos^2(\omega/2)}{1 + 2\cos^2 \omega}\right]^{1/2} \cos^2\left(\frac{\omega}{2}\right). \tag{7.49}$$

For cubic splines, the conjugate mirror filter is calculated by inserting (7.22) in (7.48). Figure 7.4 gives the graph of $|\hat{h}(\omega)|^2$. The impulse responses $h[n]$ of these filters have an infinite support but an exponential decay. For m odd, $h[n]$ is symmetric about $n = 0$. Table 7.1 gives the coefficients $h[n]$ above 10^{-4} for $m = 1, 3$.

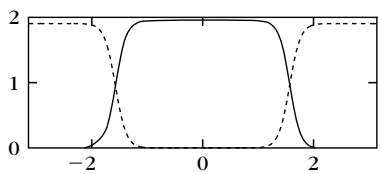

FIGURE 7.4

The solid line gives $|\hat{h}(\omega)|^2$ on $[-\pi, \pi]$ for a cubic spline multiresolution. The dotted line corresponds to $|\hat{g}(\omega)|^2$.

Table 7.1 Conjugate Mirror Filters $h[n]$ for Linear Splines $m = 1$ and Cubic Splines $m = 3$

	n	$h[n]$		n	$h[n]$
$m = 1$	0	0.817645956	$m = 3$	5, −5	0.042068328
	1, −1	0.397296430		6, −6	−0.017176331
	2, −2	−0.069101020		7, −7	−0.017982291
	3, −3	−0.051945337		8, −8	0.008685294
	4, −4	0.016974805		9, −9	0.008201477
	5, −5	0.009990599		10, −10	−0.004353840
	6, −6	−0.003883261		11, −11	−0.003882426
	7, −7	−0.002201945		12, −12	0.002186714
	8, −8	0.000923371		13, −13	0.001882120
	9, −9	0.000511636		14, −14	−0.001103748
	10, −10	−0.000224296		15, −15	−0.000927187
	11, −11	−0.000122686		16, −16	0.000559952
$m = 3$	0	0.766130398		17, −17	0.000462093
	1, −1	0.433923147		18, −18	−0.000285414
	2, −2	−0.050201753		19, −19	−0.000232304
	3, −3	−0.110036987		20, −20	0.000146098
	4, −4	0.032080869			

Note: The coefficients below 10^{-4} are not given.

7.1.4 In Which Orthogonal Wavelets Finally Arrive

Orthonormal wavelets carry the details necessary to increase the resolution of a signal approximation. The approximations of f at the scales 2^j and 2^{j-1} are, respectively, equal to their orthogonal projections on $\mathbf{V}_j$ and $\mathbf{V}_{j-1}$. We know that $\mathbf{V}_j$ is included in $\mathbf{V}_{j-1}$. Let $\mathbf{W}_j$ be the orthogonal complement of $\mathbf{V}_j$ in $\mathbf{V}_{j-1}$:

$$\mathbf{V}_{j-1} = \mathbf{V}_j \oplus \mathbf{W}_j. \tag{7.50}$$

The orthogonal projection of f on $\mathbf{V}_{j-1}$ can be decomposed as the sum of orthogonal projections on $\mathbf{V}_j$ and $\mathbf{W}_j$:

$$P_{\mathbf{V}_{j-1}} f = P_{\mathbf{V}_j} f + P_{\mathbf{W}_j} f. \tag{7.51}$$

The complement $P_{\mathbf{W}_j} f$ provides the "details" of f that appear at the scale 2^{j-1} but that disappear at the coarser scale 2^j. Theorem 7.3 [44, 362] proves that one can construct an orthonormal basis of $\mathbf{W}_j$ by scaling and translating a wavelet ψ.

Theorem 7.3: *Mallat, Meyer.* Let ϕ be a scaling function and h the corresponding conjugate mirror filter. Let ψ be the function having a Fourier transform

$$\hat{\psi}(\omega) = \frac{1}{\sqrt{2}} \hat{g}\left(\frac{\omega}{2}\right) \hat{\phi}\left(\frac{\omega}{2}\right), \tag{7.52}$$

with

$$\hat{g}(\omega) = \mathrm{e}^{-i\omega}\, \hat{h}^*(\omega + \pi). \tag{7.53}$$

Let us denote

$$\psi_{j,n}(t) = \frac{1}{\sqrt{2^j}}\,\psi\left(\frac{t-2^j n}{2^j}\right).$$

For any scale 2^j, $\{\psi_{j,n}\}_{n\in\mathbb{Z}}$ is an orthonormal basis of $\mathbf{W}_j$. For all scales, $\{\psi_{j,n}\}_{(j,n)\in\mathbb{Z}^2}$ is an orthonormal basis of $\mathbf{L^2}(\mathbb{R})$.

Proof. Let us prove first that $\hat{\psi}$ can be written as the product (7.52). Necessarily, $\psi(t/2) \in \mathbf{W}_1 \subset \mathbf{V}_0$. Thus, it can be decomposed in $\{\phi(t-n)\}_{n\in\mathbb{Z}}$, which is an orthogonal basis of $\mathbf{V}_0$:

$$\frac{1}{\sqrt{2}}\,\psi\left(\frac{t}{2}\right) = \sum_{n=-\infty}^{+\infty} g[n]\,\phi(t-n), \tag{7.54}$$

with

$$g[n] = \frac{1}{\sqrt{2}}\left\langle \psi\left(\frac{t}{2}\right), \phi(t-n)\right\rangle. \tag{7.55}$$

The Fourier transform of (7.54) yields

$$\hat{\psi}(2\omega) = \frac{1}{\sqrt{2}}\,\hat{g}(\omega)\,\hat{\phi}(\omega). \tag{7.56}$$

Lemma 7.1 gives necessary and sufficient conditions on $\hat{g}$ for designing an orthogonal wavelet.

Lemma 7.1. The family $\{\psi_{j,n}\}_{n\in\mathbb{Z}}$ is an orthonormal basis of $\mathbf{W}_j$ if and only if

$$|\hat{g}(\omega)|^2 + |\hat{g}(\omega+\pi)|^2 = 2 \tag{7.57}$$

and

$$\hat{g}(\omega)\,\hat{h}^*(\omega) + \hat{g}(\omega+\pi)\,\hat{h}^*(\omega+\pi) = 0. \tag{7.58}$$

The lemma is proved for $j=0$ from which it is easily extended to $j\neq 0$ with an appropriate scaling. As in (7.14), one can verify that $\{\psi(t-n)\}_{n\in\mathbb{Z}}$ is orthonormal if and only if

$$\forall \omega \in \mathbb{R}, \quad I(\omega) = \sum_{k=-\infty}^{+\infty} |\hat{\psi}(\omega + 2k\pi)|^2 = 1. \tag{7.59}$$

Since $\hat{\psi}(\omega) = 2^{-1/2}\,\hat{g}(\omega/2)\,\hat{\phi}(\omega/2)$ and $\hat{g}(\omega)$ is 2π periodic,

$$\begin{aligned} I(\omega) &= \sum_{k=-\infty}^{+\infty} |\hat{g}\left(\frac{\omega}{2}+k\pi\right)|^2\,|\hat{\phi}\left(\frac{\omega}{2}+k\pi\right)|^2 \\ &= |\hat{g}\Big(\frac{\omega}{2}\Big)|^2 \sum_{p=-\infty}^{+\infty} |\hat{\phi}\Big(\frac{\omega}{2}+2p\pi\Big)|^2 + |\hat{g}\Big(\frac{\omega}{2}+\pi\Big)|^2 \sum_{p=-\infty}^{+\infty} |\hat{\phi}\Big(\frac{\omega}{2}+\pi+2p\pi\Big)|^2. \end{aligned}$$

We know that $\sum_{p=-\infty}^{+\infty} |\hat{\phi}(\omega+2p\pi)|^2 = 1$, so (7.59) is equivalent to (7.57).

The space $\mathbf{W}_0$ is orthogonal to $\mathbf{V}_0$ if and only if $\{\phi(t-n)\}_{n\in\mathbb{Z}}$ and $\{\psi(t-n)\}_{n\in\mathbb{Z}}$ are orthogonal families of vectors. This means that for any $n\in\mathbb{Z}$,

$$\langle \psi(t), \phi(t-n)\rangle = \psi \star \bar{\phi}(n) = 0.$$

The Fourier transform of $\psi\star\bar{\phi}(t)$ is $\hat{\psi}(\omega)\hat{\phi}^*(\omega)$. The sampled sequence $\psi\star\bar{\phi}(n)$ is zero if its Fourier series computed with (3.3) satisfies

$$\forall \omega\in\mathbb{R}, \quad \sum_{k=-\infty}^{+\infty} \hat{\psi}(\omega+2k\pi)\,\hat{\phi}^*(\omega+2k\pi) = 0. \tag{7.60}$$

By inserting $\hat{\psi}(\omega) = 2^{-1/2}\,\hat{g}(\omega/2)\,\hat{\phi}(\omega/2)$ and $\hat{\phi}(\omega) = 2^{-1/2}\,\hat{h}(\omega/2)\,\hat{\phi}(\omega/2)$ in this equation, since $\sum_{k=-\infty}^{+\infty} |\hat{\phi}(\omega+2k\pi)|^2 = 1$, we prove as before that (7.60) is equivalent to (7.58).

We must finally verify that $\mathbf{V}_{-1} = \mathbf{V}_0 \oplus \mathbf{W}_0$. Knowing that $\{\sqrt{2}\phi(2t-n)\}_{n\in\mathbb{Z}}$ is an orthogonal basis of $\mathbf{V}_{-1}$, it is equivalent to show that for any $a[n]\in\ell^2(\mathbb{Z})$ there exist $b[n]\in\ell^2(\mathbb{Z})$ and $c[n]\in\ell^2(\mathbb{Z})$ such that

$$\sum_{n=-\infty}^{+\infty} a[n]\,\sqrt{2}\,\phi(2[t-2^{-1}n]) = \sum_{n=-\infty}^{+\infty} b[n]\,\phi(t-n) + \sum_{n=-\infty}^{+\infty} c[n]\,\psi(t-n). \tag{7.61}$$

This is done by relating $\hat{b}(\omega)$ and $\hat{c}(\omega)$ to $\hat{a}(\omega)$. The Fourier transform of (7.61) yields

$$\frac{1}{\sqrt{2}}\,\hat{a}\left(\frac{\omega}{2}\right)\hat{\phi}\left(\frac{\omega}{2}\right) = \hat{b}(\omega)\,\hat{\phi}(\omega) + \hat{c}(\omega)\,\hat{\psi}(\omega).$$

Inserting $\hat{\psi}(\omega) = 2^{-1/2}\,\hat{g}(\omega/2)\,\hat{\phi}(\omega/2)$ and $\hat{\phi}(\omega) = 2^{-1/2}\,\hat{h}(\omega/2)\,\hat{\phi}(\omega/2)$ in this equation shows that it is necessarily satisfied if

$$\hat{a}\left(\frac{\omega}{2}\right) = \hat{b}(\omega)\,\hat{h}\left(\frac{\omega}{2}\right) + \hat{c}(\omega)\,\hat{g}\left(\frac{\omega}{2}\right). \tag{7.62}$$

Let us define

$$\hat{b}(2\omega) = \frac{1}{2}\,[\hat{a}(\omega)\,\hat{h}^*(\omega) + \hat{a}(\omega+\pi)\,\hat{h}^*(\omega+\pi)]$$

and

$$\hat{c}(2\omega) = \frac{1}{2}\,[\hat{a}(\omega)\,\hat{g}^*(\omega) + \hat{a}(\omega+\pi)\,\hat{g}^*(\omega+\pi)].$$

When calculating the right side of (7.62), we verify that it is equal to the left side by inserting (7.57), (7.58), and using

$$|\hat{h}(\omega)|^2 + |\hat{h}(\omega+\pi)|^2 = 2. \tag{7.63}$$

Since $\hat{b}(\omega)$ and $\hat{c}(\omega)$ are 2π periodic they are the Fourier series of two sequences $b[n]$ and $c[n]$ that satisfy (7.61). This finishes the proof of the lemma.

The formula (7.53)

$$\hat{g}(\omega) = \mathrm{e}^{-i\omega}\,\hat{h}^*(\omega+\pi)$$

satisfies (7.57) and (7.58) because of (7.63). Thus, we derive from Lemma 7.1 that $\{\psi_{j,n}\}_{(j,n)\in\mathbb{Z}^2}$ is an orthogonal basis of $\mathbf{W}_j$.

We complete the proof of the theorem by verifying that $\{\psi_{j,n}\}_{(j,n)\in\mathbb{Z}^2}$ is an orthogonal basis of $\mathbf{L}^2(\mathbb{R})$. Observe first that the detail spaces $\{\mathbf{W}_j\}_{j\in\mathbb{Z}}$ are orthogonal. Indeed, $\mathbf{W}_j$ is

orthogonal to $\mathbf{V}_j$ and $\mathbf{W}_l \subset \mathbf{V}_{l-1} \subset \mathbf{V}_j$ for $j < l$. Thus, $\mathbf{W}_j$ and $\mathbf{W}_l$ are orthogonal. We can also decompose

$$\mathbf{L}^2(\mathbb{R}) = \oplus_{j=-\infty}^{+\infty} \mathbf{W}_j. \tag{7.64}$$

Indeed, $\mathbf{V}_{j-1} = \mathbf{W}_j \oplus \mathbf{V}_j$, and we verify by substitution that for any $L > J$,

$$\mathbf{V}_L = \oplus_{j=L-1}^{J} \mathbf{W}_j \oplus \mathbf{V}_J. \tag{7.65}$$

Since $\{\mathbf{V}_j\}_{j\in\mathbb{Z}}$ is a multiresolution approximation, $\mathbf{V}_L$ and $\mathbf{V}_J$ tend, respectively, to $\mathbf{L}^2(\mathbb{R})$ and $\{0\}$ when L and J go, respectively, to $-\infty$ and $+\infty$, which implies (7.64). Therefore, a union of orthonormal bases of all $\mathbf{W}_j$ is an orthonormal basis of $\mathbf{L}^2(\mathbb{R})$. ■

The proof of the theorem shows that $\hat{g}$ is the Fourier series of

$$g[n] = \left\langle \frac{1}{\sqrt{2}} \psi\left(\frac{t}{2}\right), \phi(t-n) \right\rangle, \tag{7.66}$$

which are the decomposition coefficients of

$$\frac{1}{\sqrt{2}} \psi\left(\frac{t}{2}\right) = \sum_{n=-\infty}^{+\infty} g[n]\, \phi(t-n). \tag{7.67}$$

Calculating the inverse Fourier transform of (7.53) yields

$$g[n] = (-1)^{1-n}\, h[1-n]. \tag{7.68}$$

This mirror filter plays an important role in the fast wavelet transform algorithm.

EXAMPLE 7.9

Figure 7.5 displays the cubic spline wavelet ψ and its Fourier transform $\hat{\psi}$ calculated by inserting in (7.52) the expressions (7.18) and (7.48) of $\hat{\phi}(\omega)$ and $\hat{h}(\omega)$. The properties of

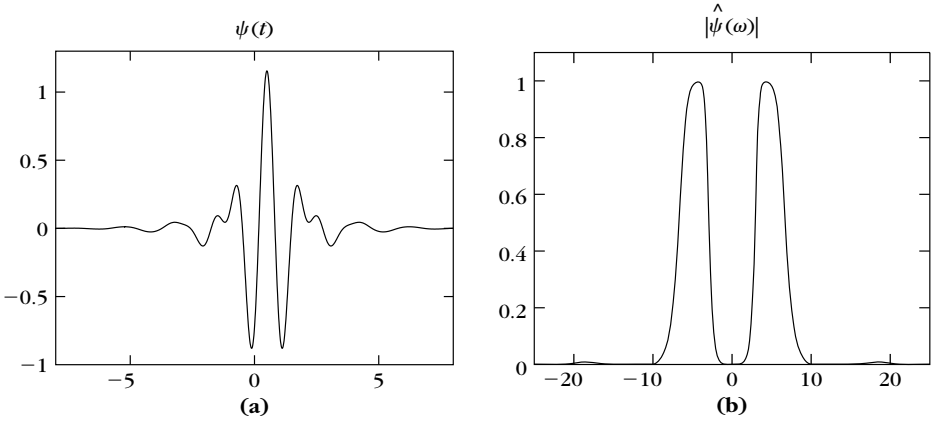

FIGURE 7.5

Battle-Lemarié cubic spline wavelet ψ **(a)** and its Fourier transform modulus **(b)**.

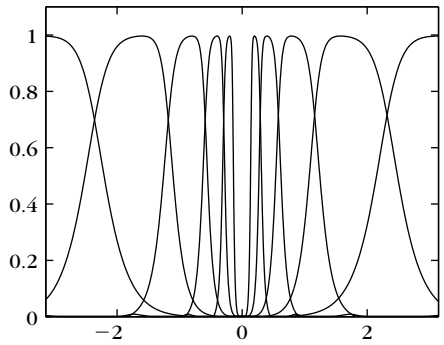

FIGURE 7.6

Graph of $|\hat{\psi}(2^j\omega)|^2$ for the cubic spline Battle-Lemarié wavelet, with $1 \leqslant j \leqslant 5$ and $\omega \in [-\pi, \pi]$.

this Battle-Lemarié spline wavelet are further studied in Section 7.2.2. Like most orthogonal wavelets, the energy of $\hat{\psi}$ is essentially concentrated in $[-2\pi, -\pi] \cup [\pi, 2\pi]$. For any ψ that generates an orthogonal basis of $\mathbf{L^2}(\mathbb{R})$, one can verify that

$$\forall \omega \in \mathbb{R} - \{0\}, \quad \sum_{j=-\infty}^{+\infty} |\hat{\psi}(2^j\omega)|^2 = 1.$$

This is illustrated in Figure 7.6.

The orthogonal projection of a signal f in a "detail" space $\mathbf{W}_j$ is obtained with a partial expansion in its wavelet basis:

$$P_{W_j} f = \sum_{n=-\infty}^{+\infty} \langle f, \psi_{j,n} \rangle \, \psi_{j,n}.$$

Thus, a signal expansion in a wavelet orthogonal basis can be viewed as an aggregation of details at all scales 2^j that go from 0 to $+\infty$:

$$f = \sum_{j=-\infty}^{+\infty} P_{\mathbf{W}_j} f = \sum_{j=-\infty}^{+\infty} \sum_{n=-\infty}^{+\infty} \langle f, \psi_{j,n} \rangle \, \psi_{j,n}.$$

Figure 7.7 gives the coefficients of a signal decomposed in the cubic spline wavelet orthogonal basis. The calculations are performed with the fast wavelet transform algorithm of Section 7.3. The up or down Diracs give the amplitudes of positive or negative wavelet coefficients at a distance $2^j n$ at each scale 2^j. Coefficients are nearly zero at fine scales where the signal is locally regular.

Wavelet Design

Theorem 7.3 constructs a wavelet orthonormal basis from any conjugate mirror filter $\hat{h}(\omega)$. This gives a simple procedure for designing and building wavelet orthogonal

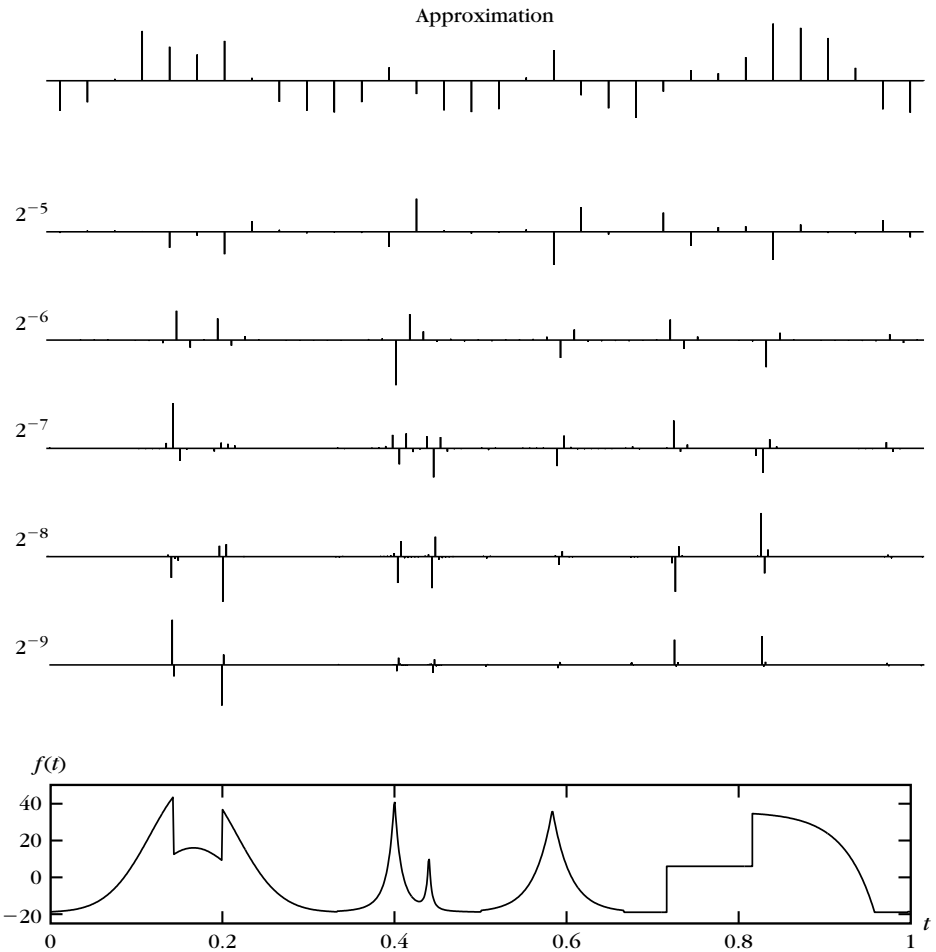

FIGURE 7.7

Wavelet coefficients $d_J[n] = \langle f, \psi_{J,n} \rangle$ calculated at scales 2^J with the cubic spline wavelet. Each up or down Dirac gives the amplitude of a positive or negative wavelet coefficient. At the top is the remaining coarse-signal approximation $a_J[n] = \langle f, \phi_{J,n} \rangle$ for $J = -5$.

bases. Conversely, we may wonder whether all wavelet orthonormal bases are associated to a multiresolution approximation and a conjugate mirror filter. If we impose that ψ has a compact support, then Lemarié [52] proved that ψ necessarily corresponds to a multiresolution approximation. It is possible, however, to construct pathological wavelets that decay like $|t|^{-1}$ at infinity, and that cannot be derived from any multiresolution approximation. Section 7.2 describes important classes of wavelet bases and explains how to design $\hat{h}$ to specify the support, the number of vanishing moments, and the regularity of ψ.

7.2 CLASSES OF WAVELET BASES

7.2.1 Choosing a Wavelet

Most applications of wavelet bases exploit their ability to efficiently approximate particular classes of functions with few nonzero wavelet coefficients. This is true not only for data compression but also for noise removal and fast calculations. Therefore, the design of ψ must be optimized to produce a maximum number of wavelet coefficients $\langle f, \psi_{j,n} \rangle$ that are close to zero. A function f has few nonnegligible wavelet coefficients if most of the fine-scale (high-resolution) wavelet coefficients are small. This depends mostly on the regularity of f, the number of vanishing moments of ψ, and the size of its support. To construct an appropriate wavelet from a conjugate mirror filter $h[n]$, we relate these properties to conditions on $\hat{h}(\omega)$.

Vanishing Moments

Let us recall that ψ has p vanishing moments if

$$\int_{-\infty}^{+\infty} t^k \, \psi(t) \, dt = 0 \quad \text{for } 0 \leq k < p. \tag{7.69}$$

This means that ψ is orthogonal to any polynomial of degree $p-1$. Section 6.1.3 proves that if f is regular and ψ has enough vanishing moments, then the wavelet coefficients $|\langle f, \psi_{j,n} \rangle|$ are small at fine scales 2^j. Indeed, if f is locally $\mathbf{C}^k$, then over a small interval it is well approximated by a Taylor polynomial of degree k. If $k < p$, then wavelets are orthogonal to this Taylor polynomial, and thus produce small-amplitude coefficients at fine scales. Theorem 7.4 relates the number of vanishing moments of ψ to the vanishing derivatives of $\hat{\psi}(\omega)$ at $\omega = 0$ and to the number of zeroes of $\hat{h}(\omega)$ at $\omega = \pi$. It also proves that polynomials of degree $p-1$ are then reproduced by the scaling functions.

Theorem 7.4: *Vanishing Moments.* Let ψ and ϕ be a wavelet and a scaling function that generate an orthogonal basis. Suppose that $|\psi(t)| = O((1+t^2)^{-p/2-1})$ and $|\phi(t)| = O((1+t^2)^{-p/2-1})$. The four following statements are equivalent:

1. The wavelet ψ has p vanishing moments.
2. $\hat{\psi}(\omega)$ and its first $p-1$ derivatives are zero at $\omega = 0$.
3. $\hat{h}(\omega)$ and its first $p-1$ derivatives are zero at $\omega = \pi$.
4. For any $0 \leq k < p$,

$$q_k(t) = \sum_{n=-\infty}^{+\infty} n^k \, \phi(t-n) \text{ is a polynomial of degree } k. \tag{7.70}$$

Proof. The decay of $|\phi(t)|$ and $|\psi(t)|$ implies that $\hat{\psi}(\omega)$ and $\hat{\phi}(\omega)$ are p times continuously differentiable. The k^{th}-order derivative $\hat{\psi}^{(k)}(\omega)$ is the Fourier transform of $(-it)^k \psi(t)$. Thus,

$$\hat{\psi}^{(k)}(0) = \int_{-\infty}^{+\infty} (-it)^k \, \psi(t) \, dt.$$

We derive that (1) is equivalent to (2).

Theorem 7.3 proves that

$$\sqrt{2}\,\hat{\psi}(2\omega) = \mathrm{e}^{-i\omega}\,\hat{h}^*(\omega+\pi)\,\hat{\phi}(\omega).$$

Since $\hat{\phi}(0) \neq 0$, by differentiating this expression we prove that (2) is equivalent to (3).

Let us now prove that (4) implies (1). Since ψ is orthogonal to $\{\phi(t-n)\}_{n\in\mathbb{Z}}$, it is also orthogonal to the polynomials q_k for $0 \leqslant k < p$. This family of polynomials is a basis of the space of polynomials of degree at most $p-1$. Thus, ψ is orthogonal to any polynomial of degree $p-1$ and in particular to t^k for $0 \leqslant k < p$. This means that ψ has p vanishing moments.

To verify that (1) implies (4) we suppose that ψ has p vanishing moments, and for $k < p$, we evaluate $q_k(t)$ defined in (7.70). This is done by computing its Fourier transform:

$$\hat{q}_k(\omega) = \hat{\phi}(\omega) \sum_{n=-\infty}^{+\infty} n^k \exp(-in\omega) = (i)^k\,\hat{\phi}(\omega)\,\frac{d^k}{d\omega^k} \sum_{n=-\infty}^{+\infty} \exp(-in\omega).$$

Let $\delta^{(k)}$ be the distribution that is the k^{th}-order derivative of a Dirac, defined in Section A.7 in the Appendix. The Poisson formula (2.4) proves that

$$\hat{q}_k(\omega) = (i)^k\,\frac{1}{2\pi}\,\hat{\phi}(\omega) \sum_{l=-\infty}^{+\infty} \delta^{(k)}(\omega - 2l\pi). \tag{7.71}$$

With several integrations by parts, we verify the distribution equality

$$\hat{\phi}(\omega)\,\delta^{(k)}(\omega-2l\pi) = \hat{\phi}(2l\pi)\,\delta^{(k)}(\omega-2l\pi) + \sum_{m=0}^{k-1} a_{m,l}^k\,\delta^{(m)}(\omega-2l\pi), \tag{7.72}$$

where $a_{m,l}^k$ is a linear combination of the derivatives $\{\hat{\phi}^{(m)}(2l\pi)\}_{0\leqslant m\leqslant k}$.

For $l \neq 0$, let us prove that $a_{m,l}^k = 0$ by showing that $\hat{\phi}^{(m)}(2l\pi) = 0$ if $0 \leqslant m < p$. For any $P > 0$, (7.27) implies

$$\hat{\phi}(\omega) = \hat{\phi}(2^{-P}\omega) \prod_{p=1}^{P} \frac{\hat{h}(2^{-p}\omega)}{\sqrt{2}}. \tag{7.73}$$

Since ψ has p vanishing moments, we showed in (3) that $\hat{h}(\omega)$ has a zero of order p at $\omega = \pm\pi$. But $\hat{h}(\omega)$ is also 2π periodic, so (7.73) implies that $\hat{\phi}(\omega) = O(|\omega - 2l\pi|^p)$ in the neighborhood of $\omega = 2l\pi$, for any $l \neq 0$. Thus, $\hat{\phi}^{(m)}(2l\pi) = 0$ if $m < p$.

Since $a_{m,l}^k = 0$ and $\phi(2l\pi) = 0$ when $l \neq 0$, it follows from (7.72) that

$$\hat{\phi}(\omega)\,\delta^{(k)}(\omega-2l\pi) = 0 \quad \text{for } l \neq 0.$$

The only term that remains in the summation (7.71) is $l = 0$, and inserting (7.72) yields

$$\hat{q}_k(\omega) = (i)^k \frac{1}{2\pi}\left(\hat{\phi}(0)\,\delta^{(k)}(\omega) + \sum_{m=0}^{k-1} a_{m,0}^k\,\delta^{(m)}(\omega)\right).$$

The inverse Fourier transform of $\delta^{(m)}(\omega)$ is $(2\pi)^{-1}(-it)^m$, and Theorem 7.2 proves that $\hat{\phi}(0) \neq 0$. Thus, the inverse Fourier transform q_k of $\hat{q}_k$ is a polynomial of degree k. ■

The hypothesis (4) is called the Fix-Strang condition [446]. The polynomials $\{q_k\}_{0 \leq k < p}$ define a basis of the space of polynomials of degree $p-1$. The Fix-Strang condition proves that ψ has p vanishing moments if and only if any polynomial of degree $p-1$ can be written as a linear expansion of $\{\phi(t-n)\}_{n \in \mathbb{Z}}$. The decomposition coefficients of the polynomials q_k do not have a finite energy because polynomials do not have a finite energy.

Size of Support

If f has an isolated singularity at t_0 and if t_0 is inside the support of $\psi_{j,n}(t) = 2^{-j/2}\psi(2^{-j}t - n)$, then $\langle f, \psi_{j,n} \rangle$ may have a large amplitude. If ψ has a compact support of size K, at each scale 2^j there are K wavelets $\psi_{j,n}$ with a support including t_0. To minimize the number of high-amplitude coefficients we must reduce the support size of ψ. Theorem 7.5 relates the support size of h to the support of ϕ and ψ.

Theorem 7.5: *Compact Support.* The scaling function ϕ has a compact support if and only if h has a compact support and their supports are equal. If the support of h and ϕ is $[N_1, N_2]$, then the support of ψ is $[(N_1 - N_2 + 1)/2\,,\ (N_2 - N_1 + 1)/2]$.

Proof. If ϕ has a compact support, since

$$h[n] = \frac{1}{\sqrt{2}} \left\langle \phi\left(\frac{t}{2}\right), \phi(t-n) \right\rangle,$$

we derive that h also has a compact support. Conversely, the scaling function satisfies

$$\frac{1}{\sqrt{2}}\,\phi\left(\frac{t}{2}\right) = \sum_{n=-\infty}^{+\infty} h[n]\,\phi(t-n). \tag{7.74}$$

If h has a compact support then one can prove [194] that ϕ has a compact support. The proof is not reproduced here.

To relate the support of ϕ and h, we suppose that $h[n]$ is nonzero for $N_1 \leq n \leq N_2$ and that ϕ has a compact support $[K_1, K_2]$. The support of $\phi(t/2)$ is $[2K_1, 2K_2]$. The sum at the right of (7.74) is a function with a support of $[N_1 + K_1, N_2 + K_2]$. The equality proves that the support of ϕ is $[K_1, K_2] = [N_1, N_2]$.

Let us recall from (7.68) and (7.67) that

$$\frac{1}{\sqrt{2}}\,\psi\left(\frac{t}{2}\right) = \sum_{n=-\infty}^{+\infty} g[n]\,\phi(t-n) = \sum_{n=-\infty}^{+\infty} (-1)^{1-n}\,h[1-n]\,\phi(t-n).$$

If the supports of ϕ and h are equal to $[N_1, N_2]$, the sum on the right side has a support equal to $[N_1 - N_2 + 1, N_2 - N_1 + 1]$. Thus, ψ has a support equal to $[(N_1 - N_2 + 1)/2, (N_2 - N_1 + 1)/2]$. ■

If h has a finite impulse response in $[N_1, N_2]$, Theorem 7.5 proves that ψ has a support of size $N_2 - N_1$ centered at $1/2$. To minimize the size of the support, we must synthesize conjugate mirror filters with as few nonzero coefficients as possible.

Support versus Moments

The support size of a function and the number of vanishing moments are a priori independent. However, we shall see in Theorem 7.7 that the constraints imposed on orthogonal wavelets imply that if ψ has p vanishing moments, then its support is at least of size $2p-1$. Daubechies wavelets are optimal in the sense that they have a minimum size support for a given number of vanishing moments. When choosing a particular wavelet, we face a trade-off between the number of vanishing moments and the support size. If f has few isolated singularities and is very regular between singularities, we must choose a wavelet with many vanishing moments to produce a large number of small wavelet coefficients $\langle f, \psi_{j,n}\rangle$. If the density of singularities increases, it might be better to decrease the size of its support at the cost of reducing the number of vanishing moments. Indeed, wavelets that overlap the singularities create high-amplitude coefficients.

The multiwavelet construction of Geronimo, Hardin, and Massupust [271] offers more design flexibility by introducing several scaling functions and wavelets. Exercise 7.16 gives an example. Better trade-off can be obtained between the multiwavelets supports and their vanishing moments [447]. However, multiwavelet decompositions are implemented with a slightly more complicated filter bank algorithm than a standard orthogonal wavelet transform.

Regularity

The regularity of ψ has mostly a cosmetic influence on the error introduced by thresholding or quantizing the wavelet coefficients. When reconstructing a signal from its wavelet coefficients

$$f = \sum_{j=-\infty}^{+\infty} \sum_{n=-\infty}^{+\infty} \langle f, \psi_{j,n}\rangle \, \psi_{j,n},$$

an error ε added to a coefficient $\langle f, \psi_{j,n}\rangle$ will add the wavelet component $\varepsilon \psi_{j,n}$ to the reconstructed signal. If ψ is smooth, then $\varepsilon \psi_{j,n}$ is a smooth error. For image-coding applications, a smooth error is often less visible than an irregular error, even though they have the same energy. Better-quality images are obtained with wavelets that are continuously differentiable than with the discontinuous Haar wavelet. Theorem 7.6 due to Tchamitchian [454] relates the uniform Lipschitz regularity of ϕ and ψ to the number of zeroes of $\hat{h}(\omega)$ at $\omega = \pi$.

Theorem 7.6: *Tchamitchian.* Let $\hat{h}(\omega)$ be a conjugate mirror filter with p zeroes at π and that satisfies the sufficient conditions of Theorem 7.2. Let us perform the factorization

$$\hat{h}(\omega) = \sqrt{2} \left(\frac{1+e^{i\omega}}{2}\right)^p \hat{l}(\omega).$$

If $\sup_{\omega\in\mathbb{R}} |\hat{l}(\omega)| = B$, then ψ and ϕ are uniformly Lipschitz α for

$$\alpha < \alpha_0 = p - \log_2 B - 1. \tag{7.75}$$

Proof. This result is proved by showing that there exist $C_1 > 0$ and $C_2 > 0$ such that for all $\omega \in \mathbb{R}$

$$|\hat{\phi}(\omega)| \leqslant C_1 \, (1 + |\omega|)^{-p + \log_2 B} \tag{7.76}$$

$$|\hat{\psi}(\omega)| \leqslant C_2 \, (1 + |\omega|)^{-p + \log_2 B}. \tag{7.77}$$

The Lipschitz regularity of ϕ and ψ is then derived from Theorem 6.1, which shows that if $\int_{-\infty}^{+\infty} (1 + |\omega|^{\alpha}) \, |\hat{f}(\omega)| \, d\omega < +\infty$, then f is uniformly Lipschitz α.

We proved in (7.32) that $\hat{\phi}(\omega) = \prod_{j=1}^{+\infty} 2^{-1/2} \, \hat{h}(2^{-j}\omega)$. One can verify that

$$\prod_{j=1}^{+\infty} \frac{1 + \exp(i 2^{-j} \omega)}{2} = \frac{1 - \exp(i\omega)}{i\,\omega},$$

thus,

$$|\hat{\phi}(\omega)| = \frac{|1 - \exp(i\omega)|^p}{|\omega|^p} \prod_{j=1}^{+\infty} |\hat{l}(2^{-j}\omega)|. \tag{7.78}$$

Let us now compute an upper bound for $\prod_{j=1}^{+\infty} |\hat{l}(2^{-j}\omega)|$. At $\omega = 0$, we have $\hat{h}(0) = \sqrt{2}$ so $\hat{l}(0) = 1$. Since $\hat{h}(\omega)$ is continuously differentiable at $\omega = 0$, $\hat{l}(\omega)$ is also continuously differentiable at $\omega = 0$. Thus, we derive that there exists $\varepsilon > 0$ such that if $|\omega| < \varepsilon$, then $|\hat{l}(\omega)| \leqslant 1 + K|\omega|$. Consequently,

$$\sup_{|\omega| \leqslant \varepsilon} \prod_{j=1}^{+\infty} |\hat{l}(2^{-j}\omega)| \leqslant \sup_{|\omega| \leqslant \varepsilon} \prod_{j=1}^{+\infty} (1 + K|2^{-j}\omega|) \leqslant \mathrm{e}^{K\varepsilon}. \tag{7.79}$$

If $|\omega| > \varepsilon$, there exists $J \geqslant 1$ such that $2^{J-1}\varepsilon \leqslant |\omega| \leqslant 2^J \varepsilon$, and we decompose

$$\prod_{j=1}^{+\infty} \hat{l}(2^{-j}\omega) = \prod_{j=1}^{J} |\hat{l}(2^{-j}\omega)| \prod_{j=1}^{+\infty} |\hat{l}(2^{-j-J}\omega)|. \tag{7.80}$$

Since $\sup_{\omega \in \mathbb{R}} |\hat{l}(\omega)| = B$, inserting (7.79) yields for $|\omega| > \varepsilon$

$$\prod_{j=1}^{+\infty} \hat{l}(2^{-j}\omega) \leqslant B^J \, \mathrm{e}^{K\varepsilon} = \mathrm{e}^{K\varepsilon} \, 2^{J \log_2 B}. \tag{7.81}$$

Since $2^J \leqslant \varepsilon^{-1} 2|\omega|$, this proves that

$$\forall \omega \in \mathbb{R}, \quad \prod_{j=1}^{+\infty} \hat{l}(2^{-j}\omega) \leqslant \mathrm{e}^{K\varepsilon} \left(1 + \frac{|2\omega|^{\log_2 B}}{\varepsilon^{\log_2 B}}\right).$$

Equation (7.76) is derived from (7.78) and this last inequality. Since $|\hat{\psi}(2\omega)| = 2^{-1/2} \, |\hat{h}(\omega + \pi)| \, |\hat{\phi}(\omega)|$, (7.77) is obtained from (7.76). ■

This theorem proves that if $B < 2^{p-1}$, then $\alpha_0 > 0$. It means that ϕ and ψ are uniformly continuous. For any $m > 0$, if $B < 2^{p-1-m}$, then $\alpha_0 > m$, so ψ and ϕ are m times continuously differentiable. Theorem 7.4 shows that the number p of zeros of $\hat{h}(\omega)$ at π is equal to the number of vanishing moments of ψ. A priori, we are

not guaranteed that increasing p will improve the wavelet regularity since B might increase as well. However, for important families of conjugate mirror filters such as splines or Daubechies filters, B increases more slowly than p, which implies that wavelet regularity increases with the number of vanishing moments. Let us emphasize that the number of vanishing moments and the regularity of orthogonal wavelets are related but it is the number of vanishing moments and not the regularity that affects the amplitude of the wavelet coefficients at fine scales.

7.2.2 Shannon, Meyer, Haar, and Battle-Lemarié Wavelets

We study important classes of wavelets with Fourier transforms that are derived from the general formula proved in Theorem 7.3,

$$\hat{\psi}(\omega) = \frac{1}{\sqrt{2}}\,\hat{g}\left(\frac{\omega}{2}\right)\,\hat{\phi}\left(\frac{\omega}{2}\right) = \frac{1}{\sqrt{2}}\,\exp\left(\frac{-i\omega}{2}\right)\,\hat{h}^*\left(\frac{\omega}{2}+\pi\right)\hat{\phi}\left(\frac{\omega}{2}\right). \tag{7.82}$$

Shannon Wavelet

The Shannon wavelet is constructed from the Shannon multiresolution approximation, which approximates functions by their restriction to low-frequency intervals. It corresponds to $\hat{\phi} = \mathbf{1}_{[-\pi,\pi]}$ and $\hat{h}(\omega) = \sqrt{2}\,\mathbf{1}_{[-\pi/2,\pi/2]}(\omega)$ for $\omega \in [-\pi, \pi]$. We derive from (7.82) that

$$\hat{\psi}(\omega) = \begin{cases} \exp(-i\omega/2) & \text{if } \omega \in [-2\pi, -\pi] \cup [\pi, 2\pi] \\ 0 & \text{otherwise,} \end{cases} \tag{7.83}$$

and thus,

$$\psi(t) = \frac{\sin 2\pi(t-1/2)}{2\pi(t-1/2)} - \frac{\sin \pi(t-1/2)}{\pi(t-1/2)}.$$

This wavelet is $\mathbf{C}^\infty$ but has a slow asymptotic time decay. Since $\hat{\psi}(\omega)$ is zero in the neighborhood of $\omega = 0$, all its derivatives are zero at $\omega = 0$. Thus, Theorem 7.4 implies that ψ has an infinite number of vanishing moments.

Since $\hat{\psi}(\omega)$ has a compact support we know that $\psi(t)$ is $\mathbf{C}^\infty$. However, $|\psi(t)|$ decays only like $|t|^{-1}$ at infinity because $\hat{\psi}(\omega)$ is discontinuous at $\pm\pi$ and $\pm 2\pi$.

Meyer Wavelets

A Meyer wavelet [375] is a frequency band-limited function that has a Fourier transform that is smooth, unlike the Fourier transform of the Shannon wavelet. This smoothness provides a much faster asymptotic decay in time. These wavelets are constructed with conjugate mirror filters $\hat{h}(\omega)$ that are $\mathbf{C}^n$ and satisfy

$$\hat{h}(\omega) = \begin{cases} \sqrt{2} & \text{if } \omega \in [-\pi/3, \pi/3] \\ 0 & \text{if } \omega \in [-\pi, -2\pi/3] \cup [2\pi/3, \pi]. \end{cases} \tag{7.84}$$

The only degree of freedom is the behavior of $\hat{h}(\omega)$ in the transition bands $[-2\pi/3, -\pi/3] \cup [\pi/3, 2\pi/3]$. It must satisfy the quadrature condition

$$|\hat{h}(\omega)|^2 + |\hat{h}(\omega+\pi)|^2 = 2, \tag{7.85}$$

and to obtain $\mathbf{C}^n$ junctions at $|\omega| = \pi/3$ and $|\omega| = 2\pi/3$, the n first derivatives must vanish at these abscissa. One can construct such functions that are $\mathbf{C}^\infty$.

The scaling function $\hat{\phi}(\omega) = \prod_{p=1}^{+\infty} 2^{-1/2}\, \hat{h}(2^{-p}\omega)$ has a compact support and one can verify that

$$\hat{\phi}(\omega) = \begin{cases} 2^{-1/2}\, \hat{h}(\omega/2) & \text{if } |\omega| \leqslant 4\pi/3 \\ 0 & \text{if } |\omega| > 4\pi/3. \end{cases} \tag{7.86}$$

The resulting wavelet (7.82) is

$$\hat{\psi}(\omega) = \begin{cases} 0 & \text{if } |\omega| \leqslant 2\pi/3 \\ 2^{-1/2}\, \hat{g}(\omega/2) & \text{if } 2\pi/3 \leqslant |\omega| \leqslant 4\pi/3 \\ 2^{-1/2}\, \exp(-i\omega/2)\, \hat{h}(\omega/4) & \text{if } 4\pi/3 \leqslant |\omega| \leqslant 8\pi/3 \\ 0 & \text{if } |\omega| > 8\pi/3. \end{cases} \tag{7.87}$$

The functions ϕ and ψ are $\mathbf{C}^\infty$ because their Fourier transforms have a compact support. Since $\hat{\psi}(\omega) = 0$ in the neighborhood of $\omega = 0$, all its derivatives are zero at $\omega = 0$, which proves that ψ has an infinite number of vanishing moments.

If $\hat{h}$ is $\mathbf{C}^n$, then $\hat{\psi}$ and $\hat{\phi}$ are also $\mathbf{C}^n$. The discontinuities of the $(n+1)^{\text{th}}$ derivative of $\hat{h}$ are generally at the junction of the transition band $|\omega| = \pi/3\,,\ 2\pi/3$, in which case one can show that there exists A such that

$$|\phi(t)| \leqslant A\,(1+|t|)^{-n-1} \quad \text{and} \quad |\psi(t)| \leqslant A\,(1+|t|)^{-n-1}.$$

Although the asymptotic decay of ψ is fast when n is large, its effective numerical decay may be relatively slow, which is reflected by the fact that A is quite large. As a consequence, a Meyer wavelet transform is generally implemented in the Fourier domain. Section 8.4.2 relates these wavelet bases to lapped orthogonal transforms applied in the Fourier domain. One can prove [19] that there exists no orthogonal wavelet that is $\mathbf{C}^\infty$ and has an exponential decay.

EXAMPLE 7.10

To satisfy the quadrature condition (7.85), one can verify that $\hat{h}$ in (7.84) may be defined on the transition bands by

$$\hat{h}(\omega) = \sqrt{2}\, \cos\left[\frac{\pi}{2}\beta\left(\frac{3|\omega|}{\pi} - 1\right)\right] \quad \text{for} \quad |\omega| \in [\pi/3, 2\pi/3],$$

where $\beta(x)$ is a function that goes from 0 to 1 on the interval $[0, 1]$ and satisfies

$$\forall x \in [0, 1], \quad \beta(x) + \beta(1-x) = 1. \tag{7.88}$$

An example due to Daubechies [19] is

$$\beta(x) = x^4\,(35 - 84x + 70x^2 - 20x^3). \tag{7.89}$$

The resulting $\hat{h}(\omega)$ has $n = 3$ vanishing derivatives at $|\omega| = \pi/3\,,\ 2\pi/3$. Figure 7.8 displays the corresponding wavelet ψ.

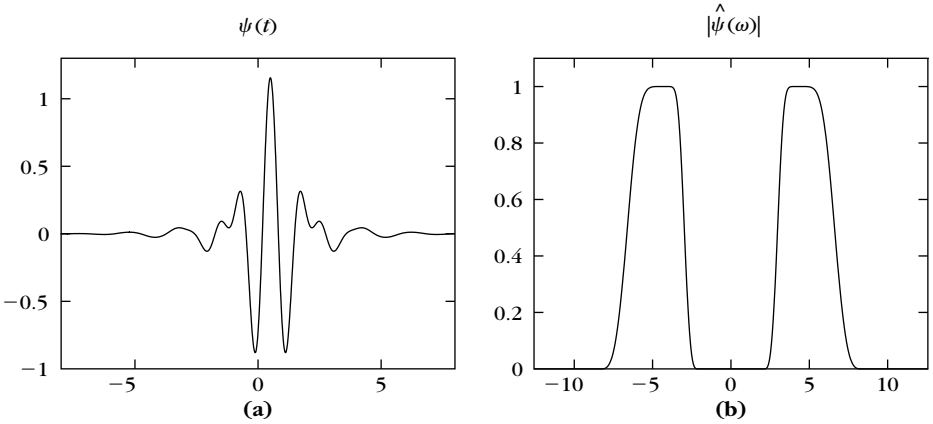

FIGURE 7.8

Meyer wavelet ψ **(a)** and its Fourier transform modulus computed with (7.89) **(b)**.

Haar Wavelets

The Haar basis is obtained with a multiresolution of piecewise constant functions. The scaling function is $\phi = \mathbf{1}_{[0,1]}$. The filter $h[n]$ given in (7.46) has two nonzero coefficients equal to $2^{-1/2}$ at $n = 0$ and $n = 1$. Thus,

$$\frac{1}{\sqrt{2}}\psi\left(\frac{t}{2}\right) = \sum_{n=-\infty}^{+\infty} (-1)^{1-n} h[1-n]\,\phi(t-n) = \frac{1}{\sqrt{2}}\Big(\phi(t-1) - \phi(t)\Big),$$

so

$$\psi(t) = \begin{cases} -1 & \text{if } 0 \leqslant t < 1/2 \\ 1 & \text{if } 1/2 \leqslant t < 1 \\ 0 & \text{otherwise.} \end{cases} \tag{7.90}$$

The Haar wavelet has the shortest support among all orthogonal wavelets. It is not well adapted to approximating smooth functions because it has only one vanishing moment.

Battle-Lemarié Wavelets

Polynomial spline wavelets introduced by Battle [99] and Lemarié [345] are computed from spline multiresolution approximations. The expressions of $\hat{\phi}(\omega)$ and $\hat{h}(\omega)$ are given, respectively, by (7.18) and (7.48). For splines of degree m, $\hat{h}(\omega)$ and its first m derivatives are zero at $\omega = \pi$. Theorem 7.4 derives that ψ has $m+1$ vanishing moments. It follows from (7.82) that

$$\hat{\psi}(\omega) = \frac{\exp(-i\omega/2)}{\omega^{m+1}} \sqrt{\frac{S_{2m+2}(\omega/2+\pi)}{S_{2m+2}(\omega)\, S_{2m+2}(\omega/2)}}.$$

This wavelet ψ has an exponential decay. Since it is a polynomial spline of degree m, it is $m-1$ times continuously differentiable. Polynomial spline wavelets are less

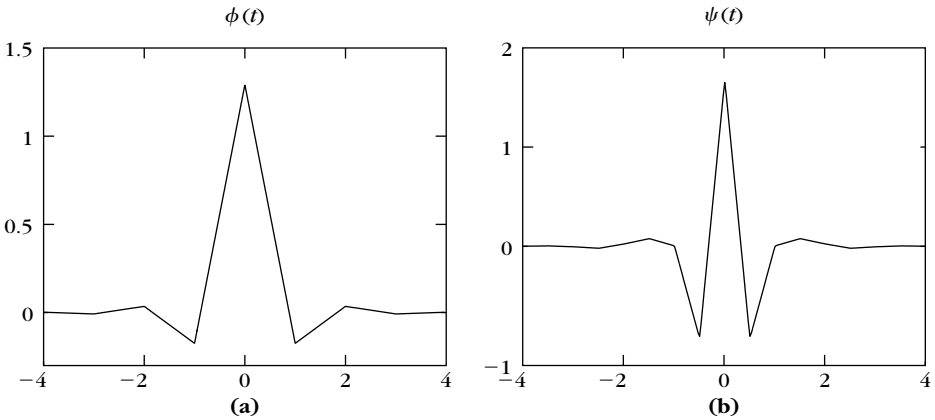

FIGURE 7.9

Linear spline Battle-Lemarié scaling function ϕ **(a)** and wavelet ψ **(b)**.

regular than Meyer wavelets but have faster time asymptotic decay. For m odd, ψ is symmetric about $1/2$. For m even, it is antisymmetric about $1/2$. Figure 7.5 gives the graph of the cubic spline wavelet ψ corresponding to $m = 3$. For $m = 1$, Figure 7.9 displays linear splines ϕ and ψ. The properties of these wavelets are further studied in [15, 106, 164].

7.2.3 Daubechies Compactly Supported Wavelets

Daubechies wavelets have a support of minimum size for any given number p of vanishing moments. Theorem 7.5 proves that wavelets of compact support are computed with finite impulse-response conjugate mirror filters h. We consider real causal filters $h[n]$, which implies that $\hat{h}$ is a trigonometric polynomial:

$$\hat{h}(\omega) = \sum_{n=0}^{N-1} h[n]\, \mathrm{e}^{-in\omega}.$$

To ensure that ψ has p vanishing moments, Theorem 7.4 shows that $\hat{h}$ must have a zero of order p at $\omega = \pi$. To construct a trigonometric polynomial of minimal size, we factor $(1 + \mathrm{e}^{-i\omega})^p$, which is a minimum-size polynomial having p zeros at $\omega = \pi$:

$$\hat{h}(\omega) = \sqrt{2}\left(\frac{1 + \mathrm{e}^{-i\omega}}{2}\right)^p R(\mathrm{e}^{-i\omega}). \tag{7.91}$$

The difficulty is to design a polynomial $R(\mathrm{e}^{-i\omega})$ of minimum degree m such that $\hat{h}$ satisfies

$$|\hat{h}(\omega)|^2 + |\hat{h}(\omega + \pi)|^2 = 2. \tag{7.92}$$

As a result, h has $N = m + p + 1$ nonzero coefficients. Theorem 7.7 by Daubechies [194] proves that the minimum degree of R is $m = p - 1$.

Theorem 7.7: *Daubechies.* A real conjugate mirror filter h, such that $\hat{h}(\omega)$ has p zeroes at $\omega = \pi$, has at least $2p$ nonzero coefficients. Daubechies filters have $2p$ nonzero coefficients.

Proof. The proof is constructive and computes Daubechies filters. Since $h[n]$ is real, $|\hat{h}(\omega)|^2$ is an even function and can be written as a polynomial in $\cos\omega$. Thus, $|R(e^{-i\omega})|^2$ defined in (7.91) is a polynomial in $\cos\omega$ that we can also write as a polynomial $P(\sin^2(\omega/2))$,

$$|\hat{h}(\omega)|^2 = 2\left(\cos\frac{\omega}{2}\right)^{2p} P\left(\sin^2\frac{\omega}{2}\right). \tag{7.93}$$

The quadrature condition (7.92) is equivalent to

$$(1-y)^p P(y) + y^p P(1-y) = 1, \tag{7.94}$$

for any $y = \sin^2(\omega/2) \in [0, 1]$. To minimize the number of nonzero terms of the finite Fourier series $\hat{h}(\omega)$, we must find the solution $P(y) \geqslant 0$ of minimum degree, which is obtained with the Bezout theorem on polynomials. ■

Theorem 7.8: *Bezout.* Let $Q_1(y)$ and $Q_2(y)$ be two polynomials of degrees n_1 and n_2 with no common zeroes. There exist two unique polynomials $P_1(y)$ and $P_2(y)$ of degrees $n_2 - 1$ and $n_1 - 1$ such that

$$P_1(y)\,Q_1(y) + P_2(y)\,Q_2(y) = 1. \tag{7.95}$$

The proof of this classical result is in [19]. Since $Q_1(y) = (1-y)^p$ and $Q_2(y) = y^p$ are two polynomials of degree p with no common zeros, the Bezout theorem proves that there exist two unique polynomials $P_1(y)$ and $P_2(y)$ such that

$$(1-y)^p P_1(y) + y^p P_2(y) = 1.$$

The reader can verify that $P_2(y) = P_1(1-y) = P(1-y)$ with

$$P(y) = \sum_{k=0}^{p-1} \binom{p-1+k}{k} y^k. \tag{7.96}$$

Clearly, $P(y) \geqslant 0$ for $y \in [0, 1]$. Thus, $P(y)$ is the polynomial of minimum degree satisfying (7.94) with $P(y) \geqslant 0$.

Now we need to construct a minimum-degree polynomial

$$R(e^{-i\omega}) = \sum_{k=0}^{m} r_k\, e^{-ik\omega} = r_0 \prod_{k=0}^{m} (1 - a_k\, e^{-i\omega})$$

such that $|R(e^{-i\omega})|^2 = P(\sin^2(\omega/2))$. Since its coefficients are real, $R^*(e^{-i\omega}) = R(e^{i\omega})$, and thus,

$$|R(e^{-i\omega})|^2 = R(e^{-i\omega})\,R(e^{i\omega}) = P\left(\frac{2 - e^{i\omega} - e^{-i\omega}}{4}\right) = Q(e^{-i\omega}). \tag{7.97}$$

This factorization is solved by extending it to the whole complex plane with the variable $z = e^{-i\omega}$:

$$R(z)\,R(z^{-1}) = r_0^2 \prod_{k=0}^{m} (1 - a_k z)\,(1 - a_k z^{-1}) = Q(z) = P\left(\frac{2 - z - z^{-1}}{4}\right). \tag{7.98}$$

Let us compute the roots of $Q(z)$. Since $Q(z)$ has real coefficients if c_k is a root, then c_k^* is also a root, and since it is a function of $z+z^{-1}$ if c_k is a root, then $1/c_k$ and thus $1/c_k^*$ are also roots. To design $R(z)$ that satisfies (7.98), we choose each root a_k of $R(z)$ among a pair $(c_k, 1/c_k)$ and include a_k^* as a root to obtain real coefficients. This procedure yields a polynomial of minimum degree $m = p-1$, with $r_0^2 = Q(0) = P(1/2) = 2^{p-1}$. The resulting filter h of minimum size has $N = p+m+1 = 2p$ nonzero coefficients.

Among all possible factorizations, the minimum-phase solution $R(e^{i\omega})$ is obtained by choosing a_k among $(c_k, 1/c_k)$ to be inside the unit circle $|a_k| \leqslant 1$ [51]. The resulting causal filter h has an energy maximally concentrated at small abscissa $n \geqslant 0$. It is a Daubechies filter of order p.

The constructive proof of this theorem synthesizes causal conjugate mirror filters of size $2p$. Table 7.2 gives the coefficients of these Daubechies filters for $2 \leqslant p \leqslant 10$. Theorem 7.9 derives that Daubechies wavelets calculated with these conjugate mirror filters have a support of minimum size.

Theorem 7.9: *Daubechies.* If ψ is a wavelet with p vanishing moments that generates an orthonormal basis of $\mathbf{L^2}(\mathbb{R})$, then it has a support of size larger than or equal to $2p-1$. A Daubechies wavelet has a minimum-size support equal to $[-p+1, p]$. The support of the corresponding scaling function ϕ is $[0, 2p-1]$.

This theorem is a direct consequence of Theorem 7.7. The support of the wavelet, and that of the scaling function, are calculated with Theorem 7.5. When $p=1$ we get the Haar wavelet. Figure 7.10 displays the graphs of ϕ and ψ for $p = 2, 3, 4$.

The regularity of ϕ and ψ is the same since $\psi(t)$ is a finite linear combination of $\phi(2t-n)$. However, this regularity is difficult to estimate precisely. Let $B = \sup_{\omega \in \mathbb{R}} |R(e^{-i\omega})|$ where $R(e^{-i\omega})$ is the trigonometric polynomial defined in (7.91). Theorem 7.6 proves that ψ is at least uniformly Lipschitz α for $\alpha < p - \log_2 B - 1$. For Daubechies wavelets, B increases more slowly than p, and Figure 7.10 shows indeed that the regularity of these wavelets increases with p. Daubechies and Lagarias [198] have established a more precise technique that computes the exact Lipschitz regularity of ψ. For $p=2$ the wavelet ψ is only Lipschitz 0.55, but for $p=3$ it is Lipschitz 1.08, which means that it is already continuously differentiable. For p large, ϕ and ψ are uniformly Lipschitz α, for α of the order of $0.2\,p$ [168].

Symmlets

Daubechies wavelets are very asymmetric because they are constructed by selecting the minimum-phase square root of $Q(e^{-i\omega})$ in (7.97). One can show [51] that filters corresponding to a minimum-phase square root have their energy optimally concentrated near the starting point of their support. Thus, they are highly nonsymmetric, which yields very asymmetric wavelets.

To obtain a symmetric or antisymmetric wavelet, the filter h must be symmetric or antisymmetric with respect to the center of its support, which means that $\hat{h}(\omega)$ has a linear complex phase. Daubechies proved [194] that the Haar filter is the

Table 7.2 Daubechies Filters for Wavelets with p Vanishing Moments

	n	$h_p[n]$
$p=2$	0	0.482962913145
	1	0.836516303738
	2	0.224143868042
	3	−0.129409522551
$p=3$	0	0.332670552950
	1	0.806891509311
	2	0.459877502118
	3	−0.135011020010
	4	−0.085441273882
	5	0.035226291882
$p=4$	0	0.230377813309
	1	0.714846570553
	2	0.630880767930
	3	−0.027983769417
	4	−0.187034811719
	5	0.030841381836
	6	0.032883011667
	7	−0.010597401785
$p=5$	0	0.160102397974
	1	0.603829269797
	2	0.724308528438
	3	0.138428145901
	4	−0.242294887066
	5	−0.032244869585
	6	0.077571493840
	7	−0.006241490213
	8	−0.012580751999
	9	0.003335725285
$p=6$	0	0.111540743350
	1	0.494623890398
	2	0.751133908021
	3	0.315250351709
	4	−0.226264693965
	5	−0.129766867567
	6	0.097501605587
	7	0.027522865530
	8	−0.031582039317
	9	0.000553842201
	10	0.004777257511
	11	−0.001077301085
$p=7$	0	0.077852054085
	1	0.396539319482
	2	0.729132090846
	3	0.469782287405
	4	−0.143906003929
	5	−0.224036184994
	6	0.071309219267
	7	0.080612609151
	8	−0.038029936935
	9	−0.016574541631
	10	0.012550998556
	11	0.000429577973
	12	−0.001801640704
	13	0.000353713800
$p=8$	0	0.054415842243
	1	0.312871590914
	2	0.675630736297
	3	0.585354683654
	4	−0.015829105256
	5	−0.284015542962
	6	0.000472484574
	7	0.128747426620
	8	−0.017369301002
	9	−0.04408825393
	10	0.013981027917
	11	0.008746094047
	12	−0.004870352993
	13	−0.000391740373
	14	0.000675449406
	15	−0.000117476784
$p=9$	0	0.038077947364
	1	0.243834674613
	2	0.604823123690
	3	0.657288078051
	4	0.133197385825
	5	−0.293273783279
	6	−0.096840783223
	7	0.148540749338
	8	0.030725681479
	9	−0.067632829061
	10	0.000250947115
	11	0.022361662124
	12	−0.004723204758
	13	−0.004281503682
	14	0.001847646883
	15	0.000230385764
	16	−0.000251963189
	17	0.000039347320
$p=10$	0	0.026670057901
	1	0.188176800078
	2	0.527201188932
	3	0.688459039454
	4	0.281172343661
	5	−0.249846424327
	6	−0.195946274377
	7	0.127369340336
	8	0.093057364604
	9	−0.071394147166
	10	−0.029457536822
	11	0.033212674059
	12	0.003606553567
	13	−0.010733175483
	14	0.001395351747
	15	0.001992405295
	16	−0.000685856695
	17	−0.000116466855
	18	0.000093588670
	19	−0.000013264203

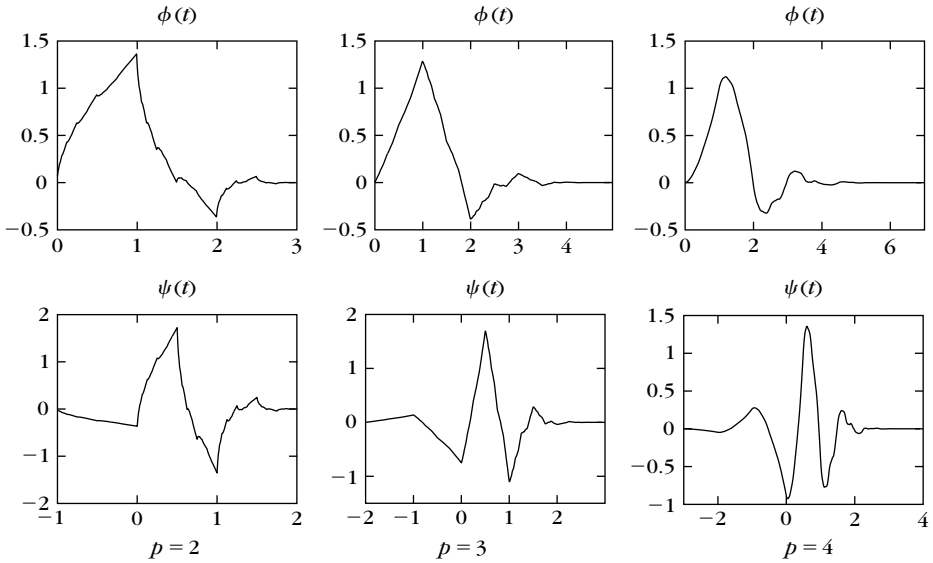

FIGURE 7.10

Daubechies scaling function ϕ and wavelet ψ with p vanishing moments.

only real compactly supported conjugate mirror filter that has a linear phase. The Daubechies *symmlet* filters are obtained by optimizing the choice of the square root $R(e^{-i\omega})$ of $Q(e^{-i\omega})$ to obtain an almost linear phase. The resulting wavelets still have a minimum support $[-p+1, p]$ with p vanishing moments, but they are more symmetric, as illustrated by Figure 7.11 for $p = 8$. The coefficients of the symmlet filters are in WaveLab. Complex conjugate mirror filters with a compact support and a linear phase can be constructed [352], but they produce complex wavelet coefficients that have real and imaginary parts that are redundant when the signal is real.

Coiflets

For an application in numerical analysis, Coifman asked Daubechies [194] to construct a family of wavelets ψ that have p vanishing moments and a minimum-size support, with scaling functions that also satisfy

$$\int_{-\infty}^{+\infty} \phi(t)\, dt = 1 \quad \text{and} \quad \int_{-\infty}^{+\infty} t^k\, \phi(t)\, dt = 0 \quad \text{for } 1 \leq k < p. \tag{7.99}$$

Such scaling functions are useful in establishing precise quadrature formulas. If f is $\mathbf{C}^k$ in the neighborhood of $2^J n$ with $k < p$, then a Taylor expansion of f up to order k shows that

$$2^{-J/2} \langle f, \phi_{J,n} \rangle \approx f(2^J n) + O(2^{(k+1)J}). \tag{7.100}$$

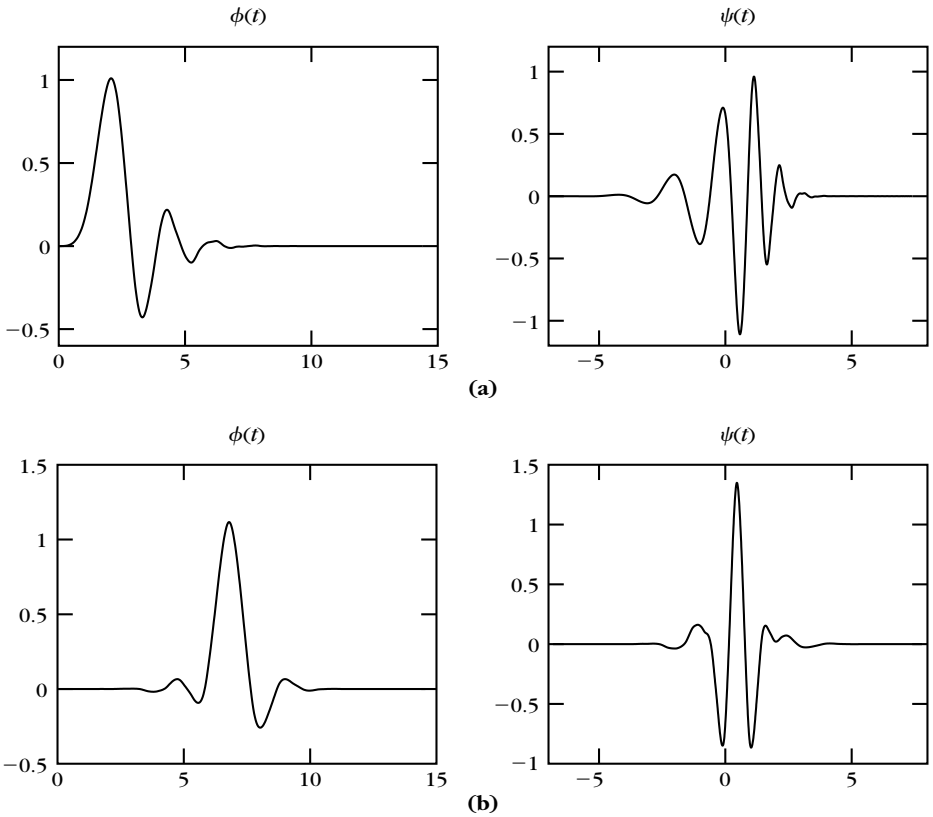

FIGURE 7.11

Daubechies **(a)** and symmlet **(b)** scaling functions and wavelets with $p = 8$ vanishing moments.

Thus, at a fine scale 2^J, the scaling coefficients are closely approximated by the signal samples. The order of approximation increases with p. The supplementary condition (7.99) requires increasing the support of ψ; the resulting coiflet has a support of size $3p - 1$ instead of $2p - 1$ for a Daubechies wavelet. The corresponding conjugate mirror filters are tabulated in WaveLab.

Audio Filters

The first conjugate mirror filters with finite impulse response were constructed in 1986 by Smith and Barnwell [443] in the context of perfect filter bank reconstruction, explained in Section 7.3.2. These filters satisfy the quadrature condition $|\hat{h}(\omega)|^2 + |\hat{h}(\omega + \pi)|^2 = 2$, which is necessary and sufficient for filter bank reconstruction. However, $\hat{h}(0) \neq \sqrt{2}$, so the infinite product of such filters does not yield a wavelet basis of $\mathbf{L^2}(\mathbb{R})$. Instead of imposing any vanishing moments, Smith and Barnwell [443], and later Vaidyanathan and Hoang [470], designed their filters to

reduce the size of the transition band, where $|\hat{h}(\omega)|$ decays from nearly $\sqrt{2}$ to nearly 0 in the neighborhood of $\pm\pi/2$. This constraint is important in optimizing the transform code of audio signals (see Section 10.3.3). However, many cascades of these filters exhibit wild behavior. The Vaidyanathan-Hoang filters are tabulated in WaveLab. Many other classes of conjugate mirror filters with finite impulse response have been constructed [69, 79]. Recursive conjugate mirror filters may also be designed [300] to minimize the size of the transition band for a given number of zeroes at $\omega = \pi$. These filters have a fast but noncausal recursive implementation for signals of finite size.

7.3 WAVELETS AND FILTER BANKS

Decomposition coefficients in a wavelet orthogonal basis are computed with a fast algorithm that cascades discrete convolutions with h and g, and subsamples the output. Section 7.3.1 derives this result from the embedded structure of multiresolution approximations. A direct filter bank analysis is performed in Section 7.3.2, which gives more general perfect reconstruction conditions on the filters. Section 7.3.3 shows that perfect reconstruction filter banks decompose signals in a basis of $\ell^2(\mathbb{Z})$. This basis is orthogonal for conjugate mirror filters.

7.3.1 Fast Orthogonal Wavelet Transform

We describe a fast filter bank algorithm that computes the orthogonal wavelet coefficients of a signal measured at a finite resolution. A fast wavelet transform decomposes successively each approximation $P_{\mathbf{V}_j} f$ into a coarser approximation $P_{\mathbf{V}_{j+1}} f$, plus the wavelet coefficients carried by $P_{\mathbf{W}_{j+1}} f$. In the other direction, the reconstruction from wavelet coefficients recovers each $P_{\mathbf{V}_j} f$ from $P_{\mathbf{V}_{j+1}} f$ and $P_{\mathbf{W}_{j+1}} f$.

Since $\{\phi_{j,n}\}_{n\in\mathbb{Z}}$ and $\{\psi_{j,n}\}_{n\in\mathbb{Z}}$ are orthonormal bases of $\mathbf{V}_j$ and $\mathbf{W}_j$, the projection in these spaces is characterized by

$$a_j[n] = \langle f, \phi_{j,n}\rangle \quad \text{and} \quad d_j[n] = \langle f, \psi_{j,n}\rangle.$$

Theorem 7.10 [360, 361] shows that these coefficients are calculated with a cascade of discrete convolutions and subsamplings. We denote $\bar{x}[n] = x[-n]$ and

$$\check{x}[n] = \begin{cases} x[p] & \text{if } n = 2p \\ 0 & \text{if } n = 2p+1. \end{cases} \tag{7.101}$$

Theorem 7.10: *Mallat.* At the decomposition,

$$a_{j+1}[p] = \sum_{n=-\infty}^{+\infty} h[n-2p]\, a_j[n] = a_j \star \bar{h}[2p], \tag{7.102}$$

$$d_{j+1}[p] = \sum_{n=-\infty}^{+\infty} g[n-2p]\, a_j[n] = a_j \star \bar{g}[2p]. \tag{7.103}$$

At the reconstruction,

$$\begin{aligned} a_j[p] &= \sum_{n=-\infty}^{+\infty} h[p-2n]\, a_{j+1}[n] + \sum_{n=-\infty}^{+\infty} g[p-2n]\, d_{j+1}[n] \\ &= \check{a}_{j+1} \star h[p] + \check{d}_{j+1} \star g[p]. \end{aligned} \tag{7.104}$$

Proof of (7.102). Any $\phi_{j+1,p} \in \mathbf{V}_{j+1} \subset \mathbf{V}_j$ can be decomposed in the orthonormal basis $\{\phi_{j,n}\}_{n\in\mathbb{Z}}$ of $\mathbf{V}_j$:

$$\phi_{j+1,p} = \sum_{n=-\infty}^{+\infty} \langle \phi_{j+1,p}, \phi_{j,n} \rangle\, \phi_{j,n}. \tag{7.105}$$

With the change of variable $t' = 2^{-j}t - 2p$, we obtain

$$\begin{aligned} \langle \phi_{j+1,p}, \phi_{j,n} \rangle &= \int_{-\infty}^{+\infty} \frac{1}{\sqrt{2^{j+1}}} \phi\Big(\frac{t-2^{j+1}p}{2^{j+1}}\Big) \frac{1}{\sqrt{2^j}} \phi^*\Big(\frac{t-2^j n}{2^j}\Big)\, dt \\ &= \int_{-\infty}^{+\infty} \frac{1}{\sqrt{2}} \phi\Big(\frac{t}{2}\Big) \phi^*(t-n+2p)\, dt \\ &= \Big\langle \frac{1}{\sqrt{2}} \phi\Big(\frac{t}{2}\Big), \phi(t-n+2p) \Big\rangle = h[n-2p]. \end{aligned} \tag{7.106}$$

Thus, (7.105) implies that

$$\phi_{j+1,p} = \sum_{n=-\infty}^{+\infty} h[n-2p]\, \phi_{j,n}. \tag{7.107}$$

Computing the inner product of f with the vectors on each side of this equality yields (7.102).

Proof of (7.103). Since $\psi_{j+1,p} \in \mathbf{W}_{j+1} \subset \mathbf{V}_j$, it can be decomposed as

$$\psi_{j+1,p} = \sum_{n=-\infty}^{+\infty} \langle \psi_{j+1,p}, \phi_{j,n} \rangle\, \phi_{j,n}.$$

As in (7.106), the change of variable $t' = 2^{-j}t - 2p$ proves that

$$\langle \psi_{j+1,p}, \phi_{j,n} \rangle = \Big\langle \frac{1}{\sqrt{2}} \psi\Big(\frac{t}{2}\Big), \phi(t-n+2p) \Big\rangle = g[n-2p], \tag{7.108}$$

and thus,

$$\psi_{j+1,p} = \sum_{n=-\infty}^{+\infty} g[n-2p]\, \phi_{j,n}. \tag{7.109}$$

Taking the inner product with f on each side gives (7.103).

Proof of (7.104). Since $\mathbf{W}_{j+1}$ is the orthogonal complement of $\mathbf{V}_{j+1}$ in $\mathbf{V}_j$, the union of the two bases $\{\psi_{j+1,n}\}_{n\in\mathbb{Z}}$ and $\{\phi_{j+1,n}\}_{n\in\mathbb{Z}}$ is an orthonormal basis of $\mathbf{V}_j$. Thus, any $\phi_{j,p}$ can be decomposed in this basis:

$$\phi_{j,p} = \sum_{n=-\infty}^{+\infty} \langle \phi_{j,p}, \phi_{j+1,n} \rangle \, \phi_{j+1,n} + \sum_{n=-\infty}^{+\infty} \langle \phi_{j,p}, \psi_{j+1,n} \rangle \, \psi_{j+1,n}.$$

Inserting (7.106) and (7.108) yields

$$\phi_{j,p} = \sum_{n=-\infty}^{+\infty} h[p-2n] \, \phi_{j+1,n} + \sum_{n=-\infty}^{+\infty} g[p-2n] \, \psi_{j+1,n}.$$

Taking the inner product with f on both sides of this equality gives (7.104). ■

Theorem 7.10 proves that a_{j+1} and d_{j+1} are computed by taking every other sample of the convolution of a_j with $\bar{h}$ and $\bar{g}$, respectively, as illustrated by Figure 7.12. The filter $\bar{h}$ removes the higher frequencies of the inner product sequence a_j, whereas $\bar{g}$ is a high-pass filter that collects the remaining highest frequencies. The reconstruction (7.104) is an interpolation that inserts zeroes to expand a_{j+1} and d_{j+1} and filters these signals, as shown in Figure 7.12.

An *orthogonal wavelet representation* of $a_L = \langle f, \phi_{L,n} \rangle$ is composed of wavelet coefficients of f at scales $2^L < 2^j \leqslant 2^J$, plus the remaining approximation at the largest scale 2^J:

$$\left[\{d_j\}_{L<j\leqslant J}, \; a_J \right]. \tag{7.110}$$

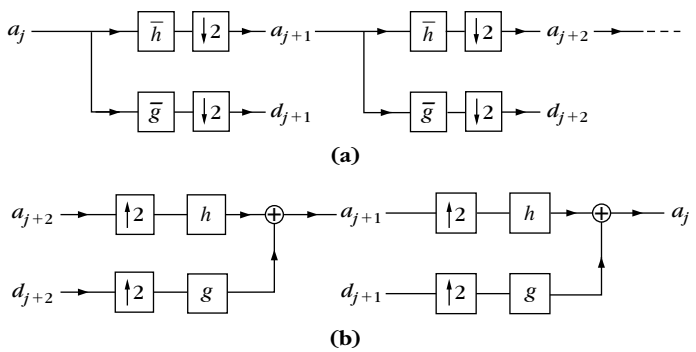

FIGURE 7.12

(a) A fast wavelet transform is computed with a cascade of filterings with $\bar{h}$ and $\bar{g}$ followed by a factor 2 subsampling. **(b)** A fast inverse wavelet transform reconstructs progressively each a_j by inserting zeroes between samples of a_{j+1} and d_{j+1}, filtering and adding the output.

It is computed from a_L by iterating (7.102) and (7.103) for $L \leqslant j < J$. Figure 7.7 gives a numerical example computed with the cubic spline filter of Table 7.1. The original signal a_L is recovered from this wavelet representation by iterating the reconstruction (7.104) for $J > j \geqslant L$.

Initialization

Most often the discrete input signal $b[n]$ is obtained by a finite-resolution device that averages and samples an analog input signal. For example, a CCD camera filters the light intensity by the optics and each photoreceptor averages the input light over its support. Thus, a pixel value measures average light intensity. If the sampling distance is N^{-1}, to define and compute the wavelet coefficients, we need to associate to $b[n]$ a function $f(t) \in \mathbf{V}_L$ approximated at the scale $2^L = N^{-1}$, and compute $a_L[n] = \langle f, \phi_{L,n} \rangle$. Exercise 7.6 explains how to compute $a_L[n] = \langle f, \phi_{L,n} \rangle$ so that $b[n] = f(N^{-1}n)$.

A simpler and faster approach considers

$$f(t) = \sum_{n=-\infty}^{+\infty} b[n]\, \phi\left(\frac{t - 2^L n}{2^L}\right) \in \mathbf{V}_L.$$

Since $\{\phi_{L,n}(t) = 2^{-L/2}\, \phi(2^{-L}t - n)\}_{n \in \mathbb{Z}}$ is orthonormal and $2^L = N^{-1}$,

$$b[n] = N^{1/2}\, \langle f, \phi_{L,n} \rangle = N^{1/2}\, a_L[n].$$

But $\hat{\phi}(0) = \int_{-\infty}^{\infty} \phi(t)\, dt = 1$, so

$$N^{1/2}\, a_L[n] = \int_{-\infty}^{+\infty} f(t)\, \frac{1}{N^{-1}}\, \phi\left(\frac{t - N^{-1}n}{N^{-1}}\right) dt$$

is a weighted average of f in the neighborhood of $N^{-1}n$ over a domain proportional to N^{-1}. Thus, if f is regular,

$$b[n] = N^{1/2}\, a_L[n] \approx f(N^{-1}n). \tag{7.111}$$

If ψ is a coiflet and $f(t)$ is regular in the neighborhood of $N^{-1}n$, then (7.100) shows that $N^{-1/2}\, a_L[n]$ is a high-order approximation of $f(N^{-1}n)$.

Finite Signals

Let us consider a signal f with a support in $[0, 1]$ and that is approximated with a uniform sampling at intervals N^{-1}. The resulting approximation a_L has $N = 2^{-L}$ samples. This is the case in Figure 7.7 with $N = 1024$. Computing the convolutions with $\bar{h}$ and $\bar{g}$ at abscissa close to 0 or close to N requires knowing the values of $a_L[n]$ beyond the boundaries $n = 0$ and $n = N - 1$. These boundary problems may be solved with one of the three approaches described in Section 7.5.

Section 7.5.1 explains the simplest algorithm, which periodizes a_L. The convolutions in Theorem 7.10 are replaced by circular convolutions. This is equivalent to decomposing f in a periodic wavelet basis of $\mathbf{L}^2[0, 1]$. This algorithm has the disadvantage of creating large wavelet coefficients at the borders.

If ψ is symmetric or antisymmetric, we can use a folding procedure described in Section 7.5.2, which creates smaller wavelet coefficients at the border. It decomposes f in a folded wavelet basis of $\mathbf{L}^2[0, 1]$. However, we mentioned in Section 7.2.3 that Haar is the only symmetric wavelet with a compact support. Higher-order spline wavelets have a symmetry, but h must be truncated in numerical calculations.

The most efficient boundary treatment is described in Section 7.5.3, but the implementation is more complicated. Boundary wavelets that keep their vanishing moments are designed to avoid creating large-amplitude coefficients when f is regular. The fast algorithm is implemented with special boundary filters and requires the same number of calculations as the two other methods.

Complexity

Suppose that h and g have K nonzero coefficients. Let a_L be a signal of size $N = 2^{-L}$. With appropriate boundary calculations, each a_j and d_j has 2^{-j} samples. Equations (7.102) and (7.103) compute a_{j+1} and d_{j+1} from a_j with $2^{-j}K$ additions and multiplications. Therefore, the wavelet representation (7.110) is calculated with at most $2KN$ additions and multiplications. The reconstruction (7.104) of a_j from a_{j+1} and d_{j+1} is also obtained with $2^{-j}K$ additions and multiplications. The original signal a_L is also recovered from the wavelet representation with at most $2KN$ additions and multiplications.

Wavelet Graphs

The graphs of ϕ and ψ are computed numerically with the inverse wavelet transform. If $f = \phi$, then $a_0[n] = \delta[n]$ and $d_j[n] = 0$ for all $L < j \leq 0$. The inverse wavelet transform computes a_L and (7.111) shows that

$$N^{1/2}\, a_L[n] \approx \phi(N^{-1}n).$$

If ϕ is regular and N is large enough, we recover a precise approximation of the graph of ϕ from a_L.

Similarly, if $f = \psi$, then $a_0[n] = 0$, $d_0[n] = \delta[n]$, and $d_j[n] = 0$ for $L < j < 0$. Then $a_L[n]$ is calculated with the inverse wavelet transform and $N^{1/2}\, a_L[n] \approx \psi(N^{-1}n)$. The Daubechies wavelets and scaling functions in Figure 7.10 are calculated with this procedure.

7.3.2 Perfect Reconstruction Filter Banks

The fast discrete wavelet transform decomposes signals into low-pass and high-pass components subsampled by 2; the inverse transform performs the reconstruction. The study of such classical multirate filter banks became a major signal-processing topic in 1976, when Croisier, Esteban, and Galand [189] discovered that it is possible to perform such decompositions and reconstructions with *quadrature mirror filters* (Exercise 7.7). However, besides the simple Haar filter, a quadrature mirror filter cannot have a finite impulse response. In 1984, Smith and Barnwell [444] and Mintzer [376] found necessary and sufficient conditions for obtaining perfect

reconstruction orthogonal filters with a finite impulse response that they called *conjugate mirror filters*. The theory was completed by the biorthogonal equations of Vetterli [471, 472] and the general paraunitary matrix theory of Vaidyanathan [469]. We follow this digital signal-processing approach, which gives a simple understanding of conjugate mirror filter conditions. More complete presentations of filter bank properties can be found in [1, 2, 63, 68, 69].

Filter Bank

A two-channel multirate filter bank convolves a signal a_0 with a low-pass filter $\bar{h}[n] = h[-n]$ and a high-pass filter $\bar{g}[n] = g[-n]$ and subsamples by 2 the output:

$$a_1[n] = a_0 \star \bar{h}[2n] \quad \text{and} \quad d_1[n] = a_0 \star \bar{g}[2n]. \tag{7.112}$$

A reconstructed signal $\tilde{a}_0$ is obtained by filtering the zero expanded signals with a dual low-pass filter $\tilde{h}$ and a dual high-pass filter $\tilde{g}$, as shown in Figure 7.13. With the zero insertion notation (7.101) it yields

$$\tilde{a}_0[n] = \check{a}_1 \star \tilde{h}[n] + \check{d}_1 \star \tilde{g}[n]. \tag{7.113}$$

We study necessary and sufficient conditions on $h, g, \tilde{h}$, and $\tilde{g}$ to guarantee a perfect reconstruction $\tilde{a}_0 = a_0$.

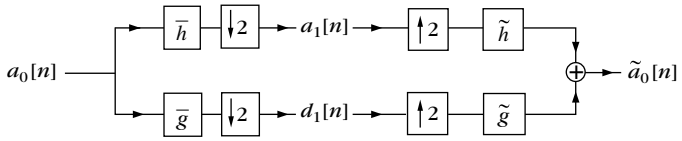

FIGURE 7.13

The input signal is filtered by a low-pass and a high-pass filter and subsampled. The reconstruction is performed by inserting zeroes and filtering with dual filters $\tilde{h}$ and $\tilde{g}$.

Subsampling and Zero Interpolation

Subsamplings and expansions with zero insertions have simple expressions in the Fourier domain. Since $\hat{x}(\omega) = \sum_{n=-\infty}^{+\infty} x[n]\, e^{-in\omega}$, the Fourier series of the subsampled signal $y[n] = x[2n]$ can be written as

$$\hat{y}(2\omega) = \sum_{n=-\infty}^{+\infty} x[2n]\, e^{-i2n\omega} = \frac{1}{2}\left(\hat{x}(\omega) + \hat{x}(\omega+\pi)\right). \tag{7.114}$$

The component $\hat{x}(\omega+\pi)$ creates a frequency folding. This *aliasing* must be canceled at the reconstruction.

The insertion of zeros defines

$$y[n] = \check{x}[n] = \begin{cases} x[p] & \text{if } n = 2p \\ 0 & \text{if } n = 2p+1, \end{cases}$$

that has a Fourier transform

$$\hat{y}(\omega) = \sum_{n=-\infty}^{+\infty} x[n]\, \mathrm{e}^{-i2n\omega} = \hat{x}(2\omega). \tag{7.115}$$

Theorem 7.11 gives Vetterli's [471] biorthogonal conditions, which guarantee that $\tilde{a}_0 = a_0$.

Theorem 7.11: *Vetterli.* The filter bank performs an exact reconstruction for any input signal if and only if

$$\hat{h}^*(\omega+\pi)\,\widehat{\tilde{h}}(\omega) + \hat{g}^*(\omega+\pi)\,\widehat{\tilde{g}}(\omega) = 0, \tag{7.116}$$

and

$$\hat{h}^*(\omega)\,\widehat{\tilde{h}}(\omega) + \hat{g}^*(\omega)\,\widehat{\tilde{g}}(\omega) = 2. \tag{7.117}$$

Proof. We first relate the Fourier transform of a_1 and d_1 to the Fourier transform of a_0. Since h and g are real, the transfer functions of $\bar{h}$ and $\bar{g}$ are, respectively, $\hat{h}(-\omega) = \hat{h}^*(\omega)$ and $\hat{g}(-\omega) = \hat{g}^*(\omega)$. By using (7.114), we derive from the definition (7.112) of a_1 and d_1 that

$$\hat{a}_1(2\omega) = \frac{1}{2}\Big(\hat{a}_0(\omega)\,\hat{h}^*(\omega) + \hat{a}_0(\omega+\pi)\,\hat{h}^*(\omega+\pi)\Big), \tag{7.118}$$

$$\hat{d}_1(2\omega) = \frac{1}{2}\big(\hat{a}_0(\omega)\,\hat{g}^*(\omega) + \hat{a}_0(\omega+\pi)\,\hat{g}^*(\omega+\pi)\big). \tag{7.119}$$

The expression (7.113) of $\tilde{a}_0$ and the zero insertion property (7.115) also imply

$$\widehat{\tilde{a}}_0(\omega) = \hat{a}_1(2\omega)\,\widehat{\tilde{h}}(\omega) + \hat{d}_1(2\omega)\,\widehat{\tilde{g}}(\omega). \tag{7.120}$$

Thus,

$$\begin{aligned}\widehat{\tilde{a}}_0(\omega) = {} & \frac{1}{2}\left(\hat{h}^*(\omega)\,\widehat{\tilde{h}}(\omega) + \hat{g}^*(\omega)\,\widehat{\tilde{g}}(\omega)\right)\hat{a}_0(\omega) \\ & + \frac{1}{2}\left(\hat{h}^*(\omega+\pi)\,\widehat{\tilde{h}}(\omega) + \hat{g}^*(\omega+\pi)\,\widehat{\tilde{g}}(\omega)\right)\hat{a}_0(\omega+\pi).\end{aligned}$$

To obtain $a_0 = \tilde{a}_0$ for all a_0, the filters must cancel the aliasing term $\hat{a}_0(\omega+\pi)$ and guarantee a unit gain for $\hat{a}_0(\omega)$, which proves equations (7.116) and (7.117). ■

Theorem 7.11 proves that the reconstruction filters $\tilde{h}$ and $\tilde{g}$ are entirely specified by the decomposition filters h and g. In matrix form, it can be rewritten

$$\begin{pmatrix} \hat{h}(\omega) & \hat{g}(\omega) \\ \hat{h}(\omega+\pi) & \hat{g}(\omega+\pi) \end{pmatrix} \times \begin{pmatrix} \widehat{\tilde{h}}^*(\omega) \\ \widehat{\tilde{g}}^*(\omega) \end{pmatrix} = \begin{pmatrix} 2 \\ 0 \end{pmatrix}. \tag{7.121}$$

The inversion of this 2×2 matrix yields

$$\begin{pmatrix} \widehat{\tilde{h}}^*(\omega) \\ \widehat{\tilde{g}}^*(\omega) \end{pmatrix} = \frac{2}{\Delta(\omega)} \begin{pmatrix} \hat{g}(\omega+\pi) \\ -\hat{h}(\omega+\pi) \end{pmatrix}, \tag{7.122}$$

where $\Delta(\omega)$ is the determinant

$$\Delta(\omega) = \hat{h}(\omega)\,\hat{g}(\omega+\pi) - \hat{h}(\omega+\pi)\,\hat{g}(\omega). \tag{7.123}$$

The reconstruction filters are stable only if the determinant does not vanish for all $\omega \in [-\pi, \pi]$. Vaidyanathan [469] has extended this result to multirate filter banks with an arbitrary number M of channels by showing that the resulting matrices of filters satisfy paraunitary properties [68].

Finite Impulse Response

When all filters have a finite impulse response, the determinant $\Delta(\omega)$ can be evaluated. This yields simpler relations between the decomposition and reconstruction filters.

Theorem 7.12. Perfect reconstruction filters satisfy

$$\hat{h}^*(\omega)\,\widehat{\tilde{h}}(\omega) + \hat{h}^*(\omega+\pi)\,\widehat{\tilde{h}}(\omega+\pi) = 2. \tag{7.124}$$

For finite impulse-response filters, there exist $a \in \mathbb{R}$ and $l \in \mathbb{Z}$ such that

$$\hat{g}(\omega) = a\,\mathrm{e}^{-i(2l+1)\omega}\,\widehat{\tilde{h}}^*(\omega+\pi) \quad \text{and} \quad \widehat{\tilde{g}}(\omega) = a^{-1}\,\mathrm{e}^{-i(2l+1)\omega}\,\hat{h}^*(\omega+\pi). \tag{7.125}$$

Proof. Equation (7.122) proves that

$$\widehat{\tilde{h}}^*(\omega) = \frac{2}{\Delta(\omega)}\,\hat{g}(\omega+\pi) \quad \text{and} \quad \widehat{\tilde{g}}^*(\omega) = \frac{-2}{\Delta(\omega)}\,\hat{h}(\omega+\pi). \tag{7.126}$$

Thus,

$$\hat{g}(\omega)\,\widehat{\tilde{g}}^*(\omega) = -\frac{\Delta(\omega+\pi)}{\Delta(\omega)}\,\widehat{\tilde{h}}^*(\omega+\pi)\,\hat{h}(\omega+\pi). \tag{7.127}$$

The definition (7.123) implies that $\Delta(\omega+\pi) = -\Delta(\omega)$. Inserting (7.127) in (7.117) yields (7.124).

The Fourier transform of finite impulse-response filters is a finite series in $\exp(\pm in\omega)$. Therefore, the determinant $\Delta(\omega)$ defined by (7.123) is a finite series. Moreover, (7.126) proves that $\Delta^{-1}(\omega)$ must also be a finite series. A finite series in $\exp(\pm in\omega)$ that has an inverse that is also a finite series must have a single term. Since $\Delta(\omega) = -\Delta(\omega+\pi)$ the exponent n must be odd. This proves that there exist $l \in \mathbb{Z}$ and $a \in \mathbb{R}$ such that

$$\Delta(\omega) = -2\,a\,\exp[i(2l+1)\omega]. \tag{7.128}$$

Inserting this expression in (7.126) yields (7.125). ■

The factor a is a gain that is inverse for the decomposition and reconstruction filters and l is a reverse shift. We generally set $a = 1$ and $l = 0$. In the time domain (7.125) can then be rewritten as

$$g[n] = (-1)^{1-n}\,\tilde{h}[1-n] \quad \text{and} \quad \tilde{g}[n] = (-1)^{1-n}\,h[1-n]. \tag{7.129}$$

The two pairs of filters (h, g) and $(\tilde{h}, \tilde{g})$ play a symmetric role and can be inverted.

Conjugate Mirror Filters

If we impose that the decomposition filter h is equal to the reconstruction filter $\tilde{h}$, then (7.124) is the condition of Smith and Barnwell [444] and Mintzer [376] that defines conjugate mirror filters:

$$|\hat{h}(\omega)|^2 + |\hat{h}(\omega+\pi)|^2 = 2. \tag{7.130}$$

It is identical to the filter condition (7.29) that is required in order to synthesize orthogonal wavelets. Section 7.3.3 proves that it is also equivalent to discrete orthogonality properties.

7.3.3 Biorthogonal Bases of $\ell^2(\mathbb{Z})$

The decomposition of a discrete signal in a multirate filter bank is interpreted as an expansion in a basis of $\ell^2(\mathbb{Z})$. Observe first that the low-pass and high-pass signals of a filter bank computed with (7.112) can be rewritten as inner products in $\ell^2(\mathbb{Z})$:

$$a_1[l] = \sum_{n=-\infty}^{+\infty} a_0[n]\, h[n-2l] = \langle a_0[n], h[n-2l]\rangle, \tag{7.131}$$

$$d_1[l] = \sum_{n=-\infty}^{+\infty} a_0[n]\, g[n-2l] = \langle a_0[n], g[n-2l]\rangle. \tag{7.132}$$

The signal recovered by the reconstructing filters is

$$a_0[n] = \sum_{l=-\infty}^{+\infty} a_1[l]\, \tilde{h}[n-2l] + \sum_{l=-\infty}^{+\infty} d_1[l]\, \tilde{g}[n-2l]. \tag{7.133}$$

Inserting (7.131) and (7.132) yields

$$a_0[n] = \sum_{l=-\infty}^{+\infty} \langle f[k], h[k-2l]\rangle\, \tilde{h}[n-2l] + \sum_{l=-\infty}^{+\infty} \langle f[k], g[k-2l]\rangle\, \tilde{g}[n-2l]. \tag{7.134}$$

We recognize the decomposition of a_0 over dual families of vectors $\{\tilde{h}[n-2l], \tilde{g}[n-2l]\}_{l\in\mathbb{Z}}$ and $\{h[n-2l], g[n-2l]\}_{l\in\mathbb{Z}}$. Theorem 7.13 proves that these two families are biorthogonal.

Theorem 7.13. If h, g, $\tilde{h}$, and $\tilde{g}$ are perfect reconstruction filters, and their Fourier transforms are bounded, then $\{\tilde{h}[n-2l], \tilde{g}[n-2l]\}_{l\in\mathbb{Z}}$ and $\{h[n-2l], g[n-2l]\}_{l\in\mathbb{Z}}$ are biorthogonal Riesz bases of $\ell^2(\mathbb{Z})$.

Proof. To prove that these families are biorthogonal we must show that for all $n \in \mathbb{Z}$

$$\langle \tilde{h}[n], h[n-2l]\rangle = \delta[l] \tag{7.135}$$

$$\langle \tilde{g}[n], g[n-2l]\rangle = \delta[l] \tag{7.136}$$

and

$$\langle \tilde{h}[n], g[n-2l]\rangle = \langle \tilde{g}[n], h[n-2l]\rangle = 0. \tag{7.137}$$

For perfect reconstruction filters, (7.124) proves that

$$\frac{1}{2}\left(\hat{h}^*(\omega)\,\widehat{\tilde{h}}(\omega)+\hat{h}^*(\omega+\pi)\,\widehat{\tilde{h}}(\omega+\pi)\right)=1.$$

In the time domain, this equation becomes

$$\bar{h}\star\tilde{h}[2l]=\sum_{k=-\infty}^{+\infty}\tilde{h}[n]\,\bar{h}[n-2l]=\delta[l], \tag{7.138}$$

which verifies (7.135). The same proof as for (7.124) shows that

$$\frac{1}{2}\left(\hat{g}^*(\omega)\,\widehat{\tilde{g}}(\omega)+\hat{g}^*(\omega+\pi)\,\widehat{\tilde{g}}(\omega+\pi)\right)=1.$$

In the time domain, this equation yields (7.136). It also follows from (7.122) that

$$\frac{1}{2}\left(\hat{g}^*(\omega)\,\widehat{\tilde{h}}(\omega)+\hat{g}^*(\omega+\pi)\,\widehat{\tilde{h}}(\omega+\pi)\right)=0,$$

and

$$\frac{1}{2}\left(\hat{h}^*(\omega)\,\widehat{\tilde{g}}(\omega)+\hat{h}^*(\omega+\pi)\,\widehat{\tilde{g}}(\omega+\pi)\right)=0.$$

The inverse Fourier transforms of these two equations yield (7.137).

To finish the proof, one must show the existence of Riesz bounds. The reader can verify that this is a consequence of the fact that the Fourier transform of each filter is bounded. ■

Orthogonal Bases

A Riesz basis is orthonormal if the dual basis is the same as the original basis. For filter banks this means that $h=\tilde{h}$ and $g=\tilde{g}$. The filter h is then a conjugate mirror filter

$$|\hat{h}(\omega)|^2+|\hat{h}(\omega+\pi)|^2=2. \tag{7.139}$$

The resulting family $\{h[n-2l],\,g[n-2l]\}_{l\in\mathbb{Z}}$ is an orthogonal basis of $\ell^2(\mathbb{Z})$.

Discrete Wavelet Bases

The construction of conjugate mirror filters is simpler than the construction of orthogonal wavelet bases of $\mathbf{L}^2(\mathbb{R})$. Why then should we bother with continuous time models of wavelets, since in any case, all computations are discrete and rely on conjugate mirror filters? The reason is that conjugate mirror filters are most often used in filter banks that cascade several levels of filterings and subsamplings. Thus, it is necessary to understand the behavior of such a cascade [407]. In a wavelet filter bank tree, the output of the low-pass filter $\bar{h}$ is subdecomposed, whereas the output of the high-pass filter $\bar{g}$ is not; this is illustrated in Figure 7.12. Suppose that the sampling distance of the original discrete signal is N^{-1}. We denote $a_L[n]$ for this discrete signal, with $2^L=N^{-1}$. At the depth $j-L\geqslant 0$ of this filter bank tree, the low-pass signal a_j and high-pass signal d_j can be written as

$$a_j[l]=a_L\star\bar{\phi}_j[2^{j-L}l]=\langle a_L[n],\,\phi_j[n-2^{j-L}l]\rangle$$

and

$$d_j[l] = a_L \star \bar{\psi}_j[2^{j-L}l] = \langle a_L[n], \psi_j[n - 2^{j-L}l] \rangle.$$

The Fourier transforms of these equivalent filters are

$$\hat{\phi}_j(\omega) = \prod_{p=0}^{j-L-1} \hat{h}(2^p\omega) \quad \text{and} \quad \hat{\psi}_j(\omega) = \hat{g}(2^{j-L-1}\omega) \prod_{p=0}^{j-L-2} \hat{h}(2^p\omega). \tag{7.140}$$

A filter bank tree of depth $J - L \geqslant 0$ decomposes a_L over the family of vectors

$$\left[\left\{ \phi_J[n - 2^{J-L}l] \right\}_{l \in \mathbb{Z}}, \quad \left\{ \psi_j[n - 2^{j-L}l] \right\}_{L < j \leqslant J,\, l \in \mathbb{Z}} \right]. \tag{7.141}$$

For conjugate mirror filters, one can verify that this family is an orthonormal basis of $\ell^2(\mathbb{Z})$. These discrete vectors are close to a uniform sampling of the continuous time-scaling functions $\phi_j(t) = 2^{-j/2}\phi(2^{-j}t)$ and wavelets $\psi_j(t) = 2^{-j/2}\phi(2^{-j}t)$. When the number $L - j$ of successive convolutions increases, one can verify that $\phi_j[n]$ and $\psi_j[n]$ converge, respectively, to $N^{-1/2}\,\phi_j(N^{-1}n)$ and $N^{-1/2}\,\psi_j(N^{-1}n)$.

The factor $N^{-1/2}$ normalizes the $\ell^2(\mathbb{Z})$ norm of these sampled functions. If $L - j = 4$, then $\phi_j[n]$ and $\psi_j[n]$ are already very close to these limit values. Thus, the impulse responses $\phi_j[n]$ and $\psi_j[n]$ of the filter bank are much closer to continuous time-scaling functions and wavelets than they are to the original conjugate mirror filters h and g. This explains why wavelets provide appropriate models for understanding the applications of these filter banks. Chapter 8 relates more general filter banks to wavelet packet bases.

If the decomposition and reconstruction filters of the filter bank are different, the resulting basis (7.141) is nonorthogonal. The stability of this discrete wavelet basis does not degrade when the depth $J - L$ of the filter bank increases. The next section shows that the corresponding continuous time wavelet $\psi(t)$ generates a Riesz basis of $\mathbf{L^2}(\mathbb{R})$.

7.4 BIORTHOGONAL WAVELET BASES

The stability and completeness properties of biorthogonal wavelet bases are described for perfect reconstruction filters h and $\tilde{h}$ having a finite impulse response. The design of linear phase wavelets with compact support is explained in Section 7.4.2.

7.4.1 Construction of Biorthogonal Wavelet Bases

An infinite cascade of perfect reconstruction filters (h, g) and $(\tilde{h}, \tilde{g})$ yields two scaling functions and wavelets having a Fourier transform that satisfies

$$\hat{\phi}(2\omega) = \frac{1}{\sqrt{2}}\,\hat{h}(\omega)\,\hat{\phi}(\omega), \quad \widehat{\tilde{\phi}}(2\omega) = \frac{1}{\sqrt{2}}\,\widehat{\tilde{h}}(\omega)\,\widehat{\tilde{\phi}}(\omega), \tag{7.142}$$

$$\hat{\psi}(2\omega) = \frac{1}{\sqrt{2}}\,\hat{g}(\omega)\,\hat{\phi}(\omega), \quad \widehat{\tilde{\psi}}(2\omega) = \frac{1}{\sqrt{2}}\,\widehat{\tilde{g}}(\omega)\,\widehat{\tilde{\phi}}(\omega). \tag{7.143}$$

In the time domain, these relations become

$$\phi(t) = \sqrt{2} \sum_{n=-\infty}^{+\infty} h[n]\, \phi(2t-n), \quad \tilde{\phi}(t) = \sqrt{2} \sum_{n=-\infty}^{+\infty} \tilde{h}[n]\, \tilde{\phi}(2t-n) \tag{7.144}$$

$$\psi(t) = \sqrt{2} \sum_{n=-\infty}^{+\infty} g[n]\, \phi(2t-n), \quad \tilde{\psi}(t) = \sqrt{2} \sum_{n=-\infty}^{+\infty} \tilde{g}[n]\, \tilde{\phi}(2t-n). \tag{7.145}$$

The perfect reconstruction conditions are given by Theorem 7.12. If we normalize the gain and shift to $a = 1$ and $l = 0$, the filters must satisfy

$$\hat{h}^*(\omega)\, \widehat{\tilde{h}}(\omega) + \hat{h}^*(\omega+\pi)\, \widehat{\tilde{h}}(\omega+\pi) = 2, \tag{7.146}$$

and

$$\hat{g}(\omega) = \mathrm{e}^{-i\omega}\, \widehat{\tilde{h}}^*(\omega+\pi), \ \widehat{\tilde{g}}(\omega) = \mathrm{e}^{-i\omega}\, \hat{h}^*(\omega+\pi). \tag{7.147}$$

Wavelets should have a zero average, which means that $\hat{\psi}(0) = \widehat{\tilde{\psi}}(0) = 0$. This is obtained by setting $\hat{g}(0) = \widehat{\tilde{g}}(0) = 0$ and thus $\hat{h}(\pi) = \widehat{\tilde{h}}(\pi) = 0$. The perfect reconstruction condition (7.146) implies that $\hat{h}^*(0)\, \widehat{\tilde{h}}(0) = 2$. Since both filters are defined up to multiplicative constants equal to λ and λ^{-1}, respectively, we adjust λ so that $\hat{h}(0) = \widehat{\tilde{h}}(0) = \sqrt{2}$.

In the following, we also suppose that h and $\tilde{h}$ are finite impulse-response filters. One can then prove [19] that

$$\hat{\phi}(\omega) = \prod_{p=1}^{+\infty} \frac{\hat{h}(2^{-p}\omega)}{\sqrt{2}} \quad \text{and} \quad \widehat{\tilde{\phi}}(\omega) = \prod_{p=1}^{+\infty} \frac{\widehat{\tilde{h}}(2^{-p}\omega)}{\sqrt{2}} \tag{7.148}$$

are the Fourier transforms of distributions of compact support. However, these distributions may exhibit wild behavior and have infinite energy. Some further conditions must be imposed to guarantee that $\hat{\phi}$ and $\widehat{\tilde{\phi}}$ are the Fourier transforms of finite energy functions. Theorem 7.14 gives sufficient conditions on the perfect reconstruction filters for synthesizing biorthogonal wavelet bases of $\mathbf{L^2}(\mathbb{R})$.

Theorem 7.14: *Cohen, Daubechies, Feauveau.* Suppose that there exist strictly positive trigonometric polynomials $P(\mathrm{e}^{i\omega})$ and $\tilde{P}(\mathrm{e}^{i\omega})$ such that

$$\left|\hat{h}\left(\frac{\omega}{2}\right)\right|^2 P(\mathrm{e}^{i\omega/2}) + \left|\hat{h}\left(\frac{\omega}{2}+\pi\right)\right|^2 P(\mathrm{e}^{i(\omega/2+\pi)}) = 2\, P(\mathrm{e}^{i\omega}), \tag{7.149}$$

$$\left|\widehat{\tilde{h}}\left(\frac{\omega}{2}\right)\right|^2 \tilde{P}(\mathrm{e}^{i\omega/2}) + \left|\widehat{\tilde{h}}\left(\frac{\omega}{2}+\pi\right)\right|^2 \tilde{P}(\mathrm{e}^{i(\omega/2+\pi)}) = 2\, \tilde{P}(\mathrm{e}^{i\omega}), \tag{7.150}$$

and that P and $\tilde{P}$ are unique (up to normalization). Suppose that

$$\inf_{\omega\in[-\pi/2,\pi/2]} |\hat{h}(\omega)| > 0, \qquad \inf_{\omega\in[-\pi/2,\pi/2]} |\widehat{\tilde{h}}(\omega)| > 0. \tag{7.151}$$

Then, the functions $\hat{\phi}$ and $\widehat{\tilde{\phi}}$ defined in (7.148) belong to $\mathbf{L^2}(\mathbb{R})$, and ϕ, $\tilde{\phi}$ satisfy biorthogonal relations

$$\langle \phi(t), \tilde{\phi}(t-n) \rangle = \delta[n]. \tag{7.152}$$

The two wavelet families $\{\psi_{j,n}\}_{(j,n)\in\mathbb{Z}^2}$ and $\{\tilde{\psi}_{j,n}\}_{(j,n)\in\mathbb{Z}^2}$ are biorthogonal Riesz bases of $\mathbf{L^2}(\mathbb{R})$.

The proof of this theorem is in [172] and [19]. The hypothesis (7.151) is also imposed by Theorem 7.2, which constructs orthogonal bases of scaling functions. The conditions (7.149) and (7.150) do not appear in the construction of wavelet orthogonal bases because they are always satisfied with $P(e^{i\omega}) = \tilde{P}(e^{i\omega}) = 1$, and one can prove that constants are the only invariant trigonometric polynomials [341].

Biorthogonality means that for any $(j, j', n, n') \in \mathbb{Z}^4$,

$$\langle \psi_{j,n}, \tilde{\psi}_{j',n'} \rangle = \delta[n - n']\,\delta[j - j']. \tag{7.153}$$

Any $f \in \mathbf{L^2}(\mathbb{R})$ has two possible decompositions in these bases:

$$f = \sum_{n,j=-\infty}^{+\infty} \langle f, \psi_{j,n} \rangle\, \tilde{\psi}_{j,n} = \sum_{n,j=-\infty}^{+\infty} \langle f, \tilde{\psi}_{j,n} \rangle\, \psi_{j,n}. \tag{7.154}$$

The Riesz stability implies that there exist $A > 0$ and $B > 0$ such that

$$A\,\|f\|^2 \leqslant \sum_{n,j=-\infty}^{+\infty} |\langle f, \psi_{j,n} \rangle|^2 \leqslant B\,\|f\|^2, \tag{7.155}$$

$$\frac{1}{B}\,\|f\|^2 \leqslant \sum_{n,j=-\infty}^{+\infty} |\langle f, \tilde{\psi}_{j,n} \rangle|^2 \leqslant \frac{1}{A}\,\|f\|^2. \tag{7.156}$$

Multiresolutions

Biorthogonal wavelet bases are related to multiresolution approximations. The family $\{\phi(t-n)\}_{n\in\mathbb{Z}}$ is a Riesz basis of the space $\mathbf{V}_0$ it generates, whereas $\{\tilde{\phi}(t-n)\}_{n\in\mathbb{Z}}$ is a Riesz basis of another space $\tilde{\mathbf{V}}_0$. Let $\mathbf{V}_j$ and $\tilde{\mathbf{V}}_j$ be the spaces defined by

$$f(t) \in \mathbf{V}_j \;\Leftrightarrow\; f(2^j t) \in \mathbf{V}_0,$$
$$f(t) \in \tilde{\mathbf{V}}_j \;\Leftrightarrow\; f(2^j t) \in \tilde{\mathbf{V}}_0.$$

One can verify that $\{\mathbf{V}_j\}_{j\in\mathbb{Z}}$ and $\{\tilde{\mathbf{V}}_j\}_{j\in\mathbb{Z}}$ are two multiresolution approximations of $\mathbf{L^2}(\mathbb{R})$. For any $j \in \mathbb{Z}$, $\{\phi_{j,n}\}_{n\in\mathbb{Z}}$ and $\{\tilde{\phi}_{j,n}\}_{n\in\mathbb{Z}}$ are Riesz bases of $\mathbf{V}_j$ and $\tilde{\mathbf{V}}_j$. The dilated wavelets $\{\psi_{j,n}\}_{n\in\mathbb{Z}}$ and $\{\tilde{\psi}_{j,n}\}_{n\in\mathbb{Z}}$ are bases of two detail spaces $\mathbf{W}_j$ and $\tilde{\mathbf{W}}_j$ such that

$$\mathbf{V}_j \oplus \mathbf{W}_j = \mathbf{V}_{j-1} \quad \text{and} \quad \tilde{\mathbf{V}}_j \oplus \tilde{\mathbf{W}}_j = \tilde{\mathbf{V}}_{j-1}.$$

The biorthogonality of the decomposition and reconstruction wavelets implies that $\mathbf{W}_j$ is not orthogonal to $\mathbf{V}_j$ but is to $\tilde{\mathbf{V}}_j$, whereas $\tilde{\mathbf{W}}_j$ is not orthogonal to $\tilde{\mathbf{V}}_j$ but is to $\mathbf{V}_j$.

Fast Biorthogonal Wavelet Transform

The perfect reconstruction filter bank discussed in Section 7.3.2 implements a fast biorthogonal wavelet transform. For any discrete signal input $b[n]$ sampled

at intervals $N^{-1} = 2^L$, there exists $f \in \mathbf{V}_L$ such that $a_L[n] = \langle f, \phi_{L,n} \rangle = N^{-1/2}\, b[n]$. The wavelet coefficients are computed by successive convolutions with $\bar{h}$ and $\bar{g}$. Let $a_j[n] = \langle f, \phi_{j,n} \rangle$ and $d_j[n] = \langle f, \psi_{j,n} \rangle$. As in Theorem 7.10, one can prove that

$$a_{j+1}[n] = a_j \star \bar{h}[2n], \quad d_{j+1}[n] = a_j \star \bar{g}[2n]. \tag{7.157}$$

The reconstruction is performed with the dual filters $\tilde{h}$ and $\tilde{g}$:

$$a_j[n] = \check{a}_{j+1} \star \tilde{h}[n] + \check{d}_{j+1} \star \tilde{g}[n]. \tag{7.158}$$

If a_L includes N nonzero samples, the biorthogonal wavelet representation $\left[\{d_j\}_{L<j\leqslant J}, a_J\right]$ is calculated with $O(N)$ operations by iterating (7.157) for $L \leqslant j < J$. The reconstruction of a_L by applying (7.158) for $J > j \geqslant L$ requires the same number of operations.

7.4.2 Biorthogonal Wavelet Design

The support size, the number of vanishing moments, the regularity, wavelet ordering, and the symmetry of biorthogonal wavelets is controlled with an appropriate design of h and $\tilde{h}$.

Support

If the perfect reconstruction filters h and $\tilde{h}$ have a finite impulse response, then the corresponding scaling functions and wavelets also have a compact support. As in Section 7.2.1, one can show that if $h[n]$ and $\tilde{h}[n]$ are nonzero, respectively, for $N_1 \leqslant n \leqslant N_2$ and $\tilde{N}_1 \leqslant n \leqslant \tilde{N}_2$, then ϕ and $\tilde{\phi}$ have a support equal to $[N_1, N_2]$ and $[\tilde{N}_1, \tilde{N}_2]$, respectively. Since

$$g[n] = (-1)^{1-n}\, h[1-n] \quad \text{and} \quad \tilde{g}[n] = (-1)^{1-n}\, \tilde{h}[1-n],$$

the supports of ψ and $\tilde{\psi}$ defined in (7.145) are, respectively,

$$\left[\frac{N_1 - \tilde{N}_2 + 1}{2}, \frac{N_2 - \tilde{N}_1 + 1}{2}\right] \quad \text{and} \quad \left[\frac{\tilde{N}_1 - N_2 + 1}{2}, \frac{\tilde{N}_2 - N_1 + 1}{2}\right]. \tag{7.159}$$

Thus, both wavelets have a support of the same size and equal to

$$l = \frac{N_2 - N_1 + \tilde{N}_2 - \tilde{N}_1}{2}. \tag{7.160}$$

Vanishing Moments

The number of vanishing moments of ψ and $\tilde{\psi}$ depends on the number of zeroes at $\omega = \pi$ of $\hat{h}(\omega)$ and $\widehat{\tilde{h}}(\omega)$. Theorem 7.4 proves that ψ has $\tilde{p}$ vanishing moments if the derivatives of its Fourier transform satisfy $\hat{\psi}^{(k)}(0) = 0$ for $k \leqslant \tilde{p}$. Since $\hat{\phi}(0) = 1$, (7.4.1) implies that it is equivalent to impose that $\hat{g}(\omega)$ has a zero of order $\tilde{p}$ at $\omega = 0$. Since $\hat{g}(\omega) = \mathrm{e}^{-i\omega}\, \widehat{\tilde{h}^*}(\omega + \pi)$, this means that $\widehat{\tilde{h}}(\omega)$ has a zero of order $\tilde{p}$ at $\omega = \pi$. Similarly, the number of vanishing moments of $\tilde{\psi}$ is equal to the number p of zeroes of $\hat{h}(\omega)$ at π.

Regularity

Although the regularity of a function is a priori independent of the number of vanishing moments, the smoothness of biorthogonal wavelets is related to their vanishing moments. The regularity of ϕ and ψ is the same because (7.145) shows that ψ is a finite linear expansion of ϕ translated. Tchamitchian's theorem (7.6) gives a sufficient condition for estimating this regularity. If $\hat{h}(\omega)$ has a zero of order p at π, we can perform the factorization

$$\hat{h}(\omega) = \left(\frac{1+e^{-i\omega}}{2}\right)^p \hat{l}(\omega). \tag{7.161}$$

Let $B = \sup_{\omega\in[-\pi,\pi]} |\hat{l}(\omega)|$. Theorem 7.6 proves that ϕ is uniformly Lipschitz α for

$$\alpha < \alpha_0 = p - \log_2 B - 1.$$

Generally, $\log_2 B$ increases more slowly than p. This implies that the regularity of ϕ and ψ increases with p, which is equal to the number of vanishing moments of $\tilde{\psi}$. Similarly, one can show that the regularity of $\tilde{\psi}$ and $\tilde{\phi}$ increases with $\tilde{p}$, which is the number of vanishing moments of ψ. If $\hat{h}$ and $\tilde{h}$ have different numbers of zeroes at π, the properties of ψ and $\tilde{\psi}$ can be very different.

Ordering of Wavelets

Since ψ and $\tilde{\psi}$ might not have the same regularity and number of vanishing moments, the two reconstruction formulas

$$f = \sum_{n,j=-\infty}^{+\infty} \langle f, \psi_{j,n}\rangle \, \tilde{\psi}_{j,n}, \tag{7.162}$$

$$f = \sum_{n,j=-\infty}^{+\infty} \langle f, \tilde{\psi}_{j,n}\rangle \, \psi_{j,n} \tag{7.163}$$

are not equivalent. The decomposition (7.162) is obtained with the filters (h, g), and the reconstruction with $(\tilde{h}, \tilde{g})$. The inverse formula (7.163) corresponds to $(\tilde{h}, \tilde{g})$ at the decomposition and (h, g) at the reconstruction.

To produce small wavelet coefficients in regular regions we must compute the inner products using the wavelet with the maximum number of vanishing moments. The reconstruction is then performed with the other wavelet, which is generally the smoothest one. If errors are added to the wavelet coefficients, for example with a quantization, a smooth wavelet at the reconstruction introduces a smooth error. The number of vanishing moments of ψ is equal to the number $\tilde{p}$ of zeroes at π of $\widehat{\tilde{h}}$. Increasing $\tilde{p}$ also increases the regularity of $\tilde{\psi}$. Thus, it is better to use h at the decomposition and $\tilde{h}$ at the reconstruction if $\hat{h}$ has fewer zeroes at π than $\widehat{\tilde{h}}$.

Symmetry

It is possible to construct smooth biorthogonal wavelets of compact support that are either symmetric or antisymmetric. This is impossible for orthogonal wavelets,

besides the particular case of the Haar basis. Symmetric or antisymmetric wavelets are synthesized with perfect reconstruction filters having a linear phase. If h and $\tilde{h}$ have an odd number of nonzero samples and are symmetric about $n = 0$, the reader can verify that ϕ and $\tilde{\phi}$ are symmetric about $t = 0$, while ψ and $\tilde{\psi}$ are symmetric with respect to a shifted center. If h and $\tilde{h}$ have an even number of nonzero samples and are symmetric about $n = 1/2$, then $\phi(t)$ and $\tilde{\phi}(t)$ are symmetric about $t = 1/2$, while ψ and $\tilde{\psi}$ are antisymmetric with respect to a shifted center. When the wavelets are symmetric or antisymmetric, wavelet bases over finite intervals are constructed with the folding procedure of Section 7.5.2.

7.4.3 Compactly Supported Biorthogonal Wavelets

We study the design of biorthogonal wavelets with a minimum-size support for a specified number of vanishing moments. Symmetric or antisymmetric compactly supported spline biorthogonal wavelet bases are constructed with a technique introduced in [172].

Theorem 7.15: *Cohen, Daubechies, Feauveau.* Biorthogonal wavelets ψ and $\tilde{\psi}$ with, respectively, $\tilde{p}$ and p vanishing moments have a support size of at least $p + \tilde{p} - 1$. CDF biorthogonal wavelets have a minimum support size $p + \tilde{p} - 1$.

Proof. The proof follows the same approach as the proof of Daubechies' theorem (7.7). One can verify that p and $\tilde{p}$ must necessarily have the same parity. We concentrate on filters $h[n]$ and $\tilde{h}[n]$ that have a symmetry with respect to $n = 0$ or $n = 1/2$. The general case proceeds similarly. We can then factor

$$\hat{h}(\omega) = \sqrt{2}\, \exp\left(\frac{-i\varepsilon\omega}{2}\right) \left(\cos\frac{\omega}{2}\right)^{p} L(\cos\omega), \tag{7.164}$$

$$\widehat{\tilde{h}}(\omega) = \sqrt{2}\, \exp\left(\frac{-i\varepsilon\omega}{2}\right) \left(\cos\frac{\omega}{2}\right)^{\tilde{p}} \tilde{L}(\cos\omega), \tag{7.165}$$

with $\varepsilon = 0$ for p and $\tilde{p}$ for even values and $\varepsilon = 1$ for odd values. Let $q = (p + \tilde{p})/2$. The perfect reconstruction condition

$$\hat{h}^*(\omega)\, \widehat{\tilde{h}}(\omega) + \hat{h}^*(\omega + \pi)\, \widehat{\tilde{h}}(\omega + \pi) = 2$$

is imposed by writing

$$L(\cos\omega)\, \tilde{L}(\cos\omega) = P\left(\sin^2\frac{\omega}{2}\right), \tag{7.166}$$

where the polynomial $P(y)$ must satisfy for all $y \in [0, 1]$

$$(1-y)^q P(y) + y^q P(1-y) = 1. \tag{7.167}$$

We saw in (7.96) that the polynomial of minimum degree satisfying this equation is

$$P(y) = \sum_{k=0}^{q-1} \binom{q-1+k}{k} y^k. \tag{7.168}$$

The spectral factorization (7.166) is solved with a root attribution similar to (7.98). The resulting minimum support of ψ and $\tilde{\psi}$ specified by (7.160) is then $p + \tilde{p} - 1$. ■

Spline Biorthogonal Wavelets

Let us choose

$$\hat{h}(\omega) = \sqrt{2}\, \exp\left(\frac{-i\varepsilon\omega}{2}\right)\left(\cos\frac{\omega}{2}\right)^{p} \tag{7.169}$$

with $\varepsilon = 0$ for p even and $\varepsilon = 1$ for p odd. The scaling function computed with (7.148) is then a box spline of degree $p-1$:

$$\hat{\phi}(\omega) = \exp\left(\frac{-i\varepsilon\omega}{2}\right)\left(\frac{\sin(\omega/2)}{\omega/2}\right)^{p}.$$

Since ψ is a linear combination of box splines $\phi(2t-n)$, it is a compactly supported polynomial spline of the same degree.

The number of vanishing moments $\tilde{p}$ of ψ is a free parameter, which must have the same parity as p. Let $q = (p+\tilde{p})/2$. The biorthogonal filter $\tilde{h}$ of minimum length is obtained by observing that $L(\cos\omega) = 1$ in (7.164). Thus, the factorization (7.166) and (7.168) imply that

$$\widehat{\tilde{h}}(\omega) = \sqrt{2}\, \exp\left(\frac{-i\varepsilon\omega}{2}\right)\left(\cos\frac{\omega}{2}\right)^{\tilde{p}} \sum_{k=0}^{q-1} \binom{q-1+k}{k} \left(\sin\frac{\omega}{2}\right)^{2k}. \tag{7.170}$$

These filters satisfy the conditions of Theorem 7.14 and therefore generate biorthogonal wavelet bases. Table 7.3 gives the filter coefficients for $(p=2, \tilde{p}=4)$ and $(p=3, \tilde{p}=7)$; see Figure 7.14 for the resulting dual wavelet and scaling functions.

Table 7.3 Perfect Reconstruction Filters h and $\tilde{h}$ for Compactly Supported Spline Wavelets

n	$p, \tilde{p}$	$h[n]$	$\tilde{h}[n]$
0		0.70710678118655	0.99436891104358
1, −1	$p=2$	0.35355339059327	0.41984465132951
2, −2	$\tilde{p}=4$		−0.17677669529664
3, −3			−0.06629126073624
4, −4			0.03314563036812
0, 1		0.53033008588991	0.95164212189718
−1, 2	$p=3$	0.17677669529664	−0.02649924094535
−2, 3	$\tilde{p}=7$		−0.30115912592284
−3, 4			0.03133297870736
−4, 5			0.07466398507402
−5, 6			−0.01683176542131
−6, 7			−0.00906325830378
−7, 8			0.00302108610126

Note: $\hat{h}$ and $\widehat{\tilde{h}}$ have, respectively, $\tilde{p}$ and p zeros at $\omega = \pi$.

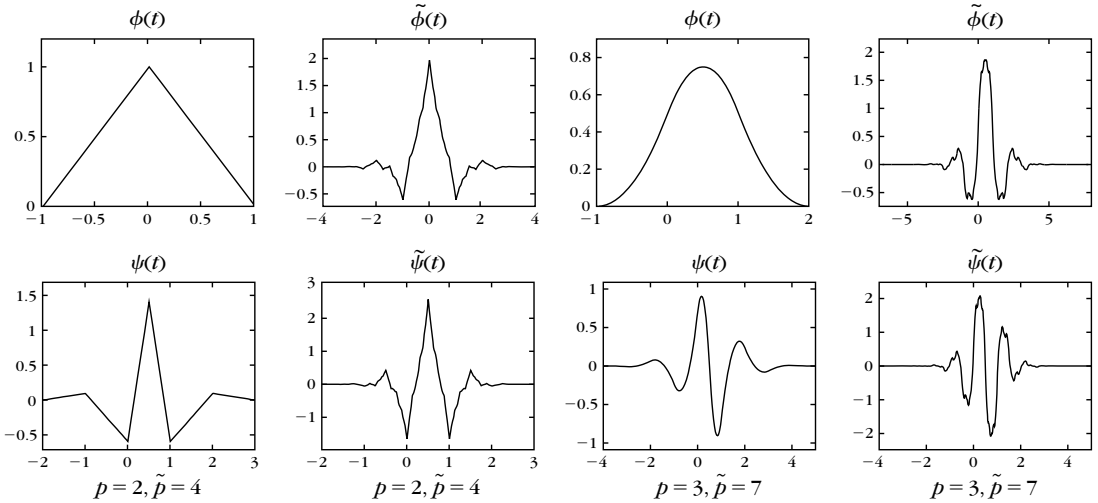

FIGURE 7.14

Spline biorthogonal wavelets and scaling functions of compact support corresponding to Table 7.3 filters.

Closer Filter Length

Biorthogonal filters h and $\tilde{h}$ of more similar length are obtained by factoring the polynomial $P(\sin^2 \frac{\omega}{2})$ in (7.166) with two polynomial $L(\cos\omega)$ and $\tilde{L}(\cos\omega)$ of similar degree. There is a limited number of possible factorizations. For $q = (p + \tilde{p})/2 < 4$, the only solution is $L(\cos\omega) = 1$. For $q = 4$ there is one nontrivial factorization, and for $q = 5$ there are two. Table 7.4 gives the resulting coefficients of the filters h and $\tilde{h}$ of most similar length, computed by Cohen, Daubechies, and Feauveau [172]. These filters also satisfy the conditions of Theorem 7.14 and therefore define biorthogonal wavelet bases.

Figure 7.15 gives the scaling functions and wavelets for $p = \tilde{p} = 2$ and $p = \tilde{p} = 4$, which correspond to filter sizes 5/3 and 9/7, respectively. For $p = \tilde{p} = 4$, ϕ, ψ are similar to $\tilde{\phi}$, $\tilde{\psi}$, which indicates that this basis is nearly orthogonal. This particular set of filters is often used in image compression and recommended for JPEG-2000. The quasi-orthogonality guarantees a good numerical stability and the symmetry allows one to use the folding procedure of Section 7.5.2 at the boundaries. There are also enough vanishing moments to create small wavelet coefficients in regular image domains. Section 7.8.5 describes their lifting implementation, which is simple and efficient. Filter sizes 5/3 are also recommended for lossless compression with JPEG-2000, because they use integer operations with a lifting algorithm. The design of other compactly supported biorthogonal filters is discussed extensively in [172, 473].

Table 7.4 Perfect Reconstruction Filters of Most Similar Length

$p, \tilde{p}$	n	$h[n]$	$\tilde{h}[n]$
$p=2$	0	1.06066017177982	0.70710678118655
$\tilde{p}=2$	−1, 1	0.35355339059327	0.35355339059327
	−2, 2	−0.17677669529664	0
	0	0.85269867900889	0.78848561640637
$p=4$	−1, 1	0.37740285561283	0.41809227322204
$\tilde{p}=4$	−2, 2	−0.11062440441844	−0.04068941760920
	−3, 3	−0.02384946501956	−0.06453888262876
	−4, 4	0.03782845554969	0
	0	0.89950610974865	0.73666018142821
$p=5$	−1, 1	0.47680326579848	0.34560528195603
$\tilde{p}=5$	−2, 2	−0.09350469740094	−0.05446378846824
	−3, 3	−0.13670658466433	0.00794810863724
	−4, 4	−0.00269496688011	0.03968708834741
	−5, 5	0.01345670945912	0
	0	0.54113273169141	1.32702528570780
$p=5$	−1, 1	0.34335173921766	0.47198693379091
$\tilde{p}=5$	−2, 2	0.06115645341349	−0.36378609009851
	−3, 3	0.00027989343090	−0.11843354319764
	−4, 4	0.02183057133337	0.05382683783789
	−5, 5	0.00992177208685	0

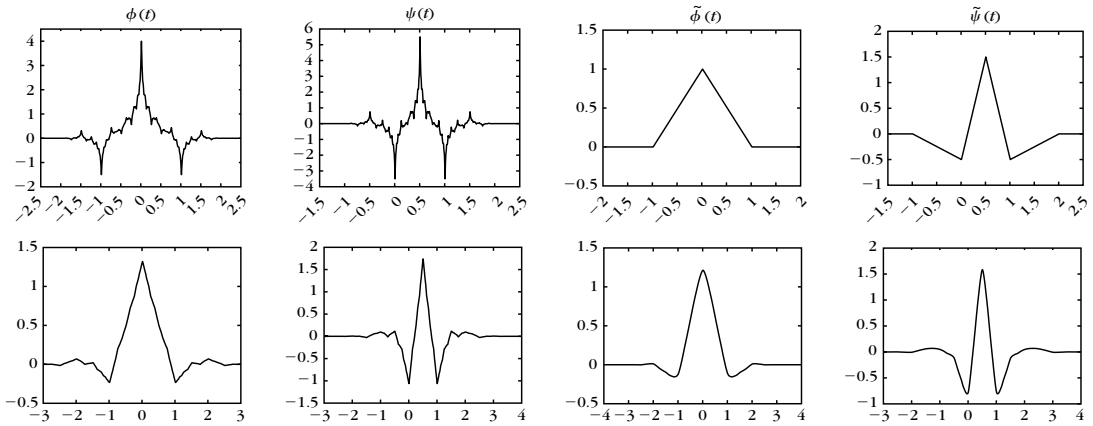

FIGURE 7.15

Biorthogonal wavelets and scaling functions calculated with the filters of Table 7.4, with $p=2$ and $\tilde{p}=2$ (*top row*) and $p=4$ and $\tilde{p}=4$ (*bottom row*).

7.5 WAVELET BASES ON AN INTERVAL

To decompose signals f defined over an interval $[0, 1]$, it is necessary to construct wavelet bases of $\mathbf{L}^2[0, 1]$. Such bases are synthesized by modifying the wavelets $\psi_{j,n}(t) = 2^{-j/2}\psi(2^{-j}t - n)$ of a basis $\{\psi_{j,n}\}_{(j,n)\in\mathbb{Z}^2}$ of $\mathbf{L}^2(\mathbb{R})$. *Inside* wavelets $\psi_{j,n}$, have a support included in $[0, 1]$, and are not modified. *Boundary* wavelets $\psi_{j,n}$, have a support that overlaps $t = 0$ or $t = 1$, and are transformed into functions having a support in $[0, 1]$, which are designed in order to provide the necessary complement to generate a basis of $\mathbf{L}^2[0, 1]$. If ψ has a compact support, then there is a constant number of boundary wavelets at each scale.

The main difficulty is to construct boundary wavelets that keep their vanishing moments. The next three sections describe different approaches to constructing boundary wavelets. Periodic wavelets have no vanishing moments at the boundary, whereas folded wavelets have one vanishing moment. The custom-designed boundary wavelets of Section 7.5.3 have as many vanishing moments as the inside wavelets but are more complicated to construct. Scaling functions $\phi_{j,n}$ are also restricted to $[0, 1]$ by modifying the scaling functions $\phi_{j,n}(t) = 2^{-j/2}\phi(2^{-j}t - n)$ associated with the wavelets $\psi_{j,n}$. The resulting wavelet basis of $\mathbf{L}^2[0, 1]$ is composed of 2^{-J} scaling functions at a coarse scale $2^J < 1$, plus 2^{-j} wavelets at each scale $2^j \leqslant 2^J$:

$$\left[\{\phi^{\text{int}}_{J,n}\}_{0\leqslant n<2^{-J}},\ \{\psi^{\text{int}}_{j,n}\}_{-\infty<j\leqslant J, 0\leqslant n<2^{-j}}\right]. \tag{7.171}$$

On any interval $[a, b]$, a wavelet orthonormal basis of $\mathbf{L}^2[a, b]$ is constructed with a dilation by $b - a$ and a translation by a of the wavelets in (7.171).

Discrete Basis of $\mathbb{C}^N$

The decomposition of a signal in a wavelet basis over an interval is computed by modifying the fast wavelet transform algorithm of Section 7.3.1. A discrete signal $b[n]$ of N samples is associated to the approximation of a signal $f \in \mathbf{L}^2[0, 1]$ at a scale $N^{-1} = 2^L$ with (7.111):

$$N^{-1/2}\, b[n] = a_L[n] = \langle f, \phi^{\text{int}}_{L,n}\rangle \quad \text{for} \quad 0 \leqslant n < 2^{-L}.$$

Its wavelet coefficients can be calculated at scales $1 \geqslant 2^j > 2^L$. We set

$$a_j[n] = \langle f, \phi^{\text{int}}_{j,n}\rangle \quad \text{and} \quad d_j[n] = \langle f, \psi^{\text{int}}_{j,n}\rangle \quad \text{for} \quad 0 \leqslant n < 2^{-j}. \tag{7.172}$$

The wavelets and scaling functions with support inside $[0, 1]$ are identical to the wavelets and scaling functions of a basis of $\mathbf{L}^2(\mathbb{R})$. Thus, the corresponding coefficients $a_j[n]$ and $d_j[n]$ can be calculated with the decomposition and reconstruction equations given by Theorem 7.10. However, these convolution formulas must be modified near the boundary where the wavelets and scaling functions are modified. Boundary calculations depend on the specific design of the boundary wavelets, as explained in the next three sections. The resulting filter bank algorithm still computes the N coefficients of the wavelet representation $\left[a_J, \{d_j\}_{L<j\leqslant J}\right]$ of a_L with $O(N)$ operations.

Wavelet coefficients can also be written as discrete inner products of a_L with discrete wavelets:

$$a_j[n] = \langle a_L[m], \phi^{\text{int}}_{j,n}[m] \rangle \quad \text{and} \quad d_j[n] = \langle a_L[m], \psi^{\text{int}}_{j,n}[m] \rangle. \tag{7.173}$$

As in Section 7.3.3, we verify that

$$\left[\{\phi^{\text{int}}_{J,n}[m]\}_{0 \leqslant n < 2^{-J}},\ \{\psi^{\text{int}}_{j,n}[m]\}_{L < j \leqslant J,\, 0 \leqslant n < 2^{-j}} \right]$$

is an orthonormal basis of $\mathbb{C}^N$.

7.5.1 Periodic Wavelets

A wavelet basis $\{\psi_{j,n}\}_{(j,n) \in \mathbb{Z}^2}$ of $\mathbf{L^2}(\mathbb{R})$ is transformed into a wavelet basis of $\mathbf{L^2}[0, 1]$ by periodizing each $\psi_{j,n}$. The periodization of $f \in \mathbf{L^2}(\mathbb{R})$ over $[0, 1]$ is defined by

$$f^{\text{pér}}(t) = \sum_{k=-\infty}^{+\infty} f(t + k). \tag{7.174}$$

The resulting periodic wavelets are

$$\psi^{\text{pér}}_{j,n}(t) = \frac{1}{\sqrt{2^j}} \sum_{k=-\infty}^{+\infty} \psi\left(\frac{t - 2^j n + k}{2^j} \right).$$

For $j \leqslant 0$, there are 2^{-j} different $\psi^{\text{pér}}_{j,n}$ indexed by $0 \leqslant n < 2^{-j}$. If the support of $\psi_{j,n}$ is included in $[0, 1]$, then $\psi^{\text{pér}}_{j,n}(t) = \psi_{j,n}(t)$ for $t \in [0, 1]$. Thus, the restriction to $[0, 1]$ of this periodization modifies only the boundary wavelets with a support that overlaps $t = 0$ or $t = 1$.

As indicated in Figure 7.16, such wavelets are transformed into boundary wavelets that have two disjoint components near $t = 0$ and $t = 1$. Taken separately, the components near $t = 0$ and $t = 1$ of these boundary wavelets have no vanishing moments, and thus create large signal coefficients, as we shall see later. Theorem 7.16 proves that periodic wavelets together with periodized scaling functions $\phi^{\text{pér}}_{j,n}$ generate an orthogonal basis of $\mathbf{L^2}[0, 1]$.

FIGURE 7.16

The restriction to $[0, 1]$ of a periodic wavelet $\psi^{\text{pér}}_{j,n}$ has two disjoint components near $t = 0$ and $t = 1$.

Theorem 7.16. For any $J \leqslant 0$,

$$\left[\{\psi^{\text{pér}}_{j,n}\}_{-\infty < j \leqslant J, 0 \leqslant n < 2^{-j}},\ \{\phi^{\text{pér}}_{J,n}\}_{0 \leqslant n < 2^{-J}} \right] \tag{7.175}$$

is an orthogonal basis of $\mathbf{L^2}[0, 1]$.

Proof. The orthogonality of this family is proved with Lemma 7.2.

Lemma 7.2. Let $\alpha(t), \beta(t) \in \mathbf{L}^2(\mathbb{R})$. If $\langle \alpha(t), \beta(t+k) \rangle = 0$ for all $k \in \mathbb{Z}$, then

$$\int_0^1 \alpha^{\text{pér}}(t)\, \beta^{\text{pér}}(t)\, dt = 0. \tag{7.176}$$

To verify (7.176) we insert the definition (7.174) of periodized functions:

$$\begin{aligned}\int_0^1 \alpha^{\text{pér}}(t)\, \beta^{\text{pér}}(t)\, dt &= \int_{-\infty}^{+\infty} \alpha(t)\, \beta^{\text{pér}}(t)\, dt \\ &= \sum_{k=-\infty}^{+\infty} \int_{-\infty}^{+\infty} \alpha(t)\, \beta(t+k)\, dt = 0.\end{aligned}$$

Since $\left[\{\psi_{j,n}\}_{-\infty<j\leqslant J, n\in\mathbb{Z}}, \{\phi_{J,n}\}_{n\in\mathbb{Z}}\right]$ is orthogonal in $\mathbf{L}^2(\mathbb{R})$, we can verify that any two different wavelets or scaling functions $\alpha^{\text{pér}}$ and $\beta^{\text{pér}}$ in (7.175) have necessarily a nonperiodized version that satisfies $\langle \alpha(t), \beta(t+k) \rangle = 0$ for all $k \in \mathbb{Z}$. Thus, this lemma proves that (7.175) is orthogonal in $\mathbf{L}^2[0, 1]$.

To prove that this family generates $\mathbf{L}^2[0, 1]$, we extend $f \in \mathbf{L}^2[0, 1]$ with zeros outside $[0, 1]$ and decompose it in the wavelet basis of $\mathbf{L}^2(\mathbb{R})$:

$$f = \sum_{j=-\infty}^{J} \sum_{n=-\infty}^{+\infty} \langle f, \psi_{j,n} \rangle\, \psi_{j,n} + \sum_{n=-\infty}^{+\infty} \langle f, \phi_{J,n} \rangle\, \phi_{J,n}. \tag{7.177}$$

This zero extension is periodized with the sum (7.174), which defines $f^{\text{pér}}(t) = f(t)$ for $t \in [0, 1]$. Periodizing (7.177) proves that f can be decomposed over the periodized wavelet family (7.175) in $\mathbf{L}^2[0, 1]$. ■

Theorem 7.16 shows that periodizing a wavelet orthogonal basis of $\mathbf{L}^2(\mathbb{R})$ defines a wavelet orthogonal basis of $\mathbf{L}^2[0, 1]$. If $J = 0$, then there is a single scaling function, and one can verify that $\phi_{0,0}(t) = 1$. The resulting scaling coefficient $\langle f, \phi_{0,0} \rangle$ is the average of f over $[0, 1]$.

Periodic wavelet bases have the disadvantage of creating high-amplitude wavelet coefficients in the neighborhood of $t = 0$ and $t = 1$, because the boundary wavelets have separate components with no vanishing moments. If $f(0) \neq f(1)$, the wavelet coefficients behave as if the signal were discontinuous at the boundaries. This can also be verified by extending $f \in \mathbf{L}^2[0, 1]$ into an infinite 1 periodic signal $f^{\text{pér}}$ and by showing that

$$\int_0^1 f(t)\, \psi_{j,n}^{\text{pér}}(t)\, dt = \int_{-\infty}^{+\infty} f^{\text{pér}}(t)\, \psi_{j,n}(t)\, dt. \tag{7.178}$$

If $f(0) \neq f(1)$, then $f^{\text{pér}}(t)$ is discontinuous at $t = 0$ and $t = 1$, which creates high-amplitude wavelet coefficients when $\psi_{j,n}$ overlaps the interval boundaries.

Periodic Discrete Transform

For $f \in \mathbf{L}^2[0, 1]$ let us consider

$$a_j[n] = \langle f, \phi_{j,n}^{\text{pér}} \rangle \quad \text{and} \quad d_j[n] = \langle f, \psi_{j,n}^{\text{pér}} \rangle.$$

We verify as in (7.178) that these inner products are equal to the coefficients of a periodic signal decomposed in a nonperiodic wavelet basis:

$$a_j[n] = \langle f^{\text{pér}}, \phi_{j,n} \rangle \quad \text{and} \quad d_j[n] = \langle f^{\text{pér}}, \psi_{j,n} \rangle.$$

Thus, the convolution formulas of Theorem 7.10 apply if we take into account the periodicity of $f^{\text{pér}}$. This means that $a_j[n]$ and $d_j[n]$ are considered as discrete signals of period 2^{-j}, and all convolutions in (7.102–7.104) must therefore be replaced by circular convolutions. Despite the poor behavior of periodic wavelets near the boundaries, they are often used because the numerical implementation is particularly simple.

7.5.2 Folded Wavelets

Decomposing $f \in \mathbf{L}^2[0, 1]$ in a periodic wavelet basis was shown in (7.178) to be equivalent to a decomposition of $f^{\text{pér}}$ in a regular basis of $\mathbf{L}^2(\mathbb{R})$. Let us extend f with zeros outside $[0, 1]$. To avoid creating discontinuities with such a periodization, the signal is folded with respect to $t = 0$: $f_0(t) = f(t) + f(-t)$. The support of f_0 is $[-1, 1]$ and it is transformed into a 2 periodic signal, as illustrated in Figure 7.17:

$$f^{\text{repl}}(t) = \sum_{k=-\infty}^{+\infty} f_0(t - 2k) = \sum_{k=-\infty}^{+\infty} f(t - 2k) + \sum_{k=-\infty}^{+\infty} f(2k - t). \tag{7.179}$$

Clearly $f^{\text{repl}}(t) = f(t)$ if $t \in [0, 1]$, and it is symmetric with respect to $t = 0$ and $t = 1$. If f is continuously differentiable, then f^{repl} is continuous at $t = 0$ and $t = 1$, but its derivative is discontinuous at $t = 0$ and $t = 1$ if $f'(0) \neq 0$ and $f'(1) \neq 0$.

Decomposing f^{repl} in a wavelet basis $\{\psi_{j,n}\}_{(j,n) \in \mathbb{Z}^2}$ is equivalent to decomposing f on a folded wavelet basis. Let $\psi_{j,n}^{\text{repl}}$ be the folding of $\psi_{j,n}$ with the summation (7.179). One can verify that

$$\int_0^1 f(t)\, \psi_{j,n}^{\text{repl}}(t)\, dt = \int_{-\infty}^{+\infty} f^{\text{repl}}(t)\, \psi_{j,n}(t)\, dt. \tag{7.180}$$

Suppose that f is regular over $[0, 1]$. Then f^{repl} is continuous at $t = 0, 1$ and produces smaller boundary wavelet coefficients than $f^{\text{pér}}$. However, it is not continuously differentiable at $t = 0, 1$, which creates bigger wavelet coefficients at the boundary than inside.

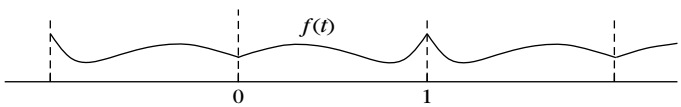

FIGURE 7.17

The folded signal $f^{\text{repl}}(t)$ is 2 periodic, symmetric about $t = 0$ and $t = 1$, and equal to $f(t)$ on $[0, 1]$.

To construct a basis of $\mathbf{L^2}[0, 1]$ with the folded wavelets $\psi_{j,n}^{\text{repl}}$, it is sufficient for $\psi(t)$ to be either symmetric or antisymmetric with respect to $t = 1/2$. The Haar wavelet is the only real compactly supported wavelet that is symmetric or antisymmetric and that generates an orthogonal basis of $\mathbf{L^2}(\mathbb{R})$. On the other hand, if we loosen up the orthogonality constraint, Section 7.4 proves that there exist biorthogonal bases constructed with compactly supported wavelets that are either symmetric or antisymmetric. Let $\{\psi_{j,n}\}_{(j,n)\in\mathbb{Z}^2}$ and $\{\tilde{\psi}_{j,n}\}_{(j,n)\in\mathbb{Z}^2}$ be such biorthogonal wavelet bases. If we fold the wavelets as well as the scaling functions, then for $J \leqslant 0$,

$$\left[\{\psi_{j,n}^{\text{repl}}\}_{-\infty<j\leqslant J, 0\leqslant n<2^{-j}}, \{\phi_{J,n}^{\text{repl}}\}_{0\leqslant n<2^{-J}}\right] \tag{7.181}$$

is a Riesz basis of $\mathbf{L^2}[0, 1]$ [174]. The biorthogonal basis is obtained by folding the dual wavelets $\tilde{\psi}_{j,n}$ and is given by

$$\left[\{\tilde{\psi}_{j,n}^{\text{repl}}\}_{-\infty<j\leqslant J, 0\leqslant n<2^{-j}}, \{\tilde{\phi}_{J,n}^{\text{repl}}\}_{0\leqslant n<2^{-J}}\right]. \tag{7.182}$$

If $J = 0$, then $\phi_{0,0}^{\text{repl}} = \tilde{\phi}_{0,0}^{\text{repl}} = 1$.

Biorthogonal wavelets of compact support are characterized by a pair of finite perfect reconstruction filters $(h, \tilde{h})$. The symmetry of these wavelets depends on the symmetry and size of the filters, as explained in Section 7.4.2. A fast folded wavelet transform is implemented with a modified filter bank algorithm, where the treatment of boundaries is slightly more complicated than for periodic wavelets. The symmetric and antisymmetric cases are considered separately.

Folded Discrete Transform

For $f \in \mathbf{L^2}[0, 1]$, we consider

$$a_j[n] = \langle f, \phi_{j,n}^{\text{repl}} \rangle \quad \text{and} \quad d_j[n] = \langle f, \psi_{j,n}^{\text{repl}} \rangle.$$

We verify as in (7.180) that these inner products are equal to the coefficients of a folded signal decomposed in a nonfolded wavelet basis:

$$a_j[n] = \langle f^{\text{repl}}, \phi_{j,n} \rangle \quad \text{and} \quad d_j[n] = \langle f^{\text{repl}}, \psi_{j,n} \rangle.$$

The convolution formulas of Theorem 7.10 apply if we take into account the symmetry and periodicity of f^{repl}. The symmetry properties of ϕ and ψ imply that $a_j[n]$ and $d_j[n]$ also have symmetry and periodicity properties, which must be taken into account in the calculations of (7.102–7.104).

Symmetric biorthogonal wavelets are constructed with perfect reconstruction filters h and $\hat{h}$ of odd size that are symmetric about $n = 0$. Then ϕ is symmetric about 0, whereas ψ is symmetric about $1/2$. As a result, one can verify that $a_j[n]$ is 2^{-j+1} periodic and symmetric about $n = 0$ and $n = 2^{-j}$. Thus, it is characterized by $2^{-j} + 1$ samples for $0 \leqslant n \leqslant 2^{-j}$. The situation is different for $d_j[n]$, which is 2^{-j+1} periodic but symmetric with respect to $-1/2$ and $2^{-j} - 1/2$. It is characterized by 2^{-j} samples for $0 \leqslant n < 2^{-j}$.

To initialize this algorithm, the original signal $a_L[n]$ defined over $0 \leqslant n < N-1$ must be extended by one sample at $n = N$, and considered to be symmetric with respect to $n = 0$ and $n = N$. The extension is done by setting $a_L[N] = a_L[N-1]$. For any $J < L$, the resulting discrete wavelet representation $\left[\{d_j\}_{L<j\leqslant J}, a_J\right]$ is characterized by $N+1$ coefficients. To avoid adding one more coefficient, one can modify symmetry at the right boundary of a_L by considering that it is symmetric with respect to $N - 1/2$ instead of N. The symmetry of the resulting a_j and d_j at the right boundary is modified accordingly by studying the properties of the convolution formula (7.157). As a result, these signals are characterized by 2^{-j} samples and the wavelet representation has N coefficients. A simpler implementation of this folding technique is given with a lifting in Section 7.8.5. This folding approach is used in most applications because it leads to simpler data structures that keep the number of coefficients constant. However, the discrete coefficients near the right boundary cannot be written as inner products of some function $f(t)$ with dilated boundary wavelets.

Antisymmetric biorthogonal wavelets are obtained with perfect reconstruction filters h and $\hat{h}$ of even size that are symmetric about $n = 1/2$. In this case, ϕ is symmetric about $1/2$ and ψ is antisymmetric about $1/2$. As a result, a_j and d_j are 2^{-j+1} periodic and, respectively, symmetric and antisymmetric about $-1/2$ and $2^{-j} - 1/2$. They are both characterized by 2^{-j} samples for $0 \leqslant n < 2^{-j}$. The algorithm is initialized by considering that $a_L[n]$ is symmetric with respect to $-1/2$ and $N - 1/2$. There is no need to add another sample. The resulting discrete wavelet representation $\left[\{d_j\}_{L<j\leqslant J}, a_J\right]$ is characterized by N coefficients.

7.5.3 Boundary Wavelets

Wavelet coefficients are small in regions where the signal is regular only if the wavelets have enough vanishing moments. The restriction of periodic and folded "boundary" wavelets to the neighborhood of $t = 0$ and $t = 1$ have, respectively, 0 and 1 vanishing moments. Therefore, these boundary wavelets cannot fully take advantage of the signal regularity. They produce large inner products, as if the signal were discontinuous or had a discontinuous derivative. To avoid creating large-amplitude wavelet coefficients at the boundaries, one must synthesize boundary wavelets that have as many vanishing moments as the original wavelet ψ. Initially introduced by Meyer, this approach has been refined by Cohen, Daubechies, and Vial [174]. The main results are given without proofs.

Multiresolution of $\mathbf{L^2}[0, 1]$

A wavelet basis of $\mathbf{L^2}[0, 1]$ is constructed with a multiresolution approximation $\{\mathbf{V}_j^{\text{int}}\}_{-\infty<j\leqslant 0}$. A wavelet has p vanishing moments if it is orthogonal to all polynomials of degree $p-1$ or smaller. Since wavelets at a scale 2^j are orthogonal to functions in $\mathbf{V}_j^{\text{int}}$, to guarantee that they have p vanishing moments we make sure that polynomials of degree $p-1$ are inside $\mathbf{V}_j^{\text{int}}$.

We define an approximation space $\mathbf{V}_j^{\text{int}} \subset \mathbf{L^2}[0,1]$ with a compactly supported Daubechies scaling function ϕ associated to a wavelet with p vanishing moments. Theorem 7.7 proves that the support of ϕ has size $2p-1$. We translate ϕ so that its support is $[-p+1, p]$. At a scale $2^j \leqslant (2p)^{-1}$, there are $2^{-j} - 2p$ scaling functions with a support inside $[0,1]$:

$$\phi_{j,n}^{\text{int}}(t) = \phi_{j,n}(t) = \frac{1}{\sqrt{2^j}}\,\phi\Big(\frac{t-2^j n}{2^j}\Big) \quad \text{for } p \leqslant n < 2^{-j} - p.$$

To construct an approximation space $\mathbf{V}_j^{\text{int}}$ of dimension 2^{-j} we add p scaling functions with a support on the left boundary near $t=0$:

$$\phi_{j,n}^{\text{int}}(t) = \frac{1}{\sqrt{2^j}}\,\phi_n^{\text{left}}\Big(\frac{t}{2^j}\Big) \quad \text{for } 0 \leqslant n < p,$$

and p scaling functions on the right boundary near $t=1$:

$$\phi_{j,n}^{\text{int}}(t) = \frac{1}{\sqrt{2^j}}\,\phi_{2^{-j}-1-n}^{\text{right}}\Big(\frac{t-1}{2^j}\Big) \quad \text{for } 2^{-j} - p \leqslant n < 2^{-j}.$$

Theorem 7.17 constructs appropriate boundary scaling functions $\{\phi_n^{\text{left}}\}_{0\leqslant n<p}$ and $\{\phi_n^{\text{right}}\}_{0\leqslant n<p}$.

Theorem 7.17: *Cohen, Daubechies, Vial.* One can construct boundary scaling functions ϕ_n^{left} and ϕ_n^{right} so that if $2^{-j} \geqslant 2p$, then $\{\phi_{j,n}^{\text{int}}\}_{0\leqslant n<2^{-j}}$ is an orthonormal basis of a space $\mathbf{V}_j^{\text{int}}$ satisfying

$$\mathbf{V}_j^{\text{int}} \subset \mathbf{V}_{j-1}^{\text{int}}$$

$$\lim_{j\to-\infty} \mathbf{V}_j^{\text{int}} = \text{Closure}\left(\bigcup_{j=-\infty}^{-\log_2(2p)} \mathbf{V}_j^{\text{int}}\right) = \mathbf{L^2}[0,1],$$

and the restrictions to $[0,1]$ of polynomials of degree $p-1$ are in $\mathbf{V}_j^{\text{int}}$.

Proof. A sketch of the proof is given. All details are in [174]. Since the wavelet ψ corresponding to ϕ has p vanishing moments, the Fix-Strang condition (7.70) implies that

$$q_k(t) = \sum_{n=-\infty}^{+\infty} n^k\,\phi(t-n) \tag{7.183}$$

is a polynomial of degree k. At any scale 2^j, $q_k(2^{-j}t)$ is still a polynomial of degree k, and for $0 \leqslant k < p$ this family defines a basis of polynomials of degree $p-1$. To guarantee that polynomials of degree $p-1$ are in $\mathbf{V}_j^{\text{int}}$ we impose that the restriction of $q_k(2^{-j}t)$ to $[0,1]$ can be decomposed in the basis of $\mathbf{V}_j^{\text{int}}$:

$$\begin{aligned} q_k(2^{-j}t)\,\mathbf{1}_{[0,1]}(t) = &\sum_{n=0}^{p-1} a[n]\,\phi_n^{\text{left}}(2^{-j}t) + \sum_{n=p}^{2^{-j}-p-1} n^k\,\phi(2^{-j}t-n) \\ &+ \sum_{n=0}^{p-1} b[n]\,\phi_n^{\text{right}}(2^{-j}t - 2^{-j}). \end{aligned} \tag{7.184}$$

Since the support of ϕ is $[-p+1, p]$, the condition (7.184) together with (7.183) can be separated into two nonoverlapping left and right conditions. With a change of variable, we verify that (7.184) is equivalent to

$$\sum_{n=-p+1}^{p} n^k \, \phi(t-n) \, \mathbf{1}_{[0,+\infty)}(t) = \sum_{n=0}^{p-1} a[n] \, \phi_n^{\text{left}}(t), \tag{7.185}$$

and

$$\sum_{n=-p}^{p-1} n^k \, \phi(t-n) \, \mathbf{1}_{(-\infty,0]}(t) = \sum_{n=0}^{p-1} b[n] \, \phi_n^{\text{right}}(t). \tag{7.186}$$

The embedding property $\mathbf{V}_j^{\text{int}} \subset \mathbf{V}_{j-1}^{\text{int}}$ is obtained by imposing that the boundary scaling functions satisfy scaling equations. We suppose that ϕ_n^{left} has a support $[0, p+n]$ and satisfies a scaling equation of the form

$$2^{-1/2} \, \phi_n^{\text{left}}(2^{-1}t) = \sum_{l=0}^{p-1} H_{n,l}^{\text{left}} \, \phi_l^{\text{left}}(t) + \sum_{m=p}^{p+2n} h_{n,m}^{\text{left}} \, \phi(t-m), \tag{7.187}$$

whereas ϕ_n^{right} has a support $[-p-n, 0]$ and satisfies a similar scaling equation on the right. The constants $H_{n,l}^{\text{left}}$, $h_{n,m}^{\text{left}}$, $H_{n,l}^{\text{right}}$, and $h_{n,m}^{\text{right}}$ are adjusted to verify the polynomial reproduction equations (7.185) and (7.186), while producing orthogonal scaling functions. The resulting family $\{\phi_{j,n}^{\text{int}}\}_{0 \leq n < 2^{-j}}$ is an orthonormal basis of a space $\mathbf{V}_j^{\text{int}}$.

The convergence of the spaces $\mathbf{V}_j^{\text{int}}$ to $\mathbf{L^2}[0, 1]$ when 2^j goes to 0 is a consequence of the fact that the multiresolution spaces $\mathbf{V}_j$ generated by the Daubechies scaling function $\{\phi_{j,n}\}_{n \in \mathbb{Z}}$ converge to $\mathbf{L^2}(\mathbb{R})$. ■

The proof constructs the scaling functions through scaling equations specified by discrete filters. At the boundaries, the filter coefficients are adjusted to construct orthogonal scaling functions with a support in $[0, 1]$, and to guarantee that polynomials of degree $p-1$ are reproduced by these scaling functions. Table 7.5 gives the filter coefficients for $p = 2$.

Wavelet Basis of $\mathbf{L^2[0, 1]}$

Let $\mathbf{W}_j^{\text{int}}$ be the orthogonal complement of $\mathbf{V}_j^{\text{int}}$ in $\mathbf{V}_{j-1}^{\text{int}}$. The support of the Daubechies wavelet ψ with p vanishing moments is $[-p+1, p]$. Since $\psi_{j,n}$ is orthogonal to any $\phi_{j,l}$, we verify that an orthogonal basis of $\mathbf{W}_j^{\text{int}}$ can be constructed with the $2^{-j} - 2p$ inside wavelets with support in $[0, 1]$:

$$\psi_{j,n}^{\text{int}}(t) = \psi_{j,n}(t) = \frac{1}{\sqrt{2^j}} \, \psi\Big(\frac{t - 2^j n}{2^j}\Big) \quad \text{for} \quad p \leqslant n < 2^{-j} - p,$$

to which are added $2p$ left and right boundary wavelets

$$\psi_{j,n}^{\text{int}}(t) = \frac{1}{\sqrt{2^j}} \, \psi_n^{\text{left}}\Big(\frac{t}{2^j}\Big) \quad \text{for} \quad 0 \leqslant n < p,$$

Table 7.5 Left and Right Border Coefficients for a Daubechies Wavelet with $p = 2$ Vanishing Moments

k	l	$H_{k,l}^{\text{left}}$	$G_{k,l}^{\text{left}}$	k	m	$h_{k,m}^{\text{left}}$	$g_{k,m}^{\text{left}}$
0	0	0.6033325119	−0.7965436169	0	2	−0.398312997	−0.2587922483
0	1	0.690895531	0.5463927140	1	2	0.8500881025	0.227428117
1	0	0.03751746045	0.01003722456	1	3	0.2238203570	−0.8366028212
1	1	0.4573276599	0.1223510431	1	4	−0.1292227434	0.4830129218
k	l	$H_{k,l}^{\text{right}}$	$G_{k,l}^{\text{right}}$	k	m	$h_{k,m}^{\text{right}}$	$g_{k,m}^{\text{left}}$
−2	−2	0.1901514184	−0.3639069596	−2	−5	0.4431490496	0.235575950
−2	−1	−0.1942334074	0.3717189665	−2	−4	0.7675566693	0.4010695194
−1	−2	0.434896998	0.8014229620	−2	−3	0.3749553316	−0.7175799994
−2	−1	0.8705087534	−0.2575129195	−1	−3	0.2303890438	−0.5398225007
		$h[-1]$	$h[0]$			$h[1]$	$h[2]$
		0.482962913145	0.836516303738			0.224143868042	−0.129409522551

Note: The inside filter coefficients are at the bottom of the table. A table of coefficients for $p \geqslant 2$ vanishing moments can be retrieved over the Internet at the FTP site ftp://math.princeton.edu/pub/user/ingrid/interval-tables.

$$\psi_{j,n}^{\text{int}}(t) = \frac{1}{\sqrt{2^j}}\, \psi_{2^{-j}-1-n}^{\text{right}}\left(\frac{t-1}{2^j}\right) \quad \text{for} \quad 2^{-j} - p \leqslant n < 2^{-j}.$$

Since $\mathbf{W}_j^{\text{int}} \subset \mathbf{V}_{j-1}^{\text{int}}$, the left and right boundary wavelets at any scale 2^j can be expanded into scaling functions at the scale 2^{j-1}. For $j = 1$ we impose that the left boundary wavelets satisfy equations of the form

$$\frac{1}{\sqrt{2}}\, \psi_n^{\text{left}}\left(\frac{t}{2}\right) = \sum_{l=0}^{p-1} G_{n,l}^{\text{left}}\, \phi_l^{\text{left}}(t) + \sum_{m=p}^{p+2n} g_{n,m}^{\text{left}}\, \phi(t-m). \tag{7.188}$$

The right boundary wavelets satisfy similar equations. The coefficients $G_{n,l}^{\text{left}}, g_{n,m}^{\text{left}}$, $G_{n,l}^{\text{right}}$, and $g_{n,m}^{\text{right}}$ are computed so that $\{\psi_{j,n}^{\text{int}}\}_{0 \leqslant n < 2^{-j}}$ is an orthonormal basis of $\mathbf{W}_j^{\text{int}}$. Table 7.5 gives the values of these coefficients for $p = 2$.

For any $2^J \leqslant (2p)^{-1}$ the multiresolution properties prove that

$$\mathbf{L^2}[0, 1] = \mathbf{V}_J^{\text{int}} \oplus_{j=-\infty}^{J} \mathbf{W}_j^{\text{int}},$$

which implies that

$$\left[\{\phi_{J,n}^{\text{int}}\}_{0 \leqslant n < 2^{-J}}, \{\psi_{j,n}^{\text{int}}\}_{-\infty < j \leqslant J, 0 \leqslant n < 2^{-j}}\right] \tag{7.189}$$

is an orthonormal wavelet basis of $\mathbf{L^2}[0, 1]$. The boundary wavelets, like the inside wavelets, have p vanishing moments because polynomials of degree $p-1$ are included in the space $\mathbf{V}_J^{\text{int}}$. Figure 7.18 displays the $2p = 4$ boundary scaling functions and wavelets.

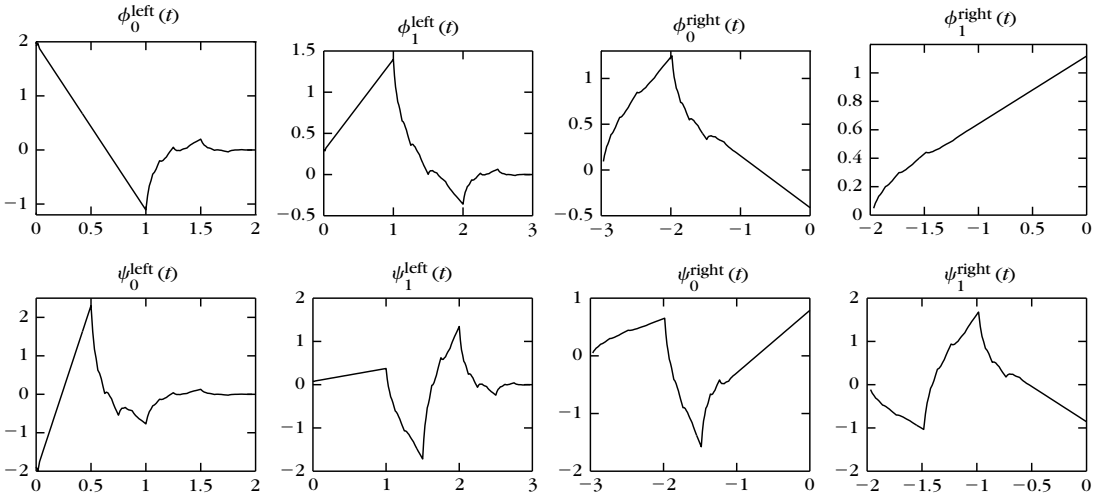

FIGURE 7.18

Boundary scaling functions and wavelets with $p = 2$ vanishing moments.

Fast Discrete Algorithm

For any $f \in \mathbf{L^2}[0, 1]$ we denote

$$a_j[n] = \langle f, \phi_{j,n}^{\text{int}} \rangle \quad \text{and} \quad d_j[n] = \langle f, \psi_{j,n}^{\text{int}} \rangle \text{ for } 0 \leqslant n \leqslant 2^{-j}.$$

Wavelet coefficients are computed with a cascade of convolutions identical to Theorem 7.10 as long as filters do not overlap signal boundaries. A Daubechies filter h is considered here to have a support located at $[-p+1, p]$. At the boundary, the usual Daubechies filters are replaced by boundary filters that relate boundary wavelets and scaling functions to the finer-scale scaling functions in (7.187) and (7.188).

Theorem 7.18: *Cohen, Daubechies, Vial.* If $0 \leqslant k < p$,

$$a_j[k] = \sum_{l=0}^{p-1} H_{k,l}^{\text{left}}\, a_{j-1}[l] + \sum_{m=p}^{p+2k} h_{k,m}^{\text{left}}\, a_{j-1}[m],$$

$$d_j[k] = \sum_{l=0}^{p-1} G_{k,l}^{\text{left}}\, a_{j-1}[l] + \sum_{m=p}^{p+2k} g_{k,m}^{\text{left}}\, a_{j-1}[m].$$

If $p \leqslant k < 2^{-j} - p$,

$$a_j[k] = \sum_{l=-\infty}^{+\infty} h[l - 2k]\, a_{j-1}[l],$$

$$d_j[k] = \sum_{l=-\infty}^{+\infty} g[l - 2k]\, a_{j-1}[l].$$

If $-p \leq k < 0$,

$$a_j[2^{-j}+k] = \sum_{l=-p}^{-1} H^{\text{right}}_{k,l}\, a_{j-1}[2^{-j+1}+l] + \sum_{m=-p+2k+1}^{-p-1} h^{\text{right}}_{k,m}\, a_{j-1}[2^{-j+1}+m],$$

$$d_j[2^{-j}+k] = \sum_{l=-p}^{-1} G^{\text{right}}_{k,l}\, a_{j-1}[2^{-j+1}+l] + \sum_{m=-p+2k+1}^{-p-1} g^{\text{right}}_{k,m}\, a_{j-1}[2^{-j+1}+m].$$

This cascade algorithm decomposes a_L into a discrete wavelet transform $\left[a_J, \{d_j\}_{L<j\leq J}\right]$ with $O(N)$ operations. The maximum scale must satisfy $2^J \leq (2p)^{-1}$, because the number of boundary coefficients remains equal to $2p$ at all scales. The implementation is more complicated than the folding and periodic algorithms described in Sections 7.5.1 and 7.5.2, but does not require more computations. The signal a_L is reconstructed from its wavelet coefficients, by inverting the decomposition formula in Theorem 7.18.

Theorem 7.19: *Cohen, Daubechies, Vial.* If $0 \leq l \leq p-1$,

$$a_{j-1}[l] = \sum_{k=0}^{p-1} H^{\text{left}}_{k,l}\, a_j[k] + \sum_{k=0}^{p-1} G^{\text{left}}_{k,l}\, d_j[k].$$

If $p \leq l \leq 3p-2$,

$$a_{j-1}[l] = \sum_{k=(l-p)/2}^{p-1} h^{\text{left}}_{k,l}\, a_j[k] + \sum_{k=-\infty}^{+\infty} h[l-2k]\, a_j[k] + \sum_{k=(l-p)/2}^{p-1} g^{\text{left}}_{k,l}\, d_j[k] + \sum_{k=-\infty}^{+\infty} g[l-2k]\, d_j[k].$$

If $3p-1 \leq l \leq 2^{-j+1}-3p$,

$$a_{j-1}[l] = \sum_{k=-\infty}^{+\infty} h[l-2k]\, a_j[k] + \sum_{k=-\infty}^{+\infty} g[l-2k]\, d_j[k].$$

If $-p-1 \geqslant l \geqslant -3p+1$,

$$a_{j-1}[2^{-j+1}+l] = \sum_{k=-p}^{(l+p-1)/2} h^{\text{right}}_{k,l}\, a_j[2^{-j}+k] + \sum_{k=-\infty}^{+\infty} h[l-2k]\, a_j[2^{-j}+k] + \sum_{k=-p}^{(l+p-1)/2} g^{\text{right}}_{k,l}\, d_j[2^{-j}+k] + \sum_{k=-\infty}^{+\infty} g[l-2k]\, d_j[2^{-j}+k].$$

If $-1 \geqslant l \geqslant -p$,

$$a_{j-1}[2^{-j+1}+l] = \sum_{k=-p}^{-1} H^{\text{right}}_{k,l}\, a_j[2^{-j}+k] + \sum_{k=-p}^{-1} G^{\text{right}}_{k,l}\, d_j[2^{-j}+k].$$

The original signal a_L is reconstructed from the orthogonal wavelet representation $\left[a_J, \{d_j\}_{L<j\leqslant J}\right]$ by iterating these equations for $L<j\leqslant J$. This reconstruction is performed with $O(N)$ operations.

7.6 MULTISCALE INTERPOLATIONS

Multiresolution approximations are closely connected to the generalized interpolations and sampling theorems studied in Section 3.1.3. Section 7.6.1 constructs general classes of interpolation functions from orthogonal scaling functions and derives new sampling theorems. Interpolation bases have the advantage of easily computing the decomposition coefficients from the sample values of the signal. Section 7.6.2 constructs interpolation wavelet bases.

7.6.1 Interpolation and Sampling Theorems

Section 3.1.3 explains that a sampling scheme approximates a signal by its orthogonal projection onto a space $\mathbf{U}_s$ and samples this projection at intervals s. The space $\mathbf{U}_s$ is constructed so that any function in $\mathbf{U}_s$ can be recovered by interpolating a uniform sampling at intervals s. We relate the construction of interpolation functions to orthogonal scaling functions and compute the orthogonal projector on $\mathbf{U}_s$.

An *interpolation function* any ϕ such that $\{\phi(t-n)\}_{n\in\mathbb{Z}}$ is a Riesz basis of the space $\mathbf{U}_1$ it generates, and that satisfies

$$\phi(n) = \begin{cases} 1 & \text{if } n = 0 \\ 0 & \text{if } n \neq 0. \end{cases} \tag{7.190}$$

Any $f \in \mathbf{U}_1$ is recovered by interpolating its samples $f(n)$:

$$f(t) = \sum_{n=-\infty}^{+\infty} f(n)\, \phi(t-n). \tag{7.191}$$

Indeed, we know that f is a linear combination of the basis vector $\{\phi(t-n)\}_{n\in\mathbb{Z}}$ and the interpolation property (7.190) yields (7.191). The Whittaker sampling Theorem 3.2 is based on the interpolation function

$$\phi(t) = \frac{\sin \pi t}{\pi t}.$$

In this case, space $\mathbf{U}_1$ is the set of functions having a Fourier transform support included in $[-\pi, \pi]$.

Scaling an interpolation function yields a new interpolation for a different sampling interval. Let us define $\phi_s(t) = \phi(t/s)$ and

$$\mathbf{U}_s = \left\{ f \in \mathbf{L}^2(\mathbb{R}) \quad \text{with} \quad f(st) \in \mathbf{U}_1 \right\}.$$

One can verify that any $f \in \mathbf{U}_s$ can be written as

$$f(t) = \sum_{n=-\infty}^{+\infty} f(ns)\, \phi_s(t-ns). \tag{7.192}$$

Scaling Autocorrelation

We denote by ϕ_o an orthogonal scaling function, defined by the fact that $\{\phi_o(t-n)\}_{n\in\mathbb{Z}}$ is an orthonormal basis of a space $\mathbf{V}_0$ of a multiresolution approximation. Theorem 7.2 proves that this scaling function is characterized by a conjugate mirror filter h_o. Theorem 7.20 defines an interpolation function from the autocorrelation of ϕ_o [423].

Theorem 7.20. Let $\bar{\phi}_o(t)=\phi_o(-t)$ and $\bar{h}_o[n]=h_o[-n]$. If $|\hat{\phi}_o(\omega)|=O((1+|\omega|)^{-1})$, then

$$\phi(t)=\int_{-\infty}^{+\infty}\phi_o(u)\,\phi_o(u-t)\,du=\phi_o\star\bar{\phi}_o(t) \tag{7.193}$$

is an interpolation function. Moreover,

$$\phi\left(\frac{t}{2}\right)=\sum_{n=-\infty}^{+\infty}h[n]\,\phi(t-n) \tag{7.194}$$

with

$$h[n]=\sum_{m=-\infty}^{+\infty}h_o[m]\,h_o[m-n]=h_o\star\bar{h}_o[n]. \tag{7.195}$$

Proof. Observe first that

$$\phi(n)=\langle\phi_o(t),\phi_o(t-n)\rangle=\delta[n],$$

which proves the interpolation property (7.190). To prove that $\{\phi(t-n)\}_{n\in\mathbb{Z}}$ is a Riesz basis of the space $\mathbf{U}_1$ it generates, we verify the condition (7.9). The autocorrelation $\phi(t)=\phi_o\star\bar{\phi}_o(t)$ has a Fourier transform $\hat{\phi}(\omega)=|\hat{\phi}_o(\omega)|^2$. Thus, condition (7.9) means that there exist $B\geqslant A>0$ such that

$$\forall\omega\in[-\pi,\pi],\quad A\leqslant\sum_{k=-\infty}^{+\infty}|\hat{\phi}_o(\omega-2k\pi)|^4\leqslant B. \tag{7.196}$$

We proved in (7.14) that the orthogonality of a family $\{\phi_o(t-n)\}_{n\in\mathbb{Z}}$ is equivalent to

$$\forall\omega\in[-\pi,\pi],\quad\sum_{k=-\infty}^{+\infty}|\hat{\phi}_o(\omega+2k\pi)|^2=1. \tag{7.197}$$

Therefore, the right inequality of (7.196) is valid for $A=1$. Let us prove the left inequality. Since $|\hat{\phi}_o(\omega)|=O((1+|\omega|)^{-1})$, one can verify that there exists $K>0$ such that for all $\omega\in[-\pi,\pi]$, $\sum_{|k|>K}|\hat{\phi}_o(\omega+2k\pi)|^2<1/2$, so (7.197) implies that $\sum_{k=-K}^{K}|\hat{\phi}_o(\omega+2k\pi)|^2\geqslant 1/2$. It follows that

$$\sum_{k=-K}^{K}|\hat{\phi}_o(\omega+2k\pi)|^4\geqslant\frac{1}{4(2K+1)},$$

which proves (7.196) for $A^{-1}=4(2K+1)$.

Since ϕ_o is a scaling function, (7.23) proves that there exists a conjugate mirror filter h_o such that

$$\frac{1}{\sqrt{2}}\,\phi_o\left(\frac{t}{2}\right) = \sum_{n=-\infty}^{+\infty} h_o[n]\,\phi_o(t-n).$$

Computing $\phi(t) = \phi_o \star \bar{\phi}_o(t)$ yields (7.194) with $h[n] = h_o \star \bar{h}_o[n]$. ■

Theorem 7.20 proves that the autocorrelation of an orthogonal scaling function ϕ_o is an interpolation function ϕ that also satisfies a scaling equation. One can design ϕ to approximate regular signals efficiently by their orthogonal projection in $\mathbf{U}_s$. Definition 6.1 measures the regularity of f with a Lipschitz exponent, which depends on the difference between f and its Taylor polynomial expansion. Theorem 7.21 gives a condition for recovering polynomials by interpolating their samples with ϕ. It derives an upper bound for the error when approximating f by its orthogonal projection in $\mathbf{U}_s$.

Theorem 7.21: *Fix, Strang.* Any polynomial $q(t)$ of degree smaller or equal to $p-1$ is decomposed into

$$q(t) = \sum_{n=-\infty}^{+\infty} q(n)\,\phi(t-n) \tag{7.198}$$

if and only if $\hat{h}(\omega)$ has a zero of order p at $\omega = \pi$.

Suppose that this property is satisfied. If f has a compact support and is uniformly Lipschitz $\alpha \leqslant p$, then there exists $C > 0$ such that

$$\forall s > 0, \quad \|f - P_{\mathbf{U}_s} f\| \leqslant C\, s^{\alpha}. \tag{7.199}$$

Proof. The main steps of the proof are given without technical detail. Let us set $s = 2^j$. One can verify that the spaces $\{\mathbf{V}_j = \mathbf{U}_{2^j}\}_{j\in\mathbb{Z}}$ define a multiresolution approximation of $\mathbf{L}^2(\mathbb{R})$. The Riesz basis of $\mathbf{V}_0$ required by Definition 7.1 is obtained with $\theta = \phi$. This basis is orthogonalized by Theorem 7.1 to obtain an orthogonal basis of scaling functions. Theorem 7.3 derives a wavelet orthonormal basis $\{\psi_{j,n}\}_{(j,n)\in\mathbb{Z}^2}$ of $\mathbf{L}^2(\mathbb{R})$.

Using Theorem 7.4, one can verify that ψ has p vanishing moments if and only if $\hat{h}(\omega)$ has p zeros at π. Although ϕ is not the orthogonal scaling function, the Fix-Strang condition (7.70) remains valid. It is also equivalent that for $k < p$,

$$q_k(t) = \sum_{n=-\infty}^{+\infty} n^k\,\phi(t-n)$$

is a polynomial of degree k. The interpolation property (7.191) implies that $q_k(n) = n^k$ for all $n \in \mathbb{Z}$, so $q_k(t) = t^k$. Since $\{t^k\}_{0\leqslant k<p}$ is a basis for polynomials of degree $p-1$, any polynomial $q(t)$ of degree $p-1$ can be decomposed over $\{\phi(t-n)\}_{n\in\mathbb{Z}}$ if and only if $\hat{h}(\omega)$ has p zeros at π.

We indicate how to prove (7.199) for $s = 2^j$. The truncated family of wavelets $\{\psi_{l,n}\}_{l\leqslant j, n\in\mathbb{Z}}$ is an orthogonal basis of the orthogonal complement of $\mathbf{U}_{2^j} = \mathbf{V}_j$ in $\mathbf{L}^2(\mathbb{R})$. Thus,

$$\|f - P_{\mathbf{U}_{2^j}} f\|^2 = \sum_{l=-\infty}^{j} \sum_{n=-\infty}^{+\infty} |\langle f, \psi_{l,n}\rangle|^2.$$

If f is uniformly Lipschitz α, since ψ has p vanishing moments, Theorem 6.3 proves that there exists $A > 0$ such that

$$|Wf(2^l n, 2^l)| = |\langle f, \psi_{l,n}\rangle| \leq A\, 2^{(\alpha+1/2)l}.$$

To simplify the argument we suppose that ψ has a compact support, although this is not required. Since f also has a compact support, one can verify that the number of nonzero $\langle f, \psi_{l,n}\rangle$ is bounded by $K\, 2^{-l}$ for some $K > 0$. Thus,

$$\|f - P_{\mathbf{U}_{2^j}} f\|^2 \leq \sum_{l=-\infty}^{j} K\, 2^{-l} A^2\, 2^{(2\alpha+1)l} \leq \frac{K A^2}{1 - 2^{-\alpha}}\, 2^{2\alpha j},$$

which proves (7.199) for $s = 2^j$. ■

As long as $\alpha \leq p$, the larger the Lipschitz exponent α, the faster the error $\|f - P_{\mathbf{U}_s} f\|$ decays to zero when the sampling interval s decreases. If a signal f is $\mathbf{C}^k$ with a compact support, then it is uniformly Lipschitz k, so Theorem 7.21 proves that $\|f - P_{\mathbf{U}_s} f\| \leq C\, s^k$.

EXAMPLE 7.11

A cubic spline–interpolation function is obtained from the linear spline–scaling function ϕ_o. The Fourier transform expression (7.5) yields

$$\hat{\phi}(\omega) = |\hat{\phi}_o(\omega)|^2 = \frac{48 \sin^4(\omega/2)}{\omega^4\,(1 + 2\cos^2(\omega/2))}. \tag{7.200}$$

Figure 7.19(a) gives the graph of ϕ, which has an infinite support but exponential decay. With Theorem 7.21, one can verify that this interpolation function recovers polynomials of degree

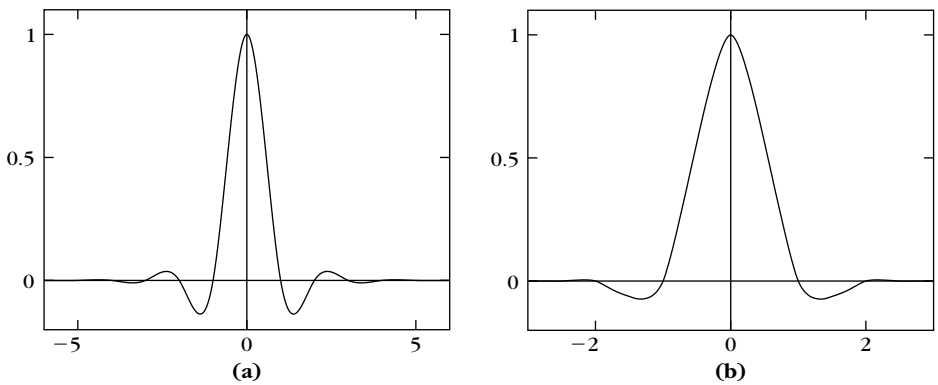

FIGURE 7.19

(a) Cubic spline–interpolation function. **(b)** Deslauriers-Dubuc interpolation function of degree 3.

3 from a uniform sampling. The performance of spline interpolation functions for generalized sampling theorems is studied in [162, 468].

EXAMPLE 7.12

Deslauriers-Dubuc [206] interpolation functions of degree $2p-1$ are compactly supported interpolation functions of minimal size that decompose polynomials of degree $2p-1$. One can verify that such an interpolation function is the autocorrelation of a scaling function ϕ_o. To reproduce polynomials of degree $2p-1$, Theorem 7.21 proves that $\hat{h}(\omega)$ must have a zero of order $2p$ at π. Since $h[n] = h_o \star \bar{h}_o[n]$, it follows that $\hat{h}(\omega) = |\hat{h}_o(\omega)|^2$, and thus $\hat{h}_o(\omega)$ has a zero of order p at π. The Daubechies theorem (7.7) designs minimum-size conjugate mirror filters h_o that satisfy this condition. Daubechies filters h_o have $2p$ nonzero coefficients and the resulting scaling function ϕ_o has a support of size $2p-1$. The autocorrelation ϕ is the Deslauriers-Dubuc interpolation function, which support $[-2p+1, 2p-1]$.

For $p=1$, $\phi_o = \mathbf{1}_{[0,1]}$ and ϕ are the piecewise linear tent functions with a support that $[-1, 1]$. For $p=2$, the Deslauriers-Dubuc interpolation function ϕ is the autocorrelation of the Daubechies 2 scaling function, shown in Figure 7.10. The graph of this interpolation function is in Figure 7.19(b). Polynomials of degree $2p-1=3$ are interpolated by this function.

The scaling equation (7.194) implies that any autocorrelation filter verifies $h[2n] = 0$ for $n \neq 0$. For any $p \geqslant 0$, the nonzero values of the resulting filter are calculated from the coefficients of the polynomial (7.168) that is factored to synthesize Daubechies filters. The support of h is $[-2p+1, 2p-1]$ and

$$h[2n+1] = (-1)^{p-n} \frac{\prod_{k=0}^{2p-1} (k-p+1/2)}{(n+1/2)\,(p-n-1)!\,(p+n)!} \quad \text{for} \quad -p \leqslant n < p. \tag{7.201}$$

Dual Basis

If $f \notin \mathbf{U}_s$, then it is approximated by its orthogonal projection $P_{\mathbf{U}_s} f$ on $\mathbf{U}_s$ before the samples at intervals s are recorded. This orthogonal projection is computed with a biorthogonal basis $\{\tilde{\phi}_s(t-ns)\}_{n\in\mathbb{Z}}$ [82]. Theorem 3.4 proves that $\tilde{\phi}_s(t) = s^{-1}\tilde{\phi}(s^{-1}t)$ where the Fourier transform of $\tilde{\phi}$ is

$$\hat{\tilde{\phi}}(\omega) = \frac{\hat{\phi}^*(\omega)}{\sum_{k=-\infty}^{+\infty} |\hat{\phi}(\omega + 2k\pi)|^2}. \tag{7.202}$$

Figure 7.20 gives the graph of the cubic spline $\tilde{\phi}$ associated to the cubic spline-interpolation function. The orthogonal projection of f over $\mathbf{U}_s$ is computed by decomposing f in the biorthogonal bases

$$P_{\mathbf{U}_s} f(t) = \sum_{n=-\infty}^{+\infty} \langle f(u), \tilde{\phi}_s(u-ns)\rangle\, \phi_s(t-ns). \tag{7.203}$$

Let $\bar{\tilde{\phi}}_s(t) = \tilde{\phi}_s(-t)$. The interpolation property (7.190) implies that

$$P_{\mathbf{U}_s} f(ns) = \langle f(u), \tilde{\phi}_s(u-ns)\rangle = f \star \bar{\tilde{\phi}}_s(ns). \tag{7.204}$$

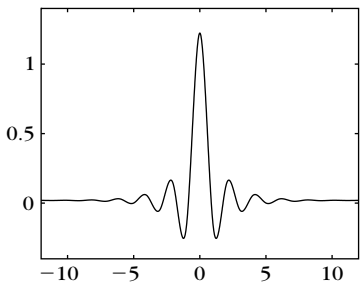

FIGURE 7.20

The dual cubic spline $\tilde{\phi}(t)$ associated to the cubic spline–interpolation function $\phi(t)$ shown in Figure 7.19(a).

Therefore, this discretization of f through a projection onto $\mathbf{U}_s$ is obtained by a filtering with $\bar{\tilde{\phi}}_s$ followed by a uniform sampling at intervals s. The best linear approximation of f is recovered with the interpolation formula (7.203).

7.6.2 Interpolation Wavelet Basis

An interpolation function ϕ can recover a signal f from a uniform sampling $\{f(ns)\}_{n\in\mathbb{Z}}$ if f belongs to an appropriate subspace $\mathbf{U}_s$ of $\mathbf{L^2}(\mathbb{R})$. Donoho [213] has extended this approach by constructing interpolation wavelet bases of the whole space of uniformly continuous signals with the supremum norm. The decomposition coefficients are calculated from sample values instead of inner product integrals.

Subdivision Scheme

Let ϕ be an interpolation function that is the autocorrelation of an orthogonal scaling function ϕ_o. Let $\phi_{j,n}(t) = \phi(2^{-j}t - n)$. The constant $2^{-j/2}$ that normalizes the energy of $\phi_{j,n}$ is not added because we shall use a supremum norm $\|f\|_\infty = \sup_{t\in\mathbb{R}} |f(t)|$ instead of the $\mathbf{L^2}(\mathbb{R})$ norm, and

$$\|\phi_{j,n}\|_\infty = \|\phi\|_\infty = |\phi(0)| = 1.$$

We define the interpolation space $\mathbf{V}_j$ of functions

$$g = \sum_{n=-\infty}^{+\infty} a[n]\,\phi_{j,n},$$

where $a[n]$ has at most a polynomial growth in n. Since ϕ is an interpolation function, $a[n] = g(2^j n)$. This space $\mathbf{V}_j$ is not included in $\mathbf{L^2}(\mathbb{R})$ since $a[n]$ may not have a finite energy. The scaling equation (7.194) implies that $\mathbf{V}_{j+1} \subset \mathbf{V}_j$ for any $j \in \mathbb{Z}$. If the autocorrelation filter h has a Fourier transform $\hat{h}(\omega)$ that has a zero of order p at $\omega = \pi$, then Theorem 7.21 proves that polynomials of a degree smaller than $p-1$ are included in $\mathbf{V}_j$.

For $f \notin \mathbf{V}_j$, we define a simple projector on $\mathbf{V}_j$ that interpolates the dyadic samples $f(2^j n)$:

$$P_{\mathbf{V}_j} f(t) = \sum_{n=-\infty}^{+\infty} f(2^j n)\, \phi_j(t - 2^j n). \tag{7.205}$$

This projector has no orthogonality property but satisfies $P_{\mathbf{V}_j} f(2^j n) = f(2^j n)$. Let $\mathbf{C}_0$ be the space of functions that are uniformly continuous over $\mathbb{R}$. Theorem 7.22 proves that any $f \in \mathbf{C}_0$ can be approximated with an arbitrary precision by $P_{\mathbf{V}_j} f$ when 2^j goes to zero.

Theorem 7.22: *Donoho.* Suppose that ϕ has an exponential decay. If $f \in \mathbf{C}_0$, then

$$\lim_{j \to -\infty} \|f - P_{\mathbf{V}_j} f\|_\infty = \lim_{j \to -\infty} \sup_{t \in \mathbb{R}} |f(t) - P_{\mathbf{V}_j} f(t)| = 0. \tag{7.206}$$

Proof. Let $\omega(\delta, f)$ denote the modulus of continuity

$$\omega(\delta, f) = \sup_{|h| \leq \delta} \sup_{t \in \mathbb{R}} |f(t+h) - f(t)|. \tag{7.207}$$

By definition, $f \in \mathbf{C}_0$ if $\lim_{\delta \to 0} \omega(\delta, f) = 0$.

Any $t \in \mathbb{R}$ can be written as $t = 2^j(n+h)$ with $n \in \mathbb{Z}$ and $|h| \leq 1$. Since $P_{\mathbf{V}_j} f(2^j n) = f(2^j n)$,

$$\begin{aligned} |f(2^j(n+h)) - P_{\mathbf{V}_j} f(2^j(n+h))| &\leq |f(2^j(n+h)) - f(2^j n)| \\ &\quad + |P_{\mathbf{V}_j} f(2^j(n+h)) - P_{\mathbf{V}_j} f(2^j n)| \\ &\leq \omega(2^j, f) + \omega(2^j, P_{\mathbf{V}_j} f). \end{aligned}$$

Lemma 7.3 proves that $\omega(2^j, P_{\mathbf{V}_j} f) \leq C_\phi\, \omega(2^j, f)$ where C_ϕ is a constant independent of j and f. Taking a supremum over $t = 2^j(n+h)$ implies the final result:

$$\sup_{t \in \mathbb{R}} |f(t) - P_{\mathbf{V}_j} f(t)| \leq (1 + C_\phi)\, \omega(2^j, f) \to 0 \quad \text{when} \quad j \to -\infty.$$

Lemma 7.3. There exists $C_\phi > 0$ such that for all $j \in \mathbb{Z}$ and $f \in \mathbf{C}_0$,

$$\omega(2^j, P_{\mathbf{V}_j} f) \leq C_\phi\, \omega(2^j, f). \tag{7.208}$$

Let us set $j = 0$. For $|h| \leq 1$, a summation by parts gives

$$P_{\mathbf{V}_0} f(t+h) - P_{\mathbf{V}_0} f(t) = \sum_{n=-\infty}^{+\infty} \big(f(n+1) - f(n)\big)\, \theta_h(t-n),$$

where

$$\theta_h(t) = \sum_{k=1}^{+\infty} \left(\phi(t+h-k) - \phi(t-k)\right).$$

Thus,

$$|P_{\mathbf{V}0}f(t+h) - P_{\mathbf{V}0}f(t)| \leqslant \sup_{n\in\mathbb{Z}} |f(n+1)-f(n)| \sum_{n=-\infty}^{+\infty} |\theta_h(t-n)|. \tag{7.209}$$

Since ϕ has an exponential decay, there exists a constant C_ϕ such that if $|h| \leqslant 1$ and $t \in \mathbb{R}$, then $\sum_{n=-\infty}^{+\infty} |\theta_h(t-n)| \leqslant C_\phi$. Taking a supremum over t in (7.209) proves that

$$\omega(1, P_{\mathbf{V}0}f) \leqslant C_\phi \sup_{n\in\mathbb{Z}} |f(n+1)-f(n)| \leqslant C_\phi\, \omega(1,f).$$

Scaling this result by 2^j yields (7.208). ■

Interpolation Wavelets

The projection $P_{\mathbf{V}_j}f(t)$ interpolates the values $f(2^j n)$. When reducing the scale by 2, we obtain a finer interpolation $P_{\mathbf{V}j-1}f(t)$ that also goes through the intermediate samples $f(2^j(n+1/2))$. This refinement can be obtained by adding "details" that compensate for the difference between $P_{\mathbf{V}_j}f(2^j(n+1/2))$ and $f(2^j(n+1/2))$. To do this, we create a "detail" space $\mathbf{W}_j$ that provides the values $f(t)$ at intermediate dyadic points $t = 2^j(n+1/2)$. This space is constructed from interpolation functions centered at these locations, namely $\phi_{j-1,2n+1}$. We call *interpolation wavelets*

$$\psi_{j,n} = \phi_{j-1,2n+1}.$$

Observe that $\psi_{j,n}(t) = \psi(2^{-j}t - n)$ with

$$\psi(t) = \phi(2t-1).$$

The function ψ is not truly a wavelet since it has no vanishing moment. However, we shall see that it plays the same role as a wavelet in this decomposition. We define $\mathbf{W}_j$ to be the space of all sums $\sum_{n=-\infty}^{+\infty} a[n]\,\psi_{j,n}$. Theorem 7.23 proves that it is a (nonorthogonal) complement of $\mathbf{V}_j$ in $\mathbf{V}_{j-1}$.

Theorem 7.23. For any $j \in \mathbb{Z}$,

$$\mathbf{V}_{j-1} = \mathbf{V}_j \oplus \mathbf{W}_j.$$

If $f \in \mathbf{V}_{j-1}$, then

$$f = \sum_{n=-\infty}^{+\infty} f(2^j n)\,\phi_{j,n} + \sum_{n=-\infty}^{+\infty} d_j[n]\,\psi_{j,n},$$

with

$$d_j[n] = f\Big(2^j\,(n+1/2)\Big) - P_{\mathbf{V}_j}f\Big(2^j\,(n+1/2)\Big). \tag{7.210}$$

Proof. Any $f \in \mathbf{V}_{j-1}$ can be written as

$$f = \sum_{n=-\infty}^{+\infty} f(2^{j-1}n)\,\phi_{j-1,n}.$$

The function $f - P_{\mathbf{V}_j} f$ belongs to $\mathbf{V}_{j-1}$ and vanishes at $\{2^j n\}_{n\in\mathbb{Z}}$. Thus, it can be decomposed over the intermediate interpolation functions $\phi_{j-1,2n+1} = \psi_{j,n}$:

$$f(t) - P_{\mathbf{V}_j} f(t) = \sum_{n=-\infty}^{+\infty} d_j[n]\, \psi_{j,n}(t) \in \mathbf{W}_j.$$

This proves that $\mathbf{V}_{j-1} \subset \mathbf{V}_j \oplus \mathbf{W}_j$. By construction we know that $\mathbf{W}_j \subset \mathbf{V}_{j-1}$, so $\mathbf{V}_{j-1} = \mathbf{V}_j \oplus \mathbf{W}_j$. Setting $t = 2^{j-1}(2n+1)$ in this formula also verifies (7.210). ■

Theorem 7.23 refines an interpolation from a coarse grid $2^j n$ to a finer grid $2^{j-1} n$ by adding "details" with coefficients $d_j[n]$ that are the interpolation errors $f(2^j(n+1/2)) - P_{\mathbf{V}_j} f(2^j(n+1/2))$. The following Theorem 7.24 defines an interpolation wavelet basis of $\mathbf{C}_0$ in the sense of uniform convergence.

Theorem 7.24. If $f \in \mathbf{C}_0$, then

$$\lim_{\substack{m\to+\infty \\ l\to-\infty}} \|f - \sum_{n=-m}^{m} f(2^J n)\, \phi_{J,n} - \sum_{j=l}^{J} \sum_{n=-m}^{m} d_j[n]\, \psi_{j,n}\|_\infty = 0. \tag{7.211}$$

The formula (7.211) decomposes f into a coarse interpolation at intervals 2^J plus layers of details that give the interpolation errors on successively finer dyadic grids. The proof is done by choosing f to be a continuous function with a compact support, in which case (7.211) is derived from Theorem 7.23 and (7.206). The density of such functions in $\mathbf{C}_0$ (for the supremum norm) allows us to extend this result to any f in $\mathbf{C}_0$. We shall write

$$f = \sum_{n=-\infty}^{+\infty} f(2^J n)\, \phi_{J,n} + \sum_{j=-\infty}^{J} \sum_{n=-\infty}^{+\infty} d_j[n]\, \psi_{j,n},$$

which means that $[\{\phi_{J,n}\}_{n\in\mathbb{Z}},\ \{\psi_{j,n}\}_{n\in\mathbb{Z}, j\leqslant J}]$ is a basis of $\mathbf{C}_0$. In $\mathbf{L^2}(\mathbb{R})$, "biorthogonal" scaling functions and wavelets are formally defined by

$$f(2^J n) = \langle f, \tilde{\phi}_{J,n} \rangle = \int_{-\infty}^{+\infty} f(t)\, \tilde{\phi}_{J,n}(t)\, dt,$$

$$d_j[n] = \langle f, \tilde{\psi}_{j,n} \rangle = \int_{-\infty}^{+\infty} f(t)\, \tilde{\psi}_{j,n}(t)\, dt. \tag{7.212}$$

Clearly, $\tilde{\phi}_{J,n}(t) = \delta(t - 2^J n)$. Similarly, (7.210) and (7.205) implies that $\tilde{\psi}_{j,n}$ is a finite sum of Diracs. These dual-scaling functions and wavelets do not have a finite energy, which illustrates the fact that $[\{\phi_{J,n}\}_{n\in\mathbb{Z}}, \{\psi_{j,n}\}_{n\in\mathbb{Z}, j\leqslant J}]$ is not a Riesz basis of $\mathbf{L^2}(\mathbb{R})$.

If $\hat{h}(\omega)$ has p zeros at π, then one can verify that $\tilde{\psi}_{j,n}$ has p vanishing moments. With similar derivations as in the proof of (6.20) in Theorem 6.4, one can show that if f is uniformly Lipschitz $\alpha \leqslant p$, then there exists $A > 0$ such that

$$|\langle f, \tilde{\psi}_{j,n} \rangle| = |d_j[n]| \leqslant A\, 2^{\alpha j}.$$

A regular signal yields small-amplitude wavelet coefficients at fine scales. Thus, we can neglect these coefficients and still reconstruct a precise approximation of f.

Fast Calculations

The interpolating wavelet transform of f is calculated at scale $1 \geqslant 2^j > N^{-1} = 2^L$ from its sample values $\{f(N^{-1}n)\}_{n\in\mathbb{Z}}$. At each scale 2^j, the values of f in between samples $\{2^j n\}_{n\in\mathbb{Z}}$ are calculated with the interpolation (7.205):

$$\begin{aligned} P_{\mathbf{V}_j} f\left(2^j\,(n+1/2)\right) &= \sum_{k=-\infty}^{+\infty} f(2^j k)\,\phi\,(n-k+1/2) \\ &= \sum_{k=-\infty}^{+\infty} f(2^j k)\,h_i[n-k], \end{aligned} \tag{7.213}$$

where the interpolation filter h_i is a subsampling of the autocorrelation filter h in (7.195):

$$h_i[n] = \phi\,(n+1/2) = h[2n+1]. \tag{7.214}$$

The wavelet coefficients are computed with (7.210):

$$d_j[n] = f\left(2^j\,(n+1/2)\right) - P_{\mathbf{V}_j} f\left(2^j\,(n+1/2)\right).$$

The reconstruction of $f(N^{-1}n)$ from the wavelet coefficients is performed recursively by recovering the samples $f(2^{j-1}n)$ from the coarser sampling $f(2^j n)$ with the interpolation (7.213) to which is added $d_j[n]$. If $h_i[n]$ is a finite filter of size K and if f has a support in $[0, 1]$, then the decomposition and reconstruction algorithms require KN multiplications and additions.

A Deslauriers-Dubuc interpolation function ϕ has the shortest support while including polynomials of degree $2p-1$ in the spaces $\mathbf{V}_j$. The corresponding interpolation filter $h_i[n]$ defined by (7.214) has $2p$ nonzero coefficients for $-p \leqslant n < p$, which are calculated in (7.201). If $p = 2$, then $h_i[1] = h_i[-2] = -1/16$ and $h_i[0] = h_i[-1] = 9/16$. Suppose that $q(t)$ is a polynomial of degree smaller or equal to $2p-1$. Since $q = P_{\mathbf{V}_j} q$, (7.213) implies a Lagrange interpolation formula

$$q\left(2^j\,(n+1/2)\right) = \sum_{k=-\infty}^{+\infty} q(2^j k)\,h_i[n-k].$$

The Lagrange filter h_i of size $2p$ is the shortest filter that recovers intermediate values of polynomials of degree $2p-1$ from a uniform sampling.

To restrict the wavelet interpolation bases to a finite interval $[0, 1]$ while reproducing polynomials of degree $2p-1$, the filter h_i is modified at the boundaries. Suppose that $f(N^{-1}n)$ is defined for $0 \leqslant n < N$. When computing the interpolation

$$P_{\mathbf{V}_j} f\left(2^j\,(n+1/2)\right) = \sum_{k=-\infty}^{+\infty} f(2^j k)\,h_i[n-k],$$

if n is too close to 0 or to $2^{-j}-1$, then h_i must be modified to ensure that the support of $h_i[n-k]$ remains inside $[0, 2^{-j}-1]$. The interpolation $P_{\mathbf{V}_j} f(2^j(n+1/2))$

is then calculated from the closest $2p$ samples $f(2^j k)$ for $2^j k \in [0, 1]$. The new interpolation coefficients are computed in order to recover exactly all polynomials of degree $2p-1$ [450]. For $p=2$, the problem occurs only at $n=0$ and the appropriate boundary coefficients are

$$h_i[0] = \frac{5}{16}, \quad h_i[-1] = \frac{15}{16}, \quad h_i[-2] = \frac{-5}{16}, \quad h_i[-3] = \frac{1}{16}.$$

The symmetric boundary filter $h_i[-n]$ is used on the other side at $n = 2^{-j} - 1$.

7.7 SEPARABLE WAVELET BASES

To any wavelet orthonormal basis $\{\psi_{j,n}\}_{(j,n)\in\mathbb{Z}^2}$ of $\mathbf{L^2}(\mathbb{R})$, one can associate a separable wavelet orthonormal basis of $\mathbf{L^2}(\mathbb{R}^2)$:

$$\left\{\psi_{j_1,n_1}(x_1)\,\psi_{j_2,n_2}(x_2)\right\}_{(j_1,j_2,n_1,n_2)\in\mathbb{Z}^4}. \tag{7.215}$$

The functions $\psi_{j_1,n_1}(x_1)\,\psi_{j_2,n_2}(x_2)$ mix information at two different scales 2^{j_1} and 2^{j_2} along x_1 and x_2, which we often want to avoid. Separable multiresolutions lead to another construction of separable wavelet bases with wavelets that are products of functions dilated at the same scale. These multiresolution approximations also have important applications in computer vision, where they are used to process images at different levels of details. Lower-resolution images are indeed represented by fewer pixels and might still carry enough information to perform a recognition task.

Signal decompositions in separable wavelet bases are computed with a separable extension of the filter bank algorithm described in Section 7.7.3. Section 7.7.4 constructs separable wavelet bases in any dimension, and explains the corresponding fast wavelet transform algorithm. Nonseparable wavelet bases can also be constructed [85, 334] but they are used less often in image processing. Section 7.8.3 gives examples of nonseparable quincunx biorthogonal wavelet bases, which have a single quasi-istropic wavelet at each scale.

7.7.1 Separable Multiresolutions

As in one dimension, the notion of resolution is formalized with orthogonal projections in spaces of various sizes. The approximation of an image $f(x_1, x_2)$ at the resolution 2^{-j} is defined as the orthogonal projection of f on a space $\mathbf{V}_j^2$ that is included in $\mathbf{L^2}(\mathbb{R}^2)$. The space $\mathbf{V}_j^2$ is the set of all approximations at the resolution 2^{-j}. When the resolution decreases, the size of $\mathbf{V}_j^2$ decreases as well. The formal definition of a multiresolution approximation $\{\mathbf{V}_j^2\}_{j\in\mathbb{Z}}$ of $\mathbf{L^2}(\mathbb{R}^2)$ is a straightforward extension of Definition 7.1 that specifies multiresolutions of $\mathbf{L^2}(\mathbb{R})$. The same causality, completeness, and scaling properties must be satisfied.

We consider the particular case of separable multiresolutions. Let $\{\mathbf{V}_j\}_{j\in\mathbb{Z}}$ be a multiresolution of $\mathbf{L}^2(\mathbb{R})$. A separable two-dimensional multiresolution is composed of the tensor product spaces

$$\mathbf{V}_j^2 = \mathbf{V}_j \otimes \mathbf{V}_j. \tag{7.216}$$

The space $\mathbf{V}_j^2$ is the set of finite energy functions $f(x_1, x_2)$ that are linear expansions of separable functions:

$$f(x_1, x_2) = \sum_{m=-\infty}^{+\infty} a[m] f_m(x_1)\, g_m(x_2) \quad \text{with} \quad f_m \in \mathbf{V}_j, \quad g_m \in \mathbf{V}_j.$$

Section A.5 reviews the properties of tensor products. If $\{\mathbf{V}_j\}_{j\in\mathbb{Z}}$ is a multiresolution approximation of $\mathbf{L}^2(\mathbb{R})$, then $\{\mathbf{V}_j^2\}_{j\in\mathbb{Z}}$ is a multiresolution approximation of $\mathbf{L}^2(\mathbb{R}^2)$.

Theorem 7.1 demonstrates the existence of a scaling function ϕ such that $\{\phi_{j,m}\}_{m\in\mathbb{Z}}$ is an orthonormal basis of $\mathbf{V}_j$. Since $\mathbf{V}_j^2 = \mathbf{V}_j \otimes \mathbf{V}_j$, Theorem A.6 proves that for $x = (x_1, x_2)$ and $n = (n_1, n_2)$,

$$\left\{ \phi_{j,n}^2(x) = \phi_{j,n_1}(x_1)\, \phi_{j,n_2}(x_2) = \frac{1}{2^j}\, \phi\Big(\frac{x_1 - 2^j n_1}{2^j}\Big)\, \phi\Big(\frac{x_2 - 2^j n_2}{2^j}\Big) \right\}_{n\in\mathbb{Z}^2}$$

is an orthonormal basis of $\mathbf{V}_j^2$. It is obtained by scaling by 2^j the two-dimensional separable scaling function $\phi^2(x) = \phi(x_1)\, \phi(x_2)$ and translating it on a two-dimensional square grid with intervals 2^j.

EXAMPLE 7.13: Piecewise Constant Approximation

Let $\mathbf{V}_j$ be the approximation space of functions that are constant on $[2^j m, 2^j(m+1)]$ for any $m \in \mathbb{Z}$. The tensor product defines a two-dimensional piecewise constant approximation. The space $\mathbf{V}_j^2$ is the set of functions that are constant on any square $[2^j n_1, 2^j(n_1+1)] \times [2^j n_2, 2^j(n_2+1)]$, for $(n_1, n_2) \in \mathbb{Z}^2$. The two-dimensional scaling function is

$$\phi^2(x) = \phi(x_1)\, \phi(x_2) = \begin{cases} 1 & \text{if } 0 \leqslant x_1 \leqslant 1 \text{ and } 0 \leqslant x_2 \leqslant 1 \\ 0 & \text{otherwise.} \end{cases}.$$

EXAMPLE 7.14: Shannon Approximation

Let $\mathbf{V}_j$ be the space of functions with Fourier transforms that have a support included in $[-2^{-j}\pi, 2^{-j}\pi]$. Space $\mathbf{V}_j^2$ is the set of functions the two-dimensional Fourier transforms of which have a support included in the low-frequency square $[-2^{-j}\pi, 2^{-j}\pi] \times [-2^{-j}\pi, 2^{-j}\pi]$. The two-dimensional scaling function is a perfect two-dimensional low-pass filter the Fourier transform of which is

$$\hat{\phi}(\omega_1)\, \hat{\phi}(\omega_2) = \begin{cases} 1 & \text{if } |\omega_1| \leqslant 2^{-j}\pi \text{ and } |\omega_2| \leqslant 2^{-j}\pi \\ 0 & \text{otherwise.} \end{cases}.$$

EXAMPLE 7.15: Spline Approximation

Let $\mathbf{V}_j$ be the space of polynomial spline functions of degree p that are $\mathbf{C}^{p-1}$ with nodes located at $2^{-j}m$ for $m \in \mathbb{Z}$. The space $\mathbf{V}_j^2$ is composed of two-dimensional polynomial spline functions that are $p-1$ times continuously differentiable. The restriction of $f(x_1, x_2) \in \mathbf{V}_j^2$ to any square $[2^j n_1, 2^j(n_1+1)] \times [2^j n_2, 2^j(n_2+1)]$ is a separable product $q_1(x_1)q_2(x_2)$ of two polynomials of degree at most p.

Multiresolution Vision

An image of 512×512 pixels often includes too much information for real-time vision processing. Multiresolution algorithms process less image data by selecting the relevant details that are necessary to perform a particular recognition task [58]. The human visual system uses a similar strategy. The distribution of photoreceptors on the retina is not uniform. The visual acuity is greatest at the center of the retina where the density of receptors is maximum. When moving apart from the center, the resolution decreases proportionally to the distance from the retina center [428].

The high-resolution visual center is called the *fovea*. It is responsible for high-acuity tasks such as reading or recognition. A retina with a uniform resolution equal to the highest fovea resolution would require about 10,000 times more photoreceptors. Such a uniform resolution retina would increase considerably the size of the optic nerve that transmits the retina information to the visual cortex and the size of the visual cortex that processes these data.

Active vision strategies [83] compensate the nonuniformity of visual resolution with eye saccades, which move successively the fovea over regions of a scene with a high information content. These saccades are partly guided by the lower-resolution information gathered at the periphery of the retina. This multiresolution sensor has the advantage of providing high-resolution information at selected locations and a large field of view with relatively little data.

Multiresolution algorithms implement in software [125] the search for important high-resolution data. A uniform high-resolution image is measured by a camera but only a small part of this information is processed. Figure 7.21 displays a pyramid of progressively lower-resolution images calculated with a filter bank presented in Section 7.7.3. Coarse to fine algorithms analyze first the lower-resolution image and selectively increase the resolution in regions where more details are needed. Such algorithms have been developed for object recognition and stereo calculations [284].

7.7.2 Two-Dimensional Wavelet Bases

A separable wavelet orthonormal basis of $\mathbf{L}^2(\mathbb{R}^2)$ is constructed with separable products of a scaling function ϕ and a wavelet ψ. The scaling function ϕ is associated to a one-dimensional multiresolution approximation $\{\mathbf{V}_j\}_{j \in \mathbb{Z}}$. Let $\{\mathbf{V}_j^2\}_{j \in \mathbb{Z}}$ be the separable two-dimensional multiresolution defined by $\mathbf{V}_j^2 = \mathbf{V}_j \otimes \mathbf{V}_j$. Let $\mathbf{W}_j^2$ be the detail

FIGURE 7.21

Multiresolution approximations $a_j[n_1, n_2]$ of an image at scales 2^j for $-5 \geqslant j \geqslant -8$.

space equal to the orthogonal complement of the lower-resolution approximation space $\mathbf{V}_j^2$ in $\mathbf{V}_{j-1}^2$:

$$\mathbf{V}_{j-1}^2 = \mathbf{V}_j^2 \oplus \mathbf{W}_j^2. \tag{7.217}$$

To construct a wavelet orthonormal basis of $\mathbf{L^2}(\mathbb{R}^2)$, Theorem 7.25 builds a wavelet basis of each detail space $\mathbf{W}_j^2$.

Theorem 7.25. Let ϕ be a scaling function and ψ be the corresponding wavelet generating a wavelet orthonormal basis of $\mathbf{L^2}(\mathbb{R})$. We define three wavelets:

$$\psi^1(x) = \phi(x_1)\,\psi(x_2), \quad \psi^2(x) = \psi(x_1)\,\phi(x_2), \quad \psi^3(x) = \psi(x_1)\,\psi(x_2), \tag{7.218}$$

and denote for $1 \leqslant k \leqslant 3$,

$$\psi_{j,n}^k(x) = \frac{1}{2^j}\,\psi^k\left(\frac{x_1 - 2^j n_1}{2^j}, \frac{x_2 - 2^j n_2}{2^j}\right).$$

The wavelet family

$$\left\{\psi_{j,n}^1, \psi_{j,n}^2, \psi_{j,n}^3\right\}_{n \in \mathbb{Z}^2} \tag{7.219}$$

is an orthonormal basis of $\mathbf{W}_j^2$, and

$$\left\{\psi_{j,n}^1, \psi_{j,n}^2, \psi_{j,n}^3\right\}_{(j,n) \in \mathbb{Z}^3} \tag{7.220}$$

is an orthonormal basis of $\mathbf{L^2}(\mathbb{R}^2)$.

Proof. Equation (7.217) is rewritten as

$$\mathbf{V}_{j-1} \otimes \mathbf{V}_{j-1} = (\mathbf{V}_j \otimes \mathbf{V}_j) \oplus \mathbf{W}_j^2. \tag{7.221}$$

The one-dimensional multiresolution space $\mathbf{V}_{j-1}$ can also be decomposed into $\mathbf{V}_{j-1} = \mathbf{V}_j \oplus \mathbf{W}_j$. By inserting this in (7.221), the distributivity of $\oplus$ with respect to $\otimes$ proves that

$$\mathbf{W}_j^2 = (\mathbf{V}_j \otimes \mathbf{W}_j) \oplus (\mathbf{W}_j \otimes \mathbf{V}_j) \oplus (\mathbf{W}_j \otimes \mathbf{W}_j). \tag{7.222}$$

Since $\{\phi_{j,m}\}_{m\in\mathbb{Z}}$ and $\{\psi_{j,m}\}_{m\in\mathbb{Z}}$ are orthonormal bases of $\mathbf{V}_j$ and $\mathbf{W}_j$, we derive that

$$\left\{\phi_{j,n_1}(x_1)\,\psi_{j,n_2}(x_2),\ \psi_{j,n_1}(x_1)\,\phi_{j,n_2}(x_2),\ \psi_{j,n_1}(x_1)\,\psi_{j,n_2}(x_2)\right\}_{(n_1,n_2)\in\mathbb{Z}^2}$$

is an orthonormal basis of $\mathbf{W}_j^2$. As in the one-dimensional case, the overall space $\mathbf{L^2}(\mathbb{R}^2)$ can be decomposed as an orthogonal sum of the detail spaces at all resolutions:

$$\mathbf{L^2}(\mathbb{R}^2) = \oplus_{j=-\infty}^{+\infty} \mathbf{W}_j^2. \tag{7.223}$$

Thus,

$$\left\{\phi_{j,n_1}(x_1)\,\psi_{j,n_2}(x_2),\ \psi_{j,n_1}(x_1)\,\phi_{j,n_2}(x_2),\ \psi_{j,n_1}(x_1)\,\psi_{j,n_2}(x_2)\right\}_{(j,n_1,n_2)\in\mathbb{Z}^3}$$

is an orthonormal basis of $\mathbf{L^2}(\mathbb{R}^2)$. ■

The three wavelets extract image details at different scales and in different directions. Overpositive frequencies, $\hat{\phi}$ and $\hat{\psi}$ have an energy mainly concentrated, respectively, on $[0, \pi]$ and $[\pi, 2\pi]$. The separable wavelet expressions (7.218) imply that

$$\hat{\psi}^1(\omega_1, \omega_2) = \hat{\phi}(\omega_1)\,\hat{\psi}(\omega_2), \quad \hat{\psi}^2(\omega_1, \omega_2) = \hat{\psi}(\omega_1)\,\hat{\phi}(\omega_2),$$

and $\hat{\psi}^3(\omega_1, \omega_2) = \hat{\psi}(\omega_1)\,\hat{\psi}(\omega_2)$. Thus, $|\hat{\psi}^1(\omega_1, \omega_2)|$ is large at low horizontal frequencies ω_1 and high vertical frequencies ω_2, whereas $|\hat{\psi}^2(\omega_1, \omega_2)|$ is large at high horizontal frequencies and low vertical frequencies, and $|\hat{\psi}_3(\omega_1, \omega_2)|$ is large at high horizontal and vertical frequencies. Figure 7.22 displays the Fourier transform of separable wavelets and scaling functions calculated from a one-dimensional Daubechies 4 wavelet.

Suppose that $\psi(t)$ has p vanishing moments and is orthogonal to one-dimensional polynomials of degree $p-1$. The wavelet ψ^1 has p one-dimensional directional vanishing moments along x_2 in the sense that it is orthogonal to any function $f(x_1, x_2)$ that is a polynomial of degree $p-1$ along x_2 for x_1 fixed. It is a horizontal directional wavelet that yields large coefficients for horizontal edges, as explained in Section 5.5.1. Similarly, ψ^2 has $p-1$ directional vanishing moments along x_1 and is a vertical directional wavelet. This is illustrated by the decomposition of a square later in Figure 7.24. The wavelet ψ^3 has directional vanishing moments along both x_1 and x_2 and is therefore not a directional wavelet. It produces large coefficients

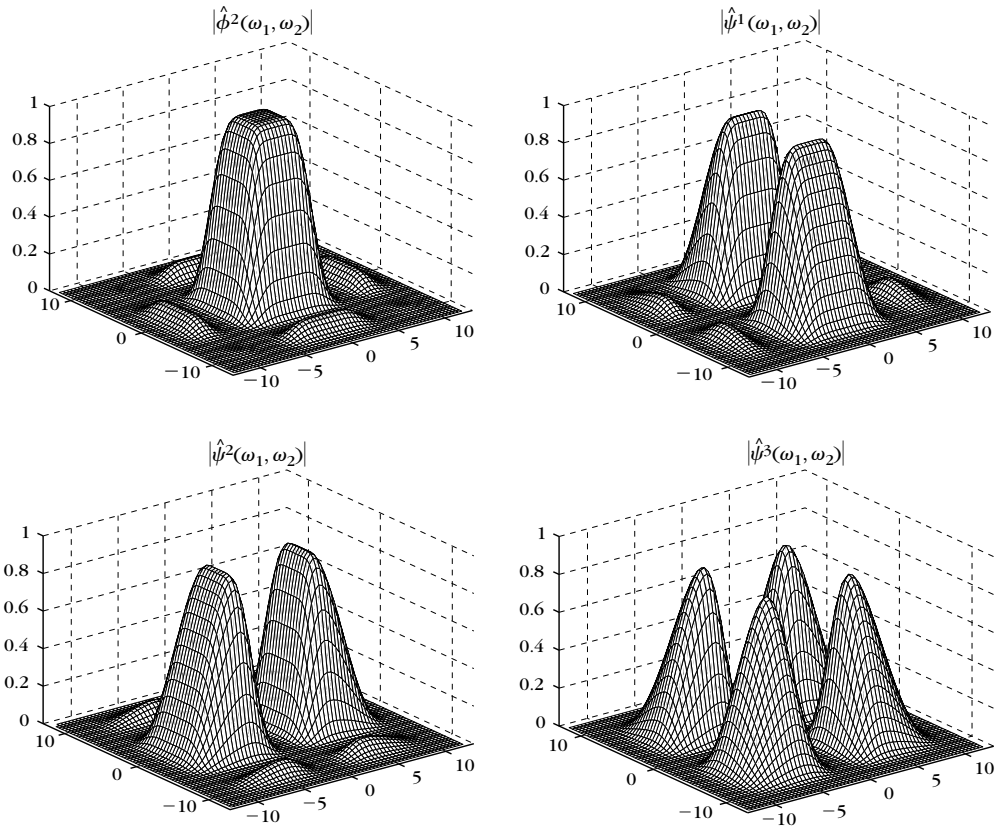

FIGURE 7.22

Fourier transforms of a separable scaling function and of three separable wavelets calculated from a one-dimensional Daubechies 4 wavelet.

at corners or junctions. The three wavelets ψ^k for $k = 1, 2, 3$ are orthogonal to two-dimensional polynomials of degree $p - 1$.

EXAMPLE 7.16

For a Shannon multiresolution approximation, the resulting two-dimensional wavelet basis paves the two-dimensional Fourier plane (ω_1, ω_2) with dilated rectangles. The Fourier transforms $\hat{\phi}$ and $\hat{\psi}$ are the indicator functions of $[-\pi, \pi]$ and $[-2\pi, -\pi] \cup [\pi, 2\pi]$, respectively. The separable space $\mathbf{V}_j^2$ contains functions with a two-dimensional Fourier transform support included in the low-frequency square $[-2^{-j}\pi, 2^{-j}\pi] \times [-2^{-j}\pi, 2^{-j}\pi]$. This corresponds to the support of $\hat{\phi}_{j,n}^2$ indicated in Figure 7.23.

The detail space $\mathbf{W}_j^2$ is the orthogonal complement of $\mathbf{V}_j^2$ in $\mathbf{V}_{j-1}^2$ and thus includes functions with Fourier transforms supported in the frequency annulus between the two squares

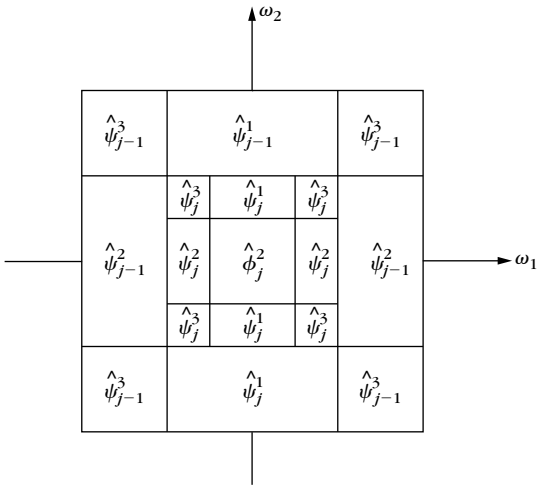

FIGURE 7.23

These dyadic rectangles indicate the regions where the energy of $\hat{\psi}^k_{j,n}$ is mostly concentrated for $1 \leq k \leq 3$. Image approximations at the scale 2^j are restricted to the lower-frequency square.

$[-2^{-j}\pi, 2^{-j}\pi] \times [-2^{-j}\pi, 2^{-j}\pi]$ and $[-2^{-j+1}\pi, 2^{-j+1}\pi] \times [-2^{-j+1}\pi, 2^{-j+1}\pi]$. As shown in Figure 7.23, this annulus is decomposed in three separable frequency regions, which are the Fourier supports of $\hat{\psi}^k_{j,n}$ for $1 \leq k \leq 3$. Dilating these supports at all scales 2^j yields an exact cover of the frequency plane (ω_1, ω_2).

For general separable wavelet bases, Figure 7.23 gives only an indication of the domains where the energy of the different wavelets is concentrated. When the wavelets are constructed with a one-dimensional wavelet of compact support, the resulting Fourier transforms have side lobes that appear in Figure 7.22.

EXAMPLE 7.17

Figure 7.24 gives two examples of wavelet transforms computed using separable Daubechies wavelets with $p = 4$ vanishing moments. They are calculated with the filter bank algorithm from Section 7.7.3. Coefficients of large amplitude in d^1_j, d^2_j, and d^3_j correspond, respectively, to vertical high frequencies (horizontal edges), horizontal high frequencies (vertical edges), and high frequencies in both directions (corners). Regions where the image intensity varies smoothly yield nearly zero coefficients, shown in gray in the figure. The large number of nearly zero coefficients makes it particularly attractive for compact image coding.

Separable Biorthogonal Bases

One-dimensional biorthogonal wavelet bases are extended to separable biorthogonal bases of $\mathbf{L^2}(\mathbb{R}^2)$ with the same approach as in Theorem 7.25. Let ϕ, ψ and $\tilde{\phi}$,

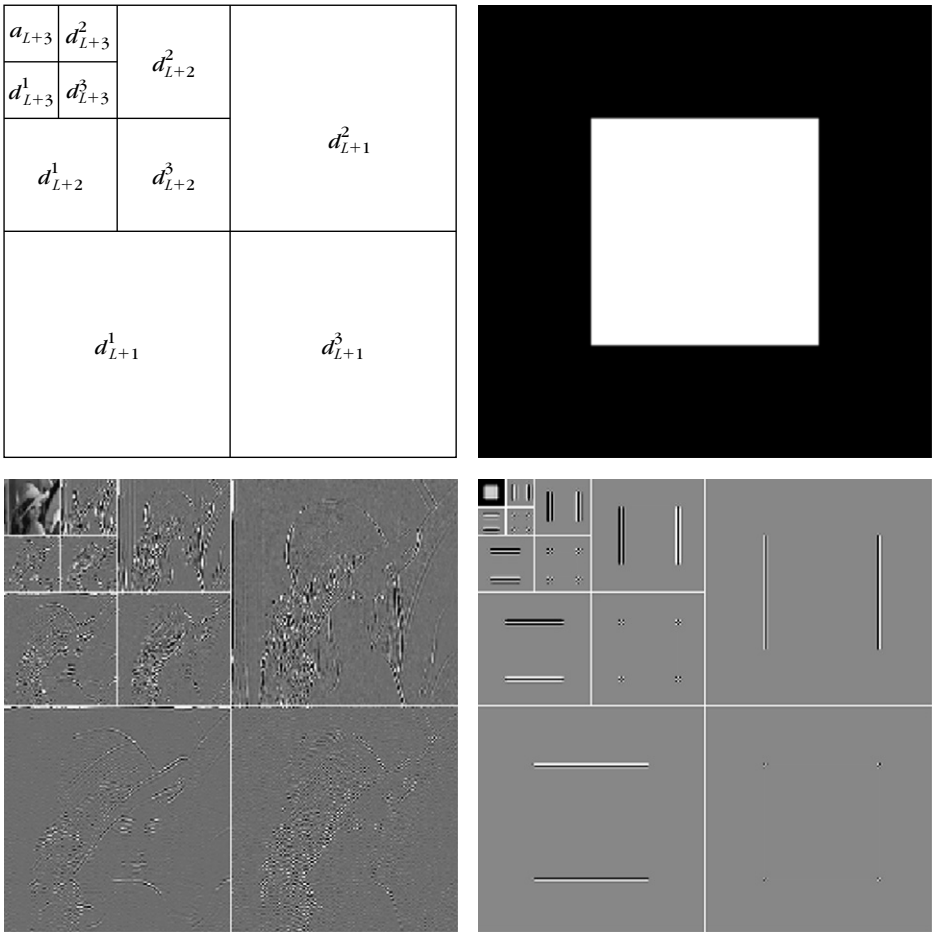

FIGURE 7.24

Separable wavelet transforms of the Lena image and of a white square in a black background, decomposed on 3 and 4 octaves, respectively. Black, gray, and white pixels correspond, respectively, to positive, zero, and negative wavelet coefficients. The disposition of wavelet image coefficients $d_j^k[n, m] = \langle f, \psi_{j,n}^k \rangle$ is illustrated on the top left.

$\tilde{\psi}$ be two dual pairs of scaling functions and wavelets that generate biorthogonal wavelet bases of $\mathbf{L^2}(\mathbb{R})$. The dual wavelets of ψ^1, ψ^2, and ψ^3 defined by (7.218) are

$$\tilde{\psi}^1(x) = \tilde{\phi}(x_1)\,\tilde{\psi}(x_2), \quad \tilde{\psi}^2(x) = \tilde{\psi}(x_1)\,\tilde{\phi}(x_2), \quad \tilde{\psi}^3(x) = \tilde{\psi}(x_1)\,\tilde{\psi}(x_2). \tag{7.224}$$

One can verify that

$$\left\{\psi_{j,n}^1, \psi_{j,n}^2, \psi_{j,n}^3\right\}_{(j,n)\in\mathbb{Z}^3} \tag{7.225}$$

and

$$\left\{\tilde{\psi}^1_{j,n}, \tilde{\psi}^2_{j,n}, \tilde{\psi}^3_{j,n}\right\}_{(j,n)\in\mathbb{Z}^3} \tag{7.226}$$

are biorthogonal Riesz bases of $\mathbf{L^2}(\mathbb{R}^2)$.

7.7.3 Fast Two-Dimensional Wavelet Transform

The fast wavelet transform algorithm presented in Section 7.3.1 is extended in two dimensions. At all scales 2^j and for any $n = (n_1, n_2)$, we denote

$$a_j[n] = \langle f, \phi^2_{j,n}\rangle \quad \text{and} \quad d^k_j[n] = \langle f, \psi^k_{j,n}\rangle \quad \text{for} \quad 1 \leqslant k \leqslant 3.$$

For any pair of one-dimensional filters $y[m]$ and $z[m]$ we write the product filter $yz[n] = y[n_1]\,z[n_2]$ and $\bar{y}[m] = y[-m]$. Let $h[m]$ and $g[m]$ be the conjugate mirror filters associated to the wavelet ψ.

The wavelet coefficients at the scale 2^{j+1} are calculated from a_j with two-dimensional separable convolutions and subsamplings. The decomposition formulas are obtained by applying the one-dimensional convolution formulas (7.102) and (7.103) of Theorem 7.10 to the separable two-dimensional wavelets and scaling functions for $n = (n_1, n_2)$:

$$a_{j+1}[n] = a_j \star \bar{h}\bar{h}[2n], \tag{7.227}$$

$$d^1_{j+1}[n] = a_j \star \bar{h}\bar{g}[2n], \tag{7.228}$$

$$d^2_{j+1}[n] = a_j \star \bar{g}\bar{h}[2n], \tag{7.229}$$

$$d^3_{j+1}[n] = a_j \star \bar{g}\bar{g}[2n]. \tag{7.230}$$

We showed in (3.70) that a separable two-dimensional convolution can be factored into one-dimensional convolutions along the rows and columns of the image. With the factorization illustrated in Figure 7.25(a), these four convolutions equations are computed with only six groups of one-dimensional convolutions. The rows of a_j are first convolved with $\bar{h}$ and $\bar{g}$ and subsampled by 2. The columns of these two output images are then convolved, respectively, with $\bar{h}$ and $\bar{g}$ and subsampled, which gives the four subsampled images $a_{j+1}, d^1_{j+1}, d^2_{j+1}$, and d^3_{j+1}.

We denote by $\check{y}[n] = \check{y}[n_1, n_2]$ the image twice the size of $y[n]$, obtained by inserting a row of zeros and a column of zeros between pairs of consecutive rows and columns. The approximation a_j is recovered from the coarser-scale approximation a_{j+1} and the wavelet coefficients d^k_{j+1} with two-dimensional separable convolutions derived from the one-dimensional reconstruction formula (7.104)

$$a_j[n] = \check{a}_{j+1} \star hh[n] + \check{d}^1_{j+1} \star hg[n] + \check{d}^2_{j+1} \star gh[n] + \check{d}^3_{j+1} \star gg[n]. \tag{7.231}$$

These four separable convolutions can also be factored into six groups of one-dimensional convolutions along rows and columns, illustrated in Figure 7.25(b).

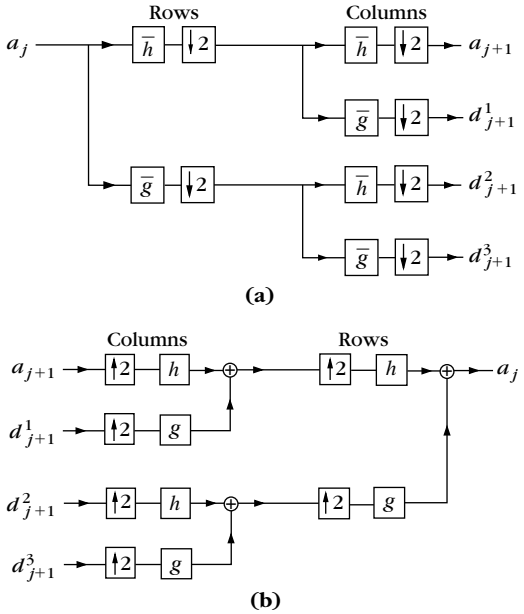

FIGURE 7.25

(a) Decomposition of a_j with six groups of one-dimensional convolutions and subsamplings along the image rows and columns. **(b)** Reconstruction of a_j by inserting zeros between the rows and columns of a_{j+1} and d^k_{j+1}, and filtering the output.

Let $b[n]$ be an input image with pixels at a distance 2^L. We associate to $b[n]$ a function $f(x) \in \mathbf{V}_L^2$ approximated at the scale 2^L. Its coefficients $a_L[n] = \langle f, \phi^2_{L,n} \rangle$ are defined like in (7.111) by

$$b[n] = 2^{-L} a_L[n] \approx f(2^L n). \tag{7.232}$$

The wavelet image representation of a_L is computed by iterating (7.227–7.230) for $L \leqslant j < J$:

$$\left[a_J, \{d^1_j, d^2_j, d^3_j\}_{L<j\leqslant J} \right]. \tag{7.233}$$

The image a_L is recovered from this wavelet representation by computing (7.231) for $J > j \geqslant L$.

Finite Image and Complexity

When a_L is a finite image of $N = N_1 N_2$ pixels, we face boundary problems when computing the convolutions (7.227–7.231). Since the decomposition algorithm is separable along rows and columns, we use one of the three one-dimensional boundary techniques described in Section 7.5. The resulting values are decomposition

coefficients in a wavelet basis of $\mathbf{L^2}[0, 1]^2$. Depending on the boundary treatment, this wavelet basis is a periodic basis, a folded basis, or a boundary adapted basis.

For square images with $N_1 = N_2$, the resulting images a_j and d_j^k have 2^{-2j} samples. Thus, the images of the wavelet representation (7.233) include a total of N samples. If h and g have size K, the reader can verify that $2K2^{-2(j-1)}$ multiplications and additions are needed to compute the four convolutions (7.227–7.230) with the factorization of Figure 7.25(a). Thus, the wavelet representation (7.233) is calculated with fewer than $8/3\ KN$ operations. The reconstruction of a_L by factoring the reconstruction equation (7.231) requires the same number of operations.

Fast Biorthogonal Wavelet Transform

The decomposition of an image in a biorthogonal wavelet basis is performed with the same fast wavelet transform algorithm. Let $(\tilde{h}, \tilde{g})$ be the perfect reconstruction filters associated to (h, g). The inverse wavelet transform is computed by replacing the filters (h, g) that appear in (7.231) by $(\tilde{h}, \tilde{g})$.

7.7.4 Wavelet Bases in Higher Dimensions

Separable wavelet orthonormal bases of $\mathbf{L^2}(\mathbb{R}^p)$ are constructed for any $p \geqslant 2$ with a procedure similar to the two-dimensional extension. Let ϕ be a scaling function and ψ a wavelet that yields an orthogonal basis of $\mathbf{L^2}(\mathbb{R})$. We denote $\theta^0 = \phi$ and $\theta^1 = \psi$. To any integer $0 \leqslant \varepsilon < 2^p$ written in binary form $\varepsilon = \varepsilon_1, \ldots, \varepsilon_p$, we associate the p-dimensional functions defined in $x = (x_1, \ldots, x_p)$ by

$$\psi^{\varepsilon}(x) = \theta^{\varepsilon_1}(x_1) \ldots \theta^{\varepsilon_n}(x_p).$$

For $\varepsilon = 0$, we obtain a p-dimensional scaling function

$$\psi^0(x) = \phi(x_1) \ldots \phi(x_p).$$

Nonzero indexes ε correspond to $2^p - 1$ wavelets. At any scale 2^j and for $n = (n_1, \ldots, n_p)$, we denote

$$\psi_{j,n}^{\varepsilon}(x) = 2^{-pj/2}\, \psi^{\varepsilon}\Big(\frac{x_1 - 2^j n_1}{2^j}, \ldots, \frac{x_p - 2^j n_p}{2^j}\Big).$$

Theorem 7.26. The family obtained by dilating and translating the $2^p - 1$ wavelets for $\varepsilon \neq 0$,

$$\left\{\psi_{j,n}^{\varepsilon}\right\}_{1 \leqslant \varepsilon < 2^p,\ (j,n) \in \mathbb{Z}^{p+1}}, \tag{7.234}$$

is an orthonormal basis of $\mathbf{L^2}(\mathbb{R}^p)$.

The proof is done by induction on p. It follows the same steps as the proof of Theorem 7.25, which associates to a wavelet basis of $\mathbf{L^2}(\mathbb{R})$ a separable wavelet basis of $\mathbf{L^2}(\mathbb{R}^2)$. For $p = 2$, we verify that the basis (7.234) includes three elementary wavelets. For $p = 3$, there are seven different wavelets.

Fast Wavelet Transform

Let $b[n]$ be an input p-dimensional discrete signal sampled at intervals 2^L. We associate $b[n]$ to an approximation f at the scale 2^L with scaling coefficients $a_L[n] = \langle f, \psi^0_{L,n} \rangle$ that satisfy

$$b[n] = 2^{-Lp/2}\, a_L[n] \approx f(2^L n).$$

The wavelet coefficients of f at scales $2^j > 2^L$ are computed with separable convolutions and subsamplings along the p signal dimensions. We denote

$$a_j[n] = \langle f, \psi^0_{j,n} \rangle \quad \text{and} \quad d^\varepsilon_j[n] = \langle f, \psi^\varepsilon_{j,n} \rangle \quad \text{for} \quad 0 < \varepsilon < 2^p.$$

The fast wavelet transform is computed with filters that are separable products of the one-dimensional filters h and g. The separable p-dimensional low-pass filter is

$$h^0[n] = h[n_1] \ldots h[n_p].$$

Let us denote $u^0[m] = h[m]$ and $u^1[m] = g[m]$. To any integer $\varepsilon = \varepsilon_1, \ldots, \varepsilon_p$ written in a binary form, we associate a separable p-dimensional band-pass filter

$$g^\varepsilon[n] = u^{\varepsilon_1}[n_1] \ldots u^{\varepsilon_p}[n_p].$$

Let $\bar{g}^\varepsilon[n] = g^\varepsilon[-n]$. One can verify that

$$a_{j+1}[n] = a_j \star \bar{h}^0[2n], \tag{7.235}$$

$$d^\varepsilon_{j+1}[n] = a_j \star \bar{g}^\varepsilon[2n]. \tag{7.236}$$

We denote by $\check{y}[n]$ the signal obtained by adding a zero between any two samples of $y[n]$ that are adjacent in the p-dimensional lattice $n = (n_1, \ldots, n_p)$. It doubles the size of $y[n]$ along each direction. If $y[n]$ has M^p samples, then $\check{y}[n]$ has $(2M)^p$ samples. The reconstruction is performed with

$$a_j[n] = \check{a}_{j+1} \star h^0[n] + \sum_{\varepsilon=1}^{2^p-1} \check{d}^\varepsilon_{j+1} \star g^\varepsilon[n]. \tag{7.237}$$

The 2^p separable convolutions needed to compute a_j and $\{d^\varepsilon_j\}_{1 \leqslant \varepsilon \leqslant 2^p}$ as well as the reconstruction (7.237) can be factored in $2^{p+1} - 2$ groups of one-dimensional convolutions along the rows of p-dimensional signals. This is a generalization of the two-dimensional case, illustrated in Figure 7.25. The wavelet representation of a_L is

$$\left[\{d^\varepsilon_j\}_{1 \leqslant \varepsilon < 2^p,\, L < j \leqslant J},\, a_J \right]. \tag{7.238}$$

It is computed by iterating (7.235) and (7.236) for $L \leqslant j < J$. The reconstruction of a_L is performed with the partial reconstruction (7.237) for $J > j \geqslant L$.

If a_L is a finite signal of size $N_1, \cdots, N_p$, the one-dimensional convolutions are modified with one of the three boundary techniques described in Section 7.5. The resulting algorithm computes decomposition coefficients in a separable wavelet

basis of $\mathbf{L^2}[0,1]^p$. If $N_1 = \cdots = N_p$, the signals a_j and d_j^ε have 2^{-pj} samples. Like a_L, the wavelet representation (7.238) is composed of N samples. If the filter h has K nonzero samples, then the separable factorization of (7.235) and (7.236) requires $pK2^{-p(j-1)}$ multiplications and additions. Thus, the wavelet representation (7.238) is computed with fewer than $p(1-2^{-p})^{-1}KN$ multiplications and additions. The reconstruction is performed with the same number of operations.

7.8 LIFTING WAVELETS

The lifting scheme, introduced by Sweldens [451, 452], factorizes orthogonal and biorthogonal wavelet transforms into elementary spatial operators called *liftings*. It has two main applications. The first one is an acceleration of the fast wavelet transform algorithm. The filter bank convolution and subsampling operations are factorized into elementary filterings on even and odd samples, which reduces the number of operations by nearly 2. Border treatments are also simplified. This is also called a *paraunitary filter bank implementation*. Readers mainly interested in this fast lifting implementation can skip directly to Section 7.8.5, which can be read independently.

The second application is the design of wavelets adapted to multidimensional-bounded domains and surfaces, which is not possible with a Fourier transform approach. Section 7.8.1 introduces biorthogonal multiresolution and wavelet bases over nonstationary grids for arbitrary domains. The lifting construction of biorthogonal wavelet bases is explained in Section 7.8.2, with the resulting fast lifting wavelet transform. Section 7.8.3 describes an application to nonseparable quincunx wavelet bases for images. The construction of wavelet bases over bounded domains and surfaces is explained in Section 7.8.4, with computer graphics examples.

7.8.1 Biorthogonal Bases over Nonstationary Grids

The lifting scheme constructs wavelet bases over an arbitrary domain Ω to represent functions of finite energy defined over Ω. This section defines biorthogonal filters and wavelets that may be modified both in space and in scale to be adapted to the domain geometry. Section 7.8.2 explains the calculation of these filters and wavelets with a lifting scheme.

Embedded Grids

Biorthogonal multiresolutions, defined in Section 7.4, are generalized by considering nested spaces

$$\{0\} \subset \ldots \subset \mathbf{V}_{j+1} \subset \mathbf{V}_j \subset \mathbf{V}_{j-1} \subset \ldots \subset \mathbf{L}^2(\Omega),$$

which are defined over embedded approximation grids $\mathcal{G}_j \subset \mathcal{G}_{j-1}$. Each index $n \in \mathcal{G}_j$ is associated to a sampling point $x_n \in \Omega$. Since the sampling grids are embedded,

this position does not change when the index is moved to finer grids $n \in \mathcal{G}_k$ for $k \leqslant j$. Each space $\mathbf{V}_j$ is equipped with a Riesz basis $\{\phi_{j,n}\}_{n\in\mathcal{G}_j}$ parameterized by the approximation grid $\mathcal{G}_j$.

Embedded grids are decomposed with complementary grids $\mathcal{C}_j$:

$$\mathcal{G}_{j-1} = \mathcal{G}_j \cup \mathcal{C}_j.$$

For example, over the interval $[0, 1]$, the grid $\mathcal{G}_{j-1}$ is the set of $2^{j-1}n \in [0, 1]$ for $0 \leqslant n < 2^{-j}$. It is decomposed into the even grid points of $2^{j-1}2n$ of $\mathcal{G}_j$ and the odd grid points $2^{j-1}(2n+1)$ of $\mathcal{C}_j$. A corresponding vector space decomposition is defined $\mathbf{V}_{j-1} = \mathbf{V}_j \oplus \mathbf{W}_j$, where the detail space $\mathbf{W}_j$ has a Riesz basis of wavelets $\{\psi_{j,m}\}_{m\in\mathcal{C}_j}$ indexed on the complementary grid $\mathcal{C}_j$.

A dual-biorthogonal wavelet family $\{\tilde{\psi}_{j,m}\}_{m\in\mathcal{G}_j}$ and a dual basis of scaling functions $\{\tilde{\phi}_{j,n}\}_{n\in\mathcal{G}_j}$ satisfy the biorthogonality conditions

$$\langle \phi_{j,n},\, \tilde{\phi}_{j,n'} \rangle = \delta[n-n'] \quad \text{and} \quad \langle \psi_{j,m},\, \tilde{\psi}_{j',m'} \rangle = \delta[j-j']\,\delta[m-m']. \tag{7.239}$$

The resulting wavelet families $\{\psi_{j,m}\}_{m\in\mathcal{G}_j, j\in\mathbb{Z}}$ and $\{\tilde{\psi}_{j,m}\}_{m\in\mathcal{G}_j, j\in\mathbb{Z}}$ are biorthogonal wavelet bases of $\mathbf{L^2}(\Omega)$, which implies that for any $f \in \mathbf{L^2}(\Omega)$,

$$f = \sum_{n\in\mathcal{G}_J} \langle f,\, \phi_{J,n} \rangle\, \tilde{\phi}_{J,n} + \sum_{j\geqslant J} \sum_{m\in\mathcal{C}_j} \langle f,\, \psi_{j,m} \rangle\, \tilde{\psi}_{j,m},$$

where 2^J is an arbitrary coarsest scale. The difference with the biorthogonal wavelets of Section 7.4 is that scaling functions and wavelets are typically not translations and dilations of mother scaling functions and wavelets to be adapted to Ω. As a result, the decomposition filters are not convolution filters.

Spatially Varying Filters

The spatially varying filters associated to this biorthogonal multiresolution satisfy

$$\phi_{j,n} = \sum_{l\in\mathcal{G}_{j-1}} h_j[n,l]\,\phi_{j-1,l} \quad \text{and} \quad \psi_{j,m} = \sum_{l\in\mathcal{G}_{j-1}} g_j[m,l]\,\phi_{j-1,l}. \tag{7.240}$$

Over a translation-invariant domain, $h_j[n,l] = h[n-2l]$ are the perfect reconstruction filters of Section 7.3.2. Dual filters $\tilde{h}$ and $\tilde{g}$ are defined similarly by

$$\tilde{\phi}_{j,n} = \sum_{l\in\mathcal{G}_{j-1}} \tilde{h}_j[n,l]\,\tilde{\phi}_{j-1,l} \quad \text{and} \quad \tilde{\psi}_{j,m} = \sum_{l\in\mathcal{G}_{j-1}} \tilde{g}_j[m,l]\,\tilde{\phi}_{j-1,l}. \tag{7.241}$$

The biorthogonality relations (7.239) between wavelets and scaling functions imply equivalent biorthogonality filter relations for all $n, n' \in \mathcal{G}_j$ and $m, m' \in \mathcal{C}_j$:

$$\sum_{l\in\mathcal{G}_{j-1}} g_j[m,l]\,\tilde{g}_j[m',l] = \delta[m-m'] \qquad \sum_{l\in\mathcal{G}_{j-1}} h_j[n,l]\,\tilde{h}_j[n',l] = \delta[n-n'], \tag{7.242}$$

$$\sum_{l\in\mathcal{G}_{j-1}} g_j[m,l]\,\tilde{h}_j[n,l] = 0 \qquad \sum_{l\in\mathcal{G}_{j-1}} h_j[n,l]\,\tilde{g}_j[m,l] = 0. \tag{7.243}$$

Wavelets and scaling functions can be written as an infinite product of these filters. If these products converge in $\mathbf{L}^2(\Omega)$ and the filters that satisfy (7.242) and (7.243), then the resulting wavelets and scaling functions define biorthogonal bases of $\mathbf{L}^2(\Omega)$, which satisfy (7.239) [452].

To simplify notations, the filters h_j and g_j are also written as matrices that transform discrete vector

$$\forall\, a \in \mathbb{C}^{|\mathcal{G}_{j-1}|}, \quad \forall\, n \in \mathcal{G}_j,\ (H_j a)[n] = \sum_{l \in \mathcal{G}_{j-1}} h_j[n,l]\, a[l]$$

$$\forall\, a \in \mathbb{C}^{|\mathcal{G}_{j-1}|}, \quad \forall\, m \in \mathcal{C}_j,\ (G_j a)[m] = \sum_{l \in \mathcal{G}_{j-1}} g_j[m,l]\, a[l]$$

and similarly for the dual matrices $\tilde{H}_j$ and $\tilde{G}_j$.

The biorthogonality conditions (7.242) are rewritten as

$$\begin{bmatrix} \tilde{H}_j \\ \tilde{G}_j \end{bmatrix} \begin{bmatrix} H_j^* & G_j^* \end{bmatrix} = \begin{bmatrix} \mathrm{Id}_{\mathcal{G}_j} & 0 \\ 0 & \mathrm{Id}_{\mathcal{C}_j} \end{bmatrix}, \tag{7.244}$$

where A^* is the complex transpose of a matrix A.

Vanishing Moments

Wavelets with p_1 vanishing moments are orthogonal to polynomials of a degree strictly smaller than p_1. Let d_1 be the dimension of the space of polynomials of degree $q-1$ in dimension d. If $d=1$, then $d_1 = p_1$, and if $d=2$, then $d_1 = p_1(p_1+1)/2$. Such wavelets are orthogonal to a basis $\{q^{(k)}\}_{0 \leq k < d_1}$ of this polynomial space, defined over $\Omega \subset \mathbb{R}^d$:

$$\forall\, j,\ \forall\, m \in \mathcal{C}_j,\ \forall\, k < d_1, \quad \int_\Omega \psi_{j,m}(x)\, q^{(k)}(x)\, dx = 0, \tag{7.245}$$

and similarly for dual wavelets with p_2 vanishing moments,

$$\forall\, j,\ \forall\, m \in \mathcal{C}_j,\ \forall\, k < d_2, \quad \int_\Omega \tilde{\psi}_{j,m}(x)\, q^{(k)}(x)\, dx = 0.$$

Lifting steps are used to increase the number of vanishing moments.

7.8.2 Lifting Scheme

The lifting scheme builds filters over arbitrary domains Ω as a succession of elementary lifting steps applied to lazy wavelets that are Diracs. Each lifting step transforms a family of biorthogonal filters into new biorthogonal filters that define wavelets with more vanishing moments.

Lazy Wavelets

A lifting begins from lazy wavelets, which are Diracs on grid points. The lazy discrete orthogonal wavelet transform just splits the coefficients of a grid $\mathcal{G}_{j-1}$ into the two

subgrids $\mathcal{G}_j$ and $\mathcal{C}_j$. It corresponds to filters that are Diracs on these grids:

$$\forall\, l \in \mathcal{G}_{j-1},\ \forall\, n \in \mathcal{G}_j,\ \forall\, m \in \mathcal{C}_j, \quad \begin{cases} h_j^o[n,l] = \tilde{h}_j^o[n,l] = \delta[n-l], \\ g_j^o[m,l] = \tilde{g}_j^o[m,l] = \delta[m-l]. \end{cases}$$

For $a \in \mathbb{C}^{|\mathcal{G}_{j-1}|}$, the vector $H_j^o a \in \mathbb{C}^{|\mathcal{G}_j|}$ is the restriction of a to $\mathcal{G}_j$, and $G_j^o a \in \mathbb{C}^{|\mathcal{C}_j|}$ is the restriction of a to $\mathcal{C}_j$.

Since each index $n \in \mathcal{G}_j$ is associated to a sampling point $x_n \in \Omega$ that does not depend on the scale index j, one can verify that $\tilde{\psi}_{j,m}^o(x) = \psi_{j,m}^o = \delta(x - x_m)$ and $\tilde{\phi}_{j,n}^o(x) = \phi_{j,n}^o = \delta(x - x_n)$, meaning that for any continuous function $f(x)$:

$$\int_\Omega f(x)\psi_{j,m}^o(x)dx = \int_\Omega f(x)\tilde{\psi}_{j,m}^o(x)dx = f(x_m).$$

This lazy wavelet basis is improved with a succession of liftings.

Increasing Vanishing Moments, Stability, and Regularity

A lifting modifies biorthogonal filters in order to increase the number of vanishing moments of the resulting biorthogonal wavelets, and hopefully their stability and regularity.

Increasing the number of vanishing moments decreases the amplitude of wavelet coefficients in regions where the signal is regular, which produces a more sparse representation. However, increasing the number of vanishing moments with a lifting also increases the wavelet support, which is an adverse effect that increases the number of large coefficients produced by isolated singularities.

Each lifting step maintains the filter biorthogonality but provides no control on the Riesz bounds and thus on the stability of the resulting wavelet biorthogonal basis. When a basis is orthogonal then the dual basis is equal to the original basis. Having a dual basis that is similar to the original basis is therefore an indication of stability. As a result, stability is generally improved when dual wavelets have as much vanishing moments as original wavelets and a support of similar size. This is why a lifting procedure also increases the number of vanishing moments of dual wavelets. It can also improve the regularity of the dual wavelet.

A lifting design is computed by adjusting the number of vanishing moments. The stability and regularity of the resulting biorthogonal wavelets are measured a posteriori, hoping for the best. This is the main weakness of this wavelet design procedure.

Prediction

Starting from an initial set of biorthogonal filters $\{h_j^o, g_j^o, \tilde{h}_j^o, \tilde{g}_j^o\}_j$, a prediction step modifies each filter g_j^o to increase the number of vanishing moments of $\psi_{j,n}$. This is done with an operator P_j that predicts the values in the grid $\mathcal{C}_j$ from samples in the grid $\mathcal{G}_j$:

$$\forall\, a \in \mathbb{C}^{|\mathcal{G}_j|},\ \forall\, m \in \mathcal{C}_j,\ (P_j a)[m] = \sum_{n \in \mathcal{G}_j} p_j[m,n]\, a[n].$$

The number of vanishing moments of $\psi_{j,n}$ is increased by modifying the filter g_j^o with this predictor

$$h_j = h_j^o \quad \text{and} \quad g_j[m,l] = g_j^o[m,l] - \sum_{n \in \mathcal{G}_j} p_j[m,n]\, h_j^o[n,l]. \tag{7.246}$$

Biorthogonality is maintained by also modifying the dual filter $\tilde{h}_j^o$:

$$\tilde{g}_j = \tilde{g}_j^o \quad \text{and} \quad \tilde{h}_j[n,l] = \tilde{h}_j^o[n,l] + \sum_{m \in \mathcal{C}_j} p_j[m,n]\, \tilde{g}_j^o[m,l].$$

The filter lifting (7.246) implies a retransformation of the scaling and wavelet coefficients computed with the original filters h_j^o and g_j^o. The lifted scaling coefficients $\{a_j[n] = \langle f,\ \phi_{j,n}\rangle\}_{n \in \mathcal{G}_j}$ and detail coefficients $\{d_j[m] = \langle f,\ \psi_{j,m}\rangle\}_{m \in \mathcal{C}_j}$ are computed from the coefficients $\{d_j^o[m], a_j^o[n]\}_{n \in \mathcal{G}_j, m \in \mathcal{C}_j}$ corresponding to h_j^o and g_j^o by applying the predict operator

$$\forall\, m \in \mathcal{C}_j, \quad d_j[m] = d_j^o[m] - \sum_{n \in \mathcal{G}_j} p_j[m,n]\, a_j^o[n],$$

while the scaling coefficients are not modified: $a_j[n] = a_j^o[n]$. If P_j is a good predictor of $d_j^o[m]$ from $a_j^o[n]$ on the coarse grid $\mathcal{G}_j$, then the resulting coefficients $d_j[m]$ are smaller, which is an indication that the wavelet has more vanishing moments.

The prediction (7.246) of the filters is rewritten with matrix notations

$$\begin{cases} H_j = H_j^o \\ G_j = G_j^o - P_j H_j^o \end{cases} \quad \text{and} \quad \begin{cases} \tilde{H}_j = \tilde{H}_j^o + P_j^* \tilde{G}_j^o \\ \tilde{G}_j = \tilde{G}_j^o. \end{cases} \tag{7.247}$$

Since $H_j = H_j^o$ is not modified, the scaling functions $\phi_{j,n} = \phi_{j,n}^o$ are not modified. In contrast, since $\tilde{H}_j^o$ is modified, both the dual-scaling and wavelet functions are modified:

$$\phi_{j,n} = \phi_{j,n}^o, \quad \psi_{j,m} = \psi_{j,m}^o - \sum_{n \in \mathcal{G}_j} p_j[m,n]\, \phi_{j,n}^o, \tag{7.248}$$

$$\tilde{\phi}_{j,n} = \sum_{l \in \mathcal{G}_{j-1}} h_j^o[n,l]\, \tilde{\phi}_{j-1,l} + \sum_{m \in \mathcal{C}_j} p_j[m,n]\, \tilde{\psi}_{j,m}, \quad \tilde{\psi}_{j,m} = \sum_{l \in \mathcal{G}_{j-1}} g_j^o[m,l]\, \tilde{\phi}_{j-1,l}. \tag{7.249}$$

Theorem 7.27 proves that this lifting step maintains the biorthogonality conditions [451].

Theorem 7.27: *Sweldens.* The prediction (7.247) transforms the biorthogonal filters $\{H_j^o, G_j^o, \tilde{H}_j^o, \tilde{G}_j^o\}$ into a new set of biorthogonal filters $\{H_j, G_j, \tilde{H}_j, \tilde{G}_j\}$.

Proof. The lifting step (7.247) is written in matrix notation as

$$\begin{bmatrix} H_j \\ G_j \end{bmatrix} = \begin{bmatrix} \mathrm{Id}_{\mathcal{G}_j} & 0 \\ -P_j & \mathrm{Id}_{\mathcal{C}_j} \end{bmatrix} \begin{bmatrix} H_j^o \\ G_j^o \end{bmatrix} \quad \text{and} \quad \begin{bmatrix} \tilde{H}_j \\ \tilde{G}_j \end{bmatrix} = \begin{bmatrix} \mathrm{Id}_{\mathcal{G}_j} & P_j^* \\ 0 & \mathrm{Id}_{\mathcal{C}_j} \end{bmatrix} \begin{bmatrix} \tilde{H}_j^o \\ \tilde{G}_j^o \end{bmatrix}.$$

The proof of the biorthogonality relation (7.244) follows from

$$\begin{bmatrix} \mathrm{Id}_{\mathcal{G}_j} & P_j \\ 0 & \mathrm{Id}_{\mathcal{C}_j} \end{bmatrix} \begin{bmatrix} \mathrm{Id}_{\mathcal{G}_j} & -P_j \\ 0 & \mathrm{Id}_{\mathcal{C}_j} \end{bmatrix} = \begin{bmatrix} \mathrm{Id}_{\mathcal{G}_j} & 0 \\ 0 & \mathrm{Id}_{\mathcal{C}_j} \end{bmatrix}.$$

■

To increase the number of vanishing moments of $\psi_{j,m}$, and get $\int_\Omega \psi_{j,m}(x) q^{(k)}(x)\, dx = 0$ for a basis of d_1 polynomial of degree p_1, (7.248) shows that predict coefficients must satisfy

$$\int_\Omega \psi^o_{j,m}(x) q^{(k)}(x)\, dx = \sum_{n \in \mathcal{G}_j} p_j[m,n] \int_\Omega \phi^o_{j,n}(x) q^{(k)}(x)\, dx \quad \text{for } 0 \leqslant k < d_1. \tag{7.250}$$

The predictor $\{p_j[m,n]\}_n$ can be chosen to have d_1 nonzero coefficients that solve this $d_1 \times d_1$ linear system for each m.

Update

The prediction (7.248) modifies $\psi_{j,n}$ but does not change $\tilde{\psi}_{j,n}$. The roles of $\psi_{j,m}$ and $\tilde{\psi}_{j,m}$ are reversed by applying a lifting step to increase the number of vanishing moments of $\tilde{\psi}_{j,m}$ as well. The goal is to obtain dual wavelets $\tilde{\psi}_{j,n}$ that are as similar as possible to $\psi_{j,n}$ in order to improve the stability of the basis. It requires the use of an *update* operator U_j defined by

$$\forall\, b \in \mathbb{C}^{|\mathcal{C}_j|},\ \forall\, n \in \mathcal{G}_j,\ (U_j b)[n] = \sum_{m \in \mathcal{C}_j} u_j[n,m]\, b[m].$$

The update step is then

$$\begin{cases} H_j = H^o_j + U_j G^o_j \\ G_j = G^o_j \end{cases} \quad \text{and} \quad \begin{cases} \tilde{H}_j = \tilde{H}^o_j \\ \tilde{G}_j = \tilde{G}^o_j - U^*_j \tilde{H}^o_j. \end{cases} \tag{7.251}$$

Since predict and update steps are equivalent operations on dual filters, Theorem 7.27 shows that this update operation defines new filters that remain biorthogonal.

Let $\{d^o_j[m], a^o_j[n]\}_{n \in \mathcal{G}_j, m \in \mathcal{C}_j}$ be the wavelet and scaling coefficients corresponding to the filters h^o_j and g^o_j. The wavelet coefficients are not modified $d_j[n] = d^o_j[n]$, and $\{a_j[n]\}_{n \in \mathcal{G}_j}$ is computed by applying the update operator

$$\forall\, n \in \mathcal{G}_j, \quad a_j[n] = a^o_j[n] + \sum_{m \in \mathcal{C}_j} u_j[n,m]\, d^o_j[m].$$

The updated scaling functions and wavelets are:

$$\phi_{j,n} = \sum_{l \in \mathcal{G}_{j-1}} h^o_j[n,l]\, \phi_{j-1,l} + \sum_{m \in \mathcal{C}_j} u_j[n,m]\, \psi_{j,m}, \quad \psi_{j,m} = \sum_{l \in \mathcal{G}_{j-1}} g^o_j[m,l]\, \phi_{j-1,l}, \tag{7.252}$$

$$\tilde{\phi}_{j,n} = \tilde{\phi}^o_{j,n}, \quad \tilde{\psi}_{j,m} = \tilde{\psi}^o_{j,m} - \sum_{n \in \mathcal{G}_j} u_j[n,m]\, \tilde{\phi}^o_{j,n}. \tag{7.253}$$

Theorem 7.28 proves that this update does not modify the number of vanishing moments of the analyzing wavelet.

Theorem 7.28. If the wavelets $\{\psi^o_{j,m}\}_{j,m}$ have p_1 vanishing moments, then the wavelets $\{\psi_{j,m}\}_{j,m}$ obtained with the update (7.252) have p_1 vanishing moments.

Proof. Equation (7.253) shows that $\tilde{\phi}^o_{j,n} = \tilde{\phi}_{j,n}$. Since the original multiresolution has p_1 vanishing moments, it is orthogonal to a basis of d_1 polynomials $\{q^{(k)}\}_{0 \leq k < d_1}$ of degree $q-1$ as defined in (7.245):

$$\forall\, k < d_1, \quad q^{(k)} = \sum_{n \in \mathcal{G}_j} \langle q^{(k)},\, \phi^o_{j,n} \rangle\, \tilde{\phi}^o_{j,n} = \sum_{n \in \mathcal{G}_j} \langle q^{(k)},\, \phi^o_{j,n} \rangle\, \tilde{\phi}_{j,n}.$$

Taking the inner product of this relation with each $\phi_{j,n'}$ leads to

$$\forall\, k < d_1, \quad \langle q^{(k)},\, \phi_{j,n'} \rangle = \sum_{n \in \mathcal{G}_j} \langle q^{(k)},\, \phi^o_{j,n} \rangle \langle \tilde{\phi}_{j,n},\, \phi_{j,n'} \rangle = \langle q^{(k)},\, \phi^o_{j,n'} \rangle. \tag{7.254}$$

Using the refinement equation (7.252) gives

$$\begin{aligned} \forall\, k < d_1, \quad \langle \psi_{j,m},\, q^{(k)} \rangle &= \sum_{l \in \mathcal{G}_{j-1}} g^o_j[m,l] \langle \phi_{j-1,l},\, q^{(k)} \rangle = \sum_{l \in \mathcal{G}_{j-1}} g^o_j[m,l] \langle \phi^o_{j-1,l},\, q^{(k)} \rangle \\ &= \Big\langle \sum_{l \in \mathcal{G}_{j-1}} g^o_j[m,l]\, \phi^o_{j-1,l},\, q^{(k)} \Big\rangle = \langle \psi^o_{j,m},\, q^{(k)} \rangle = 0, \end{aligned}$$

where we used $\langle \phi_{j-1,l},\, q^{(k)} \rangle = \langle \phi^o_{j-1,l},\, q^{(k)} \rangle$, which follows from (7.254). ■

To increase the number of vanishing moments of $\tilde{\psi}_{j,m}$ and to get $\int_\Omega \tilde{\psi}_{j,m}(x) q^{(k)}(x)\, dx = 0$ for a basis of d_2 polynomials of degree p_2 in Ω, (7.252) shows that update coefficients must satisfy

$$\forall k < d_2, \quad \int_\Omega \tilde{\psi}^o_{j,m}(x) q^{(k)}(x)\, dx = \sum_{n \in \mathcal{G}_j} u_j[n,m] \int_\Omega \tilde{\phi}^o_{j,n}(x) q^{(k)}(x)\, dx. \tag{7.255}$$

Thus, the update coefficients $\{u_j[m,n]\}_n$ can be chosen to have d_2 nonzero coefficients, which solves this $d_2 \times d_2$ linear system for each m.

Predict plus Update Design and Algorithm

Wavelets synthesized with a lifting are constructed with one predict step followed by one update step, because there is no technique that controls the wavelet stability and regularity over more lifting steps. Beginning from Dirac lazy wavelets $\{\psi^o_{j,m}, \tilde{\psi}^o_{j,m}\}_{j,m}$ with no vanishing moment, a prediction (7.247) obtains biorthogonal wavelets $\{\psi^1_{j,m}, \tilde{\psi}^1_{j,m}\}_{j,m}$ with, respectively, p_1 and zero vanishing moments. An update (7.251) then yields biorthogonal wavelets $\{\psi_{j,m}, \tilde{\psi}_{j,m}\}_{j,m}$ having, respectively, p_1 and p_2 vanishing moments.

A fast wavelet transform computes the coefficients

$$\forall\, n \in \mathcal{G}_j, \quad a_j[n] = \langle f,\, \phi_{j,n} \rangle \quad \text{and} \quad \forall\, m \in \mathcal{C}_j, \quad d_j[m] = \langle f,\, \psi_{j,m} \rangle$$

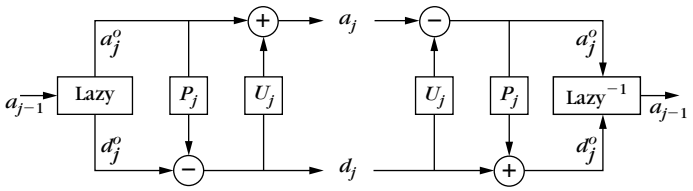

FIGURE 7.26

Predict and update decomposition of a_{j-1} into a_j and d_j, followed by the reconstruction of a_{j-1} with the same update and predict operators.

by replacing convolution with conjugate mirror filters by a succession of lifting and update steps. The algorithm takes in input a discrete signal $a_L \in \mathbb{C}^{|\mathcal{G}_L|}$ of length $N = |\mathcal{G}_L|$, and applies the lazy decomposition, a predict, and an update operator, as illustrated in Figure 7.26. For $j = L+1, \ldots, J$, it computes

1. *Split:* $\forall\, m \in \mathcal{C}_j,\ d_j^o[m] = a_{j-1}[m], \quad \forall\, n \in \mathcal{G}_j,\ a_j^o[n] = a_{j-1}[n]$.
2. *Forward predict:* $\forall\, m \in \mathcal{C}_j, \quad d_j[m] = d_j^o[m] - \sum_{n \in \mathcal{G}_j} p_j[m,n]\, a_j^o[n]$.
3. *Forward update:* $\forall\, n \in \mathcal{G}_j, \quad a_j[n] = a_j^o[n] + \sum_{m \in \mathcal{C}_j} u_j[n,m]\, d_j[m]$.

This fast biorthogonal wavelet transform (7.157) requires $O(N)$ operations.

The reconstruction of a_L from $\{d_j\}_{J \leqslant j < L}$ and a_J inverts these predict and update steps. For $j = J, \ldots, L+1$, it computes

1. *Backward update:* $\forall\, n \in \mathcal{G}_j, \quad a_j^o[n] = a_j[n] - \sum_{m \in \mathcal{C}_j} u_j[n,m]\, d_j[m]$.
2. *Backward predict:* $\forall\, m \in \mathcal{C}_j, \quad d_j^o[m] = d_j[m] + \sum_{n \in \mathcal{G}_j} p_j[m,n]\, a_j^o[n]$.
3. *Merge:* $\forall\, m \in \mathcal{C}_j, \quad a_{j-1}[m] = d_j^o[m], \quad \forall\, n \in \mathcal{G}_j, \quad a_{j-1}[n] = a_j^o[n]$.

Vanishing Moments

The predict and update filters are computed to create vanishing moments on the resulting wavelets. After the prediction applied to the lazy Diracs $\psi^0_{j,m}(x) = \delta(x - x_m)$, $\phi^0_{j,n}(x) = \delta(x - x_n)$, the resulting wavelets and scaling functions derived from (7.248) and (7.249) are:

$$\phi^1_{j,n}(x) = \delta(x - x_n), \quad \psi^1_{j,m}(x) = \delta(x - x_m) - \sum_{n \in \mathcal{G}_j} p_j[m,n]\, \delta(x - x_n) \tag{7.256}$$

$$\tilde{\phi}^1_{j,n}(x) = \delta(x - x_n) + \sum_{m \in \mathcal{C}_j} p_j[m,n]\, \delta(x - x_m), \quad \tilde{\psi}^1_{j,m}(x) = \delta(x - x_m). \tag{7.257}$$

According to (7.250), the wavelet $\psi^1_{j,m}$ has p_1 vanishing moments if for each m, the p_1 coefficients of $\{p_j[m,n]\}_n$ solve the $d_1 \times d_1$ linear system:

$$\forall\, m \in \mathcal{C}_j,\ \forall\, k < d_1, \quad q^{(k)}(x_m) = \sum_{n \in \mathcal{G}_j} p_j[m,n] q^{(k)}(x_n). \tag{7.258}$$

Following (7.253), after the update of the dual wavelet and the scaling functions, are

$$\tilde{\phi}^2_{j,n} = \tilde{\phi}^1_{j,n} = \tilde{\phi}^2_{j-1,n} + \sum_{m \in \mathcal{C}_j} p_j[m,n]\, \tilde{\phi}^2_{j-1,m} \tag{7.259}$$

$$\tilde{\psi}^2_{j,m} = \tilde{\psi}^1_{j,m} - \sum_{n \in \mathcal{G}_j} u_j[n,m]\, \tilde{\phi}^1_{j,n} = \tilde{\phi}^2_{j-1,m} - \sum_{n \in \mathcal{G}_j} u_j[n,m]\, \tilde{\phi}^2_{j,m}. \tag{7.260}$$

Theorem 7.28 proves that the vanishing moments of $\psi^1_{j,m}$ are transferred to $\psi^2_{j,m}$ after the dual lifting step. According to (7.258), the dual wavelet $\tilde{\psi}^2_{j,m}$ has p_2 vanishing moments if for each m the d_2 coefficients of $\{u_j[m,n]\}_n$ solve the $d_2 \times d_2$ linear system:

$$\forall\, k < d_2, \quad \sum_{n \in \mathcal{G}_j} I^k_j(n)\, u_j[n,m] = I^k_{j-1}(m) \quad \text{with} \quad I^k_j(n) = \langle \tilde{\phi}_{j,n},\, q^{(k)} \rangle. \tag{7.261}$$

The inner products $I^k_j(n)$ are computed iteratively with (7.259):

$$I^k_j(n) = I^k_{j-1}(n) + \sum_{m \in \mathcal{C}_j} p_j[m,n]\, I^k_{j-1}(m). \tag{7.262}$$

The recurrence is initialized at the finest scale $j = L$ by setting $I^k_L(n) = q^{(k)}(x_n)$, where $x_n \in \Omega$ is the point associated to the index $n \in \mathcal{G}_L$. More elaborated initializations using quadrature formula can also be used [427].

Linear Splines 5/3 Biorthogonal Wavelets

Linear spline wavelets are obtained with a two-step lifting construction beginning from lazy wavelets. The one-dimensional grid $\mathcal{G}_{j-1}$ is a uniform sampling at intervals 2^{j-1} and the two subgrids $\mathcal{G}_j$ and $\mathcal{C}_j$ correspond to even and odd subsampling. Figure 7.27 illustrates these embedded one-dimensional grids.

The lazy wavelet transform splits the coefficients a_{j-1} into two groups

$$\forall\, n \in \mathcal{G}_j, \quad a^o_j[n] = a_{j-1}[n], \quad \text{and} \quad \forall\, m \in \mathcal{C}_j, \quad d^o_j[m] = a_{j-1}[m].$$

The value of d^o_j in $\mathcal{C}_j$ is predicted with a linear interpolation of neighbor values in $\mathcal{G}_j$

$$\forall\, m \in \mathcal{C}_j, \quad d_j[m] = d^o_j[m] - \frac{a^o_j[n + 2^{j-1}] + a^o_j[n - 2^{j-1}]}{2}. \tag{7.263}$$

This lifting step creates wavelets with two vanishing moments because this linear interpolation predicts exactly the values of polynomials of degree 0 and 1.

A symmetric update step computes

$$\begin{aligned} \forall\, n \in \mathcal{G}_j, \quad a_j[n] = a^o_j[n] &+ (u_j[n, m - 2^{j-1}]\, d_j[m - 2^{j-1}] \\ &+ u_j[n, m + 2^{j-1}]\, d_j[m + 2^{j-1}]). \end{aligned} \tag{7.264}$$

To obtain two vanishing moments, the inner products $I^k_j(n) = \langle \tilde{\phi}_{j,n}(t),\, t^k \rangle$ are computed iteratively with (7.262), using two nonzero update coefficients $u_j[n, m -$

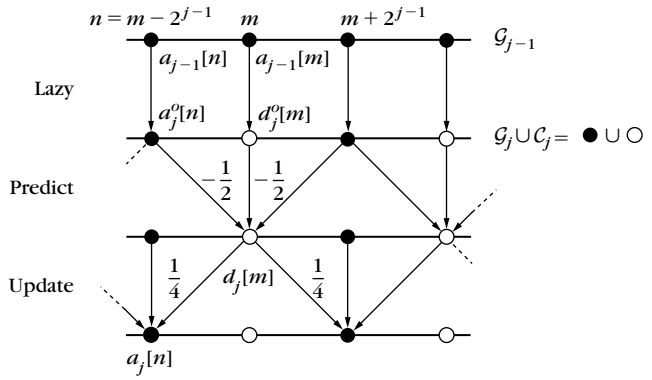

FIGURE 7.27

Predict and update steps for the construction of linear spline wavelets.

$2^{j-1}]$ and $u_j[n, m + 2^{j-1}]$ for each m. For $k = 0$ we get $I_j^0(n) = \langle \tilde{\phi}_{j,n},\ 1 \rangle = 2^{j-L}$. Since t is antisymmetric, if this equation is valid for $k = 0$ and if $u_j[n, m - 2^{j-1}] = u_j[n, m + 2^{j-1}]$, then it is valid for $k = 1$. Solving (7.261) for $k = 0$ gives $u_j[n, m - 2^{j-1}] = u_j[n, m + 2^{j-1}] = 1/4$ and thus,

$$a_j[n] = a_j^o[n] + \frac{1}{4}(d_j[m - 2^{j-1}] + d_j[m + 2^{j-1}]). \tag{7.265}$$

Figure 7.27 illustrates the succession of predict and update. One can verify (Exercise 7.20) that the resulting biorthogonal wavelets correspond to the spline biorthogonal wavelets computed with $p_1 = p_2 = 2$ vanishing moments (shown in Figure 7.15). The dual-scaling functions and wavelets are compactly supported linear splines. Higher-order biorthogonal spline wavelets are constructed with a prediction (7.263) and an update (7.264) providing more vanishing moments.

7.8.3 Quincunx Wavelet Bases

Separable two-dimensional wavelet bases are constructed in Section 7.7.2 from one-dimensional wavelet bases. They are implemented with separable filter banks that increase the scale by 2, by dividing the image grid in a coarse grid that keeps one point out of four, plus three detail grids of the same size and that correspond to three different wavelets. Other regular subsamplings of the image array lead to nonseparable wavelet bases. A quincunx subsampling divides the image grid into a coarse grid that keeps one point out of two and a detail grid of the same size that corresponds to a quincunx wavelet. Thus, the scale increases only by a factor $2^{1/2}$. A quincunx wavelet is more isotropic than separable wavelets.

Biorthogonal or orthogonal quincunx wavelets are constructed with perfect reconstruction or conjugate mirror filters, defined with a quincunx subsampling, which yields conditions on their transfer functions [170, 253, 254, 431]. Kovačević

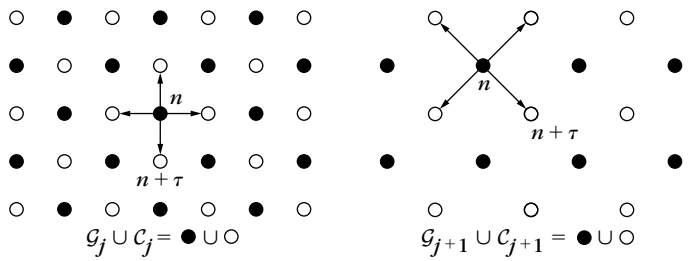

FIGURE 7.28

Two successive quincunx subsampling for j and $j+1$, where j is odd.

and Sweldens [333] give a simple construction of biorthogonal quincunx wavelets from lazy wavelets, with a predict followed by an update lifting.

We denote by $(a, b)^*$ a transposed two-dimensional vector column. Embedded quincunx grids are defined by

$$\forall j, \quad \begin{cases} \mathcal{G}_j = L^j \mathbb{Z}^2 = \{L^j (n_1, n_2)^* : n \in \mathbb{Z}^2\} \\ \mathcal{C}_j = L^j \mathbb{Z}^2 + L^{j-1} e_1 = \mathcal{G}_j + L^{j-1} e_1, \end{cases}$$

where $L = \begin{bmatrix} 1 & -1 \\ 1 & 1 \end{bmatrix}$, $e_1 = (1, 0)^*$ and $e_2 = (0, 1).^*$

Figure 7.28 shows two quincunx subsampled grids, depending on the parity of j.

Each point $n \in \mathcal{G}_j$ and $m \in \mathcal{C}_j$ have four neighbors

$$\{n + \tau\}_{\Delta_j} \subset \mathcal{C}_j \quad \text{and} \quad \{m + \tau\}_{\Delta_j} \subset \mathcal{G}_j,$$

where the set of shifts has the following four elements:

$$\Delta_j = \{\pm L^{j-1} e_1, \pm L^{j-1} e_2\}.$$

The simplest symmetric prediction operator on these grids is the symmetric averaging on the four neighbors, which performs a linear interpolation:

$$\forall\, a \in \mathbb{C}^{|\mathcal{G}_j|}, \quad \forall\, m \in \mathcal{C}_j, \quad (P_j a)[m] = \frac{1}{4} \sum_{\tau \in \Delta_j} a[m + \tau]. \tag{7.266}$$

This prediction operator applied to lazy wavelets yields a wavelet that is orthogonal to constant and linear polynomial in $\mathbb{R}^2$, which gives $p_1 = 2$ vanishing moments. The update operator is defined with the same symmetry on the four neighbors

$$\forall\, b \in \mathbb{C}^{|\mathcal{C}_j|}, \quad \forall\, n \in \mathcal{G}_j, \quad (U_j b)[n] = \lambda \sum_{\tau \in \Delta_j} b[n + \tau]. \tag{7.267}$$

Choosing $\lambda = 1/4$ satisfies the vanishing moments conditions (7.261) for constant and linear polynomials [333].

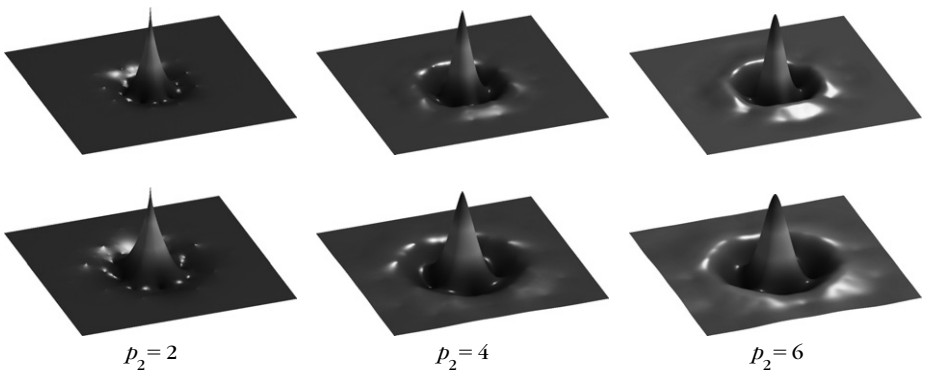

FIGURE 7.29

Quincunx dual wavelets $\tilde{\psi}_{j,m}$ and $\tilde{\psi}_{j+1,m}$ at two consecutive scales 2^j and $2^{j+1/2}$ (first and second row) with progressively more vanishing moments.

Figure 7.29 shows dual wavelets $\tilde{\psi}_{j,m}$ and $\tilde{\psi}_{j+1,m}$ at two consecutive scales 2^j and $2^{j+1/2}$, corresponding to the predict and update operators (7.266) and (7.267). They have $p_2 = 2$ vanishing moments and are nearly isotropic. The analyzing wavelets $\psi_{j,m}$ also have $p_1 = 2$ vanishing moments but are more irregular. The irregularity of analyzing wavelets is not a problem since the reconstruction is performed by dual wavelets. Wavelets with more vanishing moments are obtained by replacing the four-neighborhood linear interpolation (7.266) by higher-order polynomial interpolations [333]. Figure 7.29 shows the resulting dual wavelets $\tilde{\psi}_{j,m}$ for $p_2 = 4$ and $p_2 = 6$, which correspond to wavelets $\psi_{j,m}$ with as much vanishing moments $p_1 = p_2$, but which are more irregular. Increasing the number of vanishing moments improves the regularity of dual wavelets, but it reduces the stability of these biorthogonal bases, which limits their application.

Figure 7.30 shows an example of quincunx wavelet image transform with $p_1 = 2$ vanishing moments. It is computed with the fast lifting algorithm from Section 7.8.2 with the predict and update operators (7.266) and (7.267). The quasi-isotropic quincunx wavelet detects sharp transitions in all directions.

7.8.4 Wavelets on Bounded Domains and Surfaces

Processing three-dimensional surfaces and signals defined on surfaces is important in multimedia and computer graphics applications. Biorthogonal wavelets on triangulated meshes were introduced by Lounsbery et al. [354], and Schröder and Sweldens [427] improved these techniques with lifting schemes. Lifted wavelets are used to compress functions defined on a surface $\Omega \subset \mathbb{R}^3$, and in particular on a sphere to process geographical data on Earth. The sphere is represented with a recursively subdivided three-dimensional mesh, and the signal is processed using lifted wavelets on this embedded mesh.

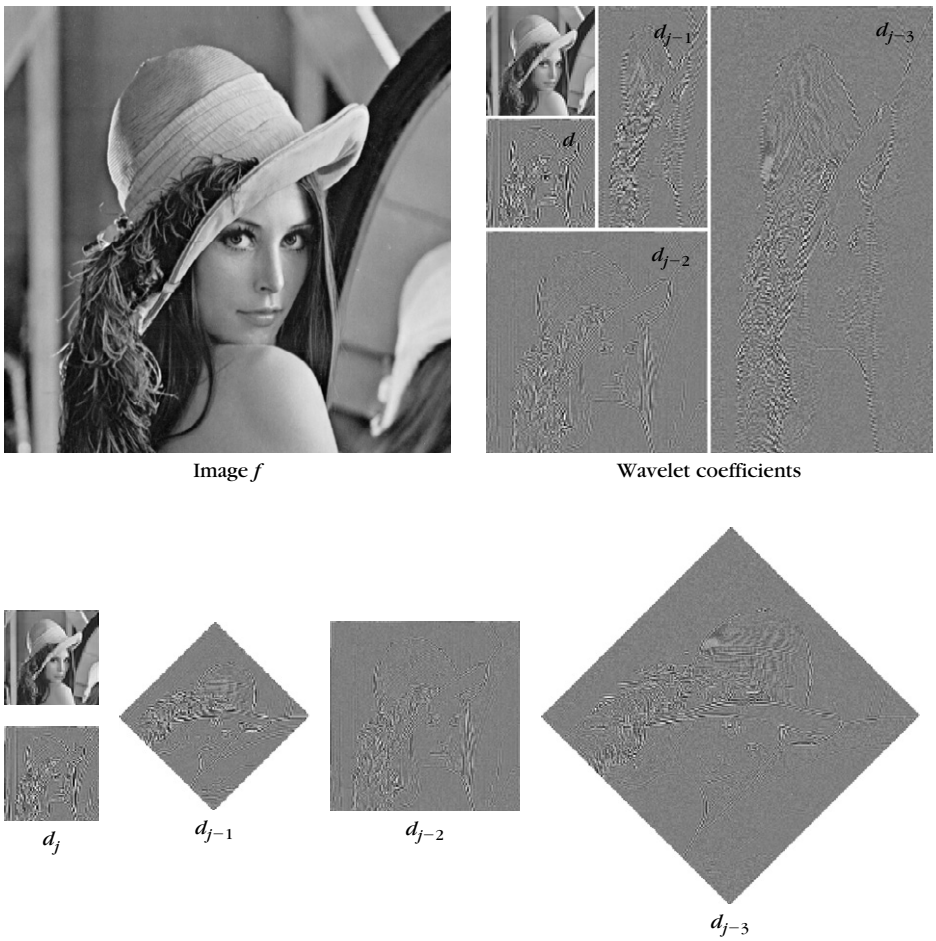

FIGURE 7.30

Image decomposition in a biorthogonal quincunx wavelet basis with $p_1 = 2$ vanishing moments. The top right image shows wavelet coefficients packed over the image-sampling array. These coefficients are displayed as square quincunx grids (*below*) with a rotation for odd scales.

Lifted wavelets are also defined on a two-dimensional parametric domain Ω with an arbitrary topology, to compress a three-dimensional surface $\mathcal{S} \subset \mathbb{R}^3$, viewed as a mapping from Ω to $\mathbb{R}^3$. The surface is represented as a three-dimensional mesh, and the lifted wavelet transform computes three coefficients for each vertex of the mesh—one per coordinate. Denoising and compression of surfaces are then implemented by thresholding and quantizing these wavelet coefficients. Such multiresolution processings have applications in video games, where a large amount of three-dimensional surface data must be displayed in real time. Lifting wavelets also

finds applications in computer-aided design, where surfaces are densely sampled to represent manufactured objects, and should be compressed to reduce the storage requirements.

Semiregular Triangulation

A triangulation is a data structure frequently used to index points $x_n \in \Omega$ on a surface. Embedded indexes $n \in \mathcal{G}_j$ with a triangulation topology are defined by recursively subdividing a coarse triangulated mesh.

For each scale j, a triangulation (E_j, T_j) is composed of edges $E_j \subset \mathcal{G}_j \times \mathcal{G}_j$ that link pairs of points on the grid, and triangles $T_j \subset \mathcal{G}_j \times \mathcal{G}_j \times \mathcal{G}_j$. Each triangle of T_j is composed of three edges in E_j. These triangulations are supposed to be embedded using the 1:4 subdivision rule of each triangle, illustrated in Figure 7.31, as follows.

- For each edge $e \in E_j$, a midpoint $\gamma(e) \in \mathcal{G}_{j-1}$ is added to the vertices
$$\mathcal{G}_{j-1} = \mathcal{G}_j \cup \{\gamma(e) : e \in E_j\}.$$
- Each edge is subdivided into two finer edges
$$\forall\, e = (n_0, n_1) \in E_j, \quad \sigma_1(e) = (n_0, \gamma(e)) \quad \text{and} \quad \sigma_2(e) = (n_1, \gamma(e)).$$
The subdivided set of edges is then
$$E_{j-1} = \{\sigma_i(e) : i = 1, 2 \text{ and } e \in E_j\}.$$
- Each triangle face $f = (n_0, n_1, n_2) \in F_j$ is subdivided into four faces
$$\mu_1(f) = (n_0, \gamma(n_0, n_1), \gamma(n_0, n_2)), \quad \mu_2(f) = (n_1, \gamma(n_1, n_0), \gamma(n_1, n_2)),$$
$$\mu_3(f) = (n_2, \gamma(n_2, n_0), \gamma(n_2, n_1)), \quad \mu_4(f) = (\gamma(n_0, n_1), \gamma(n_1, n_2), \gamma(n_2, n_0)).$$

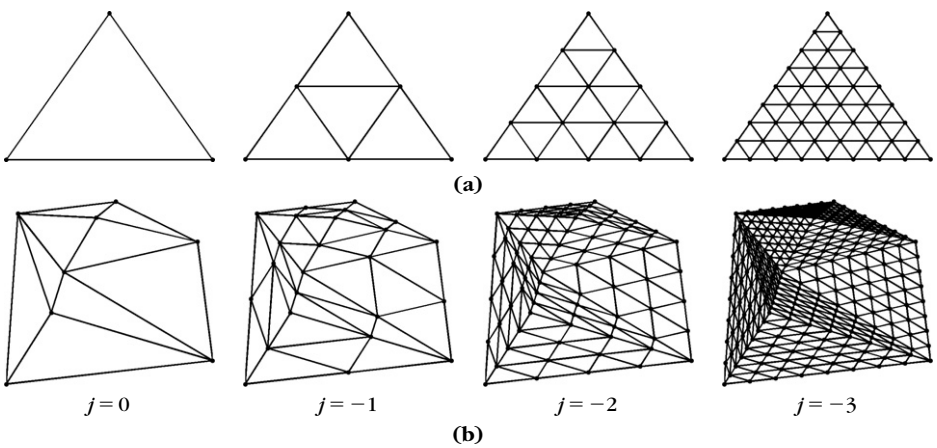

FIGURE 7.31

(a) Iterated regular subdivision 1:4 of one triangle in four equal subtriangles. **(b)** Planar triangulation $(\mathcal{G}_0, E_0, T_0)$ of a domain Ω in $\mathbb{R}^2$, successively refined with a 1:4 subdivision.

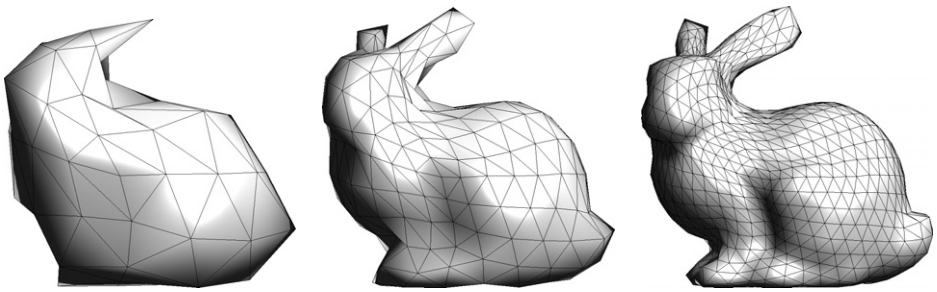

FIGURE 7.32

Examples of semiregular mesh $\{\mathcal{G}_j, E_j, T_j\}_j$ of a domain Ω that is a surface $\mathcal{S}$ in $\mathbb{R}^3$.

The subdivided set of faces is then

$$F_{j-1} = \big\{\mu_i(f) : i = 1, 2, 3, 4 \quad \text{and} \quad f \in F_j\big\}.$$

Figure 7.31 shows an example of coarse planar triangulation with points x_n in a domain Ω of $\mathbb{R}^2$.

The semiregular mesh $\{E_j, T_j\}_j$ and the corresponding sample locations x_n are usually computed from an input surface $\mathcal{S}$, represented either with a parametric continuous function or with an unstructured set of polygons. This requires using a hierarchical remeshing process to compute the embedded triangulation [354]. Figure 7.32 shows an example of semiregular triangulation of a three-dimensional surface $\mathcal{S}$, and in this case the points x_n belong to a domain Ω that is the surface $\mathcal{S}$ in $\mathbb{R}^3$.

Wavelets to Process Functions on Surfaces

Let us consider a domain $\Omega \in \mathbb{R}^3$ that is a three-dimensional surface, and each $n \in \mathcal{G}_j$ indexes a point $x_n \in \Omega$ of the surface. Figure 7.33 shows the local labeling convention for the neighboring vertices in $\mathcal{G}_j$ of a given index $m \in \mathcal{C}_j$ in a butterfly neighborhood.

A predictor P_j is computed in this local neighborhood

$$\forall\, m \in \mathcal{C}_j,\ (P_j a)[m] = \sum_{i=1,2} \lambda_i a[v_m^i] + \sum_{i=1,2} \mu_i a[w_m^i] + \sum_{i,j=1}^{2} \nu_{i,j} a[z_m^{i,j}], \tag{7.268}$$

where the parameters $\lambda_i, \mu_i, \nu_{i,j}$ are calculated by solving (7.258) to obtain vanishing moments for a collection of low-degree polynomials $\{q^{(k)}\}_{0 \leq k < d_1}$ [427].

The update operator ensures that the dual wavelets have one vanishing moment. It is calculated on the direct neighbors in $\mathcal{C}_j$ of each point $n \in \mathcal{G}_j$:

$$\forall\, n \in \mathcal{G}_j, \quad \mathcal{V}_n = \big\{m = \gamma(n, n') \in \mathcal{C}_j : (n, n') \in E_j\big\}.$$

The update operator is parameterized as follows:

$$\forall\, b \in \mathbb{C}^{|\mathcal{C}_j|},\ \ \forall\, n \in \mathcal{G}_j,\ \ (U_j b)[n] = \lambda_n \sum_{m \in \mathcal{V}_n} b[m], \tag{7.269}$$

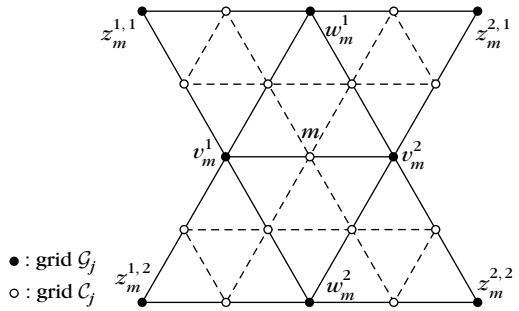

FIGURE 7.33

Labeling of points in the butterfly neighborhood of a vertex $m \in \mathcal{C}_j$.

where each λ_n is computed to solve the system (7.261) to obtain vanishing moments. This requires the iterative computation of the moments $I_j^k(n)$, as explained in (7.262), with an initialization $I_L^k(n) = 1$ at the finest scale L of the mesh. In a perfectly regular triangulation, where all the points have six neighbors, a constant weight $\lambda_n = \lambda$ can be used, and one can check that $\lambda_n = 1/24$ guarantees one vanishing moment.

Processing signals on a sphere is an important application of these wavelets on surfaces [427]. The triangulated mesh is obtained by a 1:4 subdivision of a regular polyhedron, for instance a tetrahedron. The positions of the points x_n for $n \in \mathcal{G}_j$ are defined recursively by projecting midpoints of the edges on the sphere:

$$\forall\, (n_0, n_1) \in E_j, \quad x_{\gamma(n_0,n_1)} = \frac{x_{n_0} + x_{n_1}}{\|x_{n_0} + x_{n_1}\|}.$$

The signal $f \in \mathbb{C}^{|\mathcal{G}_L|}$ is defined on the finest mesh $\mathcal{G}_L$.

A nonlinear approximation is obtained by setting to zero wavelet coefficients that satisfy $|\langle f,\ \psi_{j,m}\rangle| \leqslant T\|\psi_{j,m}\|$ where T is a given threshold. The value of $\|\psi_{j,m}\|$ can be approximated from the size of its support $\|\psi_{j,m}\| \sim \sqrt{\text{supp}(\psi_{j,n})}$ [427]. Figure 7.34 shows an example of such a nonlinear approximation with an image of Earth defined as a function on the sphere.

Wavelets to Process Surfaces

A three-dimensional surface $\mathcal{S} \subset \mathbb{R}^3$ is represented as a mapping from a two-dimensional parameter domain Ω to $\mathbb{R}^3$. This surface is discretized with a semiregular mesh $\{\mathcal{G}_j, E_j, T_j\}_{L \leqslant j \leqslant 0}$, and thus Ω can be chosen as the finest grid $\mathcal{G}_L$ viewed as an abstract domain. The surface is a discrete mapping from $\Omega = \mathcal{G}_L$ to $\mathbb{R}^3$ that assigns to each $n \in \Omega$ three values $(f_1[n], f_2[n], f_3[n]) \in \mathcal{S}$, which is a position in the three-dimensional space.

Processing the discrete surface is equivalent to processing the three signals (f_1, f_2, f_3) where each $f_i \in \mathbb{C}^{|\mathcal{G}_L|}$ is defined on the finest grid $\mathcal{G}_L$. Since points in

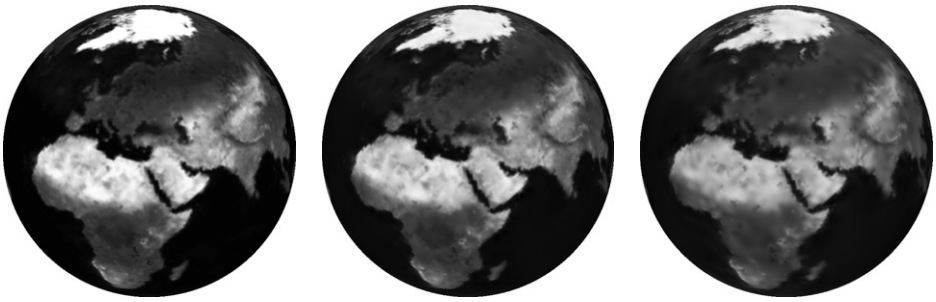

FIGURE 7.34

Nonlinear approximation of a function defined on a sphere using a decreasing number of large wavelet coefficients.

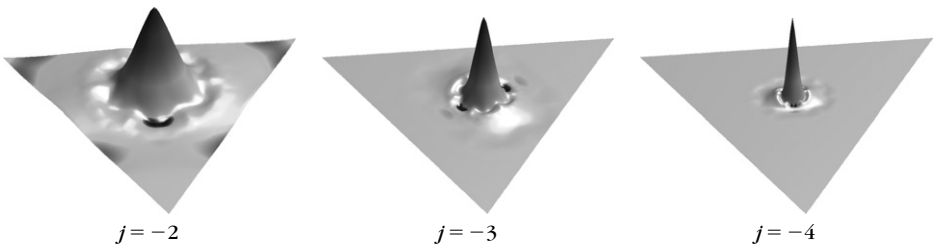

FIGURE 7.35

Example of dual wavelets $\tilde{\psi}_{j,k}(x)$ for x on a subdivided equilateral triangle. The height over the triangle indicates the value of the wavelet.

the parametric domain Ω do not have positions in Euclidean space, the notion of vanishing moments is not well defined, and the predict operator is computed using weights that are calculated as if the faces of the mesh were equilateral triangles. One can verify that the resulting parameters of the predict operator (7.268) are $\lambda_i = 1/2$, $\mu_i = 1/4$, and $\nu_{i,j} = -1/16$ [427]. Figure 7.35 shows the corresponding wavelets on a subdivided equilateral triangle.

These wavelets are used to compress each of the three signals $f_i \in \mathbb{C}^{|\mathcal{G}_L|}$ by uniformly quantizing the normalized coefficients $\langle f_i,\ \psi_{j,m}\rangle / \|\psi_{j,m}\|$. The resulting set of quantized coefficients are within strings with an entropy coder algorithm, described in Section 10.2.1. The quantization and coding of sparse signal representation is described in Section 10.4.

Figure 7.36 shows an example of three-dimensional surface approximation using biorthogonal wavelets on triangulated meshes. Wavelet coders based on lifting offer state-of-the-art results in surface compression [327]. There is no control on the Riesz bounds of the lifted wavelet basis, because the lifted basis depends on the surface properties, but good approximation results are obtained.

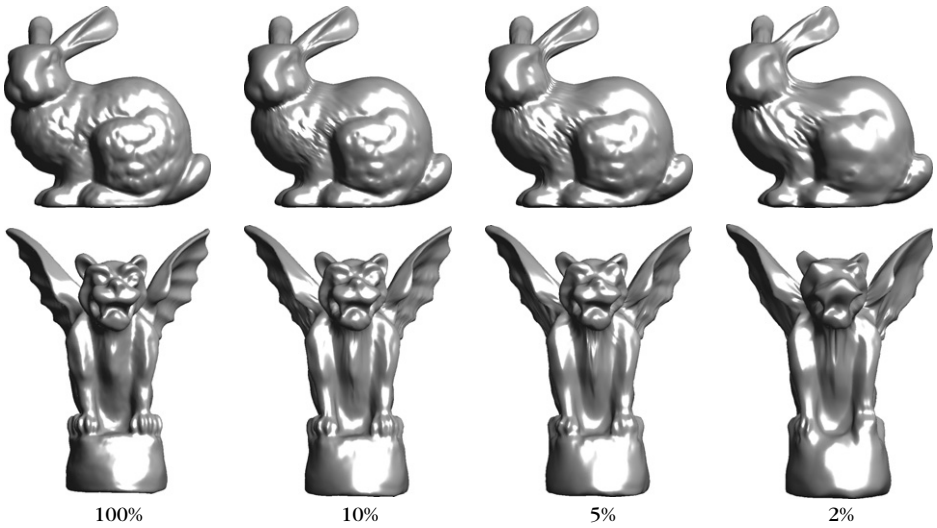

FIGURE 7.36

Nonlinear surface approximation using a decreasing proportion of large wavelet coefficients.

7.8.5 Faster Wavelet Transform with Lifting

Lifting is used to reduce the number of operations of a one-dimensional fast wavelet transform by factorizing the filter bank convolutions. It also reduces the memory requirements by implementing all operations, in place, within the input signal array.

Before the introduction of liftings for wavelet design, the factorization of filter bank convolutions was studied as paraunitary filter banks by Vaidyanathan [68] and other signal-processing researchers. Instead of implementing a filter bank with convolutions and subsamplings, specific filters are designed for even and odd signal coefficients. These filters are shown to be factorized as a succession of elementary operators that correspond to the predict and update operators of a lifting. This filtering architecture reduces by up to 2 the number of additions and multiplications, and simplifies folding border treatments for symmetric wavelets.

The fast wavelet transform algorithm in Sections 7.3.1 and 7.3.2 decomposes iteratively the scaling coefficients $a_j[n]$ at a scale 2^j into larger-scale coefficients $a_{j+1}[n]$ and detail wavelet coefficients $d_{j+1}[n]$, with convolutions and subsampling using two filters h and g. According to (7.157),

$$a_{j+1}[n] = a_j \star \bar{h}[2n], \quad d_{j+1}[n] = a_j \star \bar{g}[2n], \tag{7.270}$$

with $\bar{h}[n] = h[-n]$ and $\bar{g}[n] = g[-n]$. The reconstruction is performed with the dual filters $\tilde{h}$ and $\tilde{g}$ according to (7.158),

$$a_j[n] = \check{a}_{j+1} \star \tilde{h}[n] + \check{d}_{j+1} \star \tilde{g}[n]. \tag{7.271}$$

Sweldens and Daubechies [199] proved that the convolutions and subsamplings (7.270) can be implemented with a succession of lifting steps and the reconstruction (7.271) by inverting these liftings.

Each uniform one-dimensional signal sampling grid $\mathcal{G}_j$ of $a_j[n]$ is divided into even samples in $\mathcal{G}_{j+1}$ and odd samples in $\mathcal{C}_j$ where a_{j+1} and d_{j+1} are, respectively, defined. Starting from the lazy wavelet transform that splits even and odd samples of $a_j[n]$, K couples of predict and update convolution operators $\{P^{(k)}, U^{(k)}\}_{1 \leqslant k \leqslant K}$ are sequentially applied. Each predict operator $P^{(k)}$ corresponds to a filter $p^{(k)}[n]$ and each update operator to a filter $u^{(k)}[m]$. The filters have a small support of typically two coefficients. They are computed from the biorthogonal filters $(h, g, \tilde{h}, \tilde{g})$ with a Euclidean division algorithm [199]. A final scaling step renormalizes the filter coefficients.

Let $a_L[n]$ be the input finest-scale signal for $n \in \mathcal{G}_L$. The lifting implementation of a fast wavelet transform proceeds as follow. For $j = L+1, \ldots, J$:

1. *Even-odd split:* $\forall\, m \in \mathcal{C}_j,\ d_j^{(0)}[m] = a_{j-1}[m]$, and $\forall\, n \in \mathcal{G}_j,\ a_j^{(0)}[n] = a_{j-1}[n]$. The following steps 2 and 3 are performed for $k = 1, \ldots, K$.
2. *Forward predict:* $\forall\, m \in \mathcal{C}_j,\ d_j^{(k)}[m] = d_j^{(k-1)}[m] - \sum_{n \in \mathcal{G}_j} p^{(k)}[m-n]\, a_j^{(k-1)}[n]$.
3. *Forward update:* $\forall\, n \in \mathcal{G}_j,\ a_j^{(k)}[n] = a_j^{(k-1)}[n] + \sum_{m \in \mathcal{C}_j} u^{(k)}[n-m]\, d_j^{(k)}[m]$.
4. *Scaling:* The output coefficients are $d_j = d_j^{(K)}/\zeta$ and $a_j = \zeta\, a_j^{(K)}$.

The fast inverse wavelet transform recovers a_L from the set of wavelet coefficients $\{d_j\}_{0 \leqslant j < L}$ and a_J by inverting these predict and update operators. For $j = J, \ldots, L+1$:

1. *Inverse scaling:* Initialize $d_j^{(K)} = \zeta\, d_j$ and $a_j^{(K)} = a_j/\zeta$. The following steps, 2 and 3, are performed for $k = K, \ldots, 1$.
2. *Backward update:* $\forall\, n \in \mathcal{G}_j,\ a_j^{(k-1)}[n] = a_j^{(k)}[n] - \sum_{m \in \mathcal{C}_j} u^{(k)}[n-m]\, d_j^{(k)}[m]$.
3. *Backward predict:* $\forall\, m \in \mathcal{C}_j,\ d_j^{(k-1)}[m] = d_j^{(k)}[m] + \sum_{n \in \mathcal{G}_j} p^{(k)}[m-n]\, a_j^{(k-1)}[n]$.
4. *Merge even-odd samples:* $\forall\, m \in \mathcal{C}_j,\ a_{j-1}[m] = d_j^{(0)}[m]$ and $\forall\, n \in \mathcal{G}_j,\ a_{j-1}[n] = a_j^{(0)}[n]$.

One can verify (Exercise 7.21) that this implementation divides the number of operations by up to a factor of 2, compared to direct convolutions and subsamplings calculated in (7.270) and (7.271). Moreover, this algorithm proceeds "in place," which means that it only uses the memory of the original array $\mathcal{G}_L$ with

coefficients that are progressively modified by the lifting operations; it then stores the resulting wavelet coefficients. Similarly, the reconstruction operates in place by reconstructing progressively the coefficients in the array $\mathcal{G}_L$.

Symmetric Lifting on the Interval

The lifting implementation is described in more detail for symmetric wavelets on an interval, corresponding to symmetric biorthogonal filters $(h, g, \tilde{h}, \tilde{g})$. Predict and update convolutions are modified at the boundaries to implement folding boundary conditions.

The input sampling grid $\mathcal{G}_L$ has $N = 2^{-L}$ samples at integer positions $0 \leqslant n < N$. The embedded subgrids at scales $0 \geqslant 2^j > 2^L$ are

$$\mathcal{G}_j = \left\{ kN2^j : 0 \leqslant k < 2^{-j} \right\} \quad \text{and} \quad \mathcal{C}_j = \left\{ kN2^j + N2^{j-1} : 0 \leqslant k < 2^{-j} \right\}. \tag{7.272}$$

The resulting lifting operators $\{P^{(k)}, U^{(k)}\}_{1 \leqslant k \leqslant K}$ are two-tap symmetric convolution operators. A prediction of parameter λ is defined by

$$\forall\, m \in \mathcal{C}_j,\ m < N - N2^{j-1}, \quad (P_\lambda a)[m] = \lambda \left(a[m + N2^{j-1}] + a[m - N2^{j-1}] \right). \tag{7.273}$$

An update of parameter μ is defined as

$$\forall\, n \in \mathcal{G}_j,\ n > 0, \quad (U_\mu b)[n] = \mu \left(b[n + N2^{j-1}] + b[n - N2^{j-1}] \right). \tag{7.274}$$

At the interval boundaries, the predict and update operators must be modified for $m = N - N2^{j-1}$ in (7.273) and $n = 0$ in (7.274), because one of the two neighbors falls outside the grids $\mathcal{G}_j$ and $\mathcal{C}_j$.

Symmetric boundary conditions, described in Section 7.5.2, are implemented with a folding, which leads to the following definition of boundary predict and update operators:

$$(P_\lambda a)[N - N2^{j-1}] = 2\lambda\, a[N - N2^j] \quad \text{and} \quad (U_\mu b)[0] = 2\mu\, b[N2^{j-1}].$$

This ensures that the lifting operators have one vanishing moment, and that the resulting boundary wavelets also have one vanishing moment.

Factorization of 5/3 and 9/7 Biorthogonal Wavelets

The 9/7 biorthogonal and 5/3 wavelets in Figure 7.15 are recommended for image compression in JPEG-2000 and are often used in wavelet image-processing applications. The 5/3 biorthogonal wavelet has $p_1 = p_2 = 2$ vanishing moments, while the 9/7 wavelet has $p_1 = p_2 = 4$ vanishing moments.

The 5/3 wavelet transform is implemented with $K = 1$ pair of predict and update steps, presented in Section 7.8.2. They correspond to

$$P^{(1)} = P_{1/2}, \quad U^{(1)} = U_{1/4}, \quad \text{and} \quad \zeta = \sqrt{2}.$$

The 9/7 wavelet transform is implemented with $K = 2$ pairs of predict and update steps defined as

$$\begin{cases} P^{(1)} = P_\alpha, & U^{(1)} = U_\beta, \\ P^{(2)} = P_\gamma, & U^{(2)} = U_\delta, \end{cases} \quad \text{where} \quad \begin{cases} \alpha = 1.58613434342059, & \beta = -0.0529801185729, \\ \gamma = -0.8829110755309, & \delta = 0.4435068520439, \end{cases}$$

and the scaling constant is $\zeta = 1.14960439886 02$.

7.9 EXERCISES

7.1 [2] Let h be a conjugate mirror filter associated to a scaling function ϕ.

(a) Prove that if $\hat{h}(\omega)$ is $\mathbf{C}^p$ and has a zero of order p at π, then the lth-order derivative $\hat{\phi}^{(l)}(2k\pi) = 0$ for any $k \in \mathbb{Z} - \{0\}$ and $l < p$.

(b) Derive that if $q < p$, then $\sum_{n=-\infty}^{+\infty} n^q \, \phi(n) = \int_{-\infty}^{+\infty} t^q \, \phi(t) \, dt$.

7.2 [2] Prove that $\sum_{n=-\infty}^{+\infty} \phi(t-n) = 1$ if ϕ is an orthogonal scaling function.

7.3 [2] Let ϕ_m be the Battle-Lemarié scaling function of degree m defined in (7.18). Let ϕ be the Shannon scaling function defined by $\hat{\phi} = \mathbf{1}_{[-\pi,\pi]}$. Prove that $\lim_{m \to +\infty} \|\phi_m - \phi\| = 0$.

7.4 [3] Suppose that $h[n]$ is nonzero only for $0 \leqslant n < K$. We denote $m[n] = \sqrt{2}\, h[n]$. The scaling equation is $\phi(t) = \sum_{n=0}^{K-1} m[n] \, \phi(2t-n)$.

(a) Suppose that $K = 2$. Prove that if t is a dyadic number that can be written in binary form with i digits, $t = 0.\varepsilon_1 \varepsilon_2 \cdots \varepsilon_i$ with $\varepsilon_k \in \{0, 1\}$, then $\phi(t)$ is the product

$$\phi(t) = m[\varepsilon_0] \times m[\varepsilon_1] \times \cdots \times m[\varepsilon_i] \times \phi(0).$$

(b) For $K = 2$, show that if $m[0] = 4/3$ and $m[1] = 2/3$, then $\phi(t)$ is singular at all dyadic points. Verify numerically with WaveLab that the resulting scaling equation does not define a finite-energy function ϕ.

(c) Show that one can find two matrices $M[0]$ and $M[1]$ such that the K-dimensional vector $\Phi(t) = [\phi(t), \phi(t+1), \ldots, \phi(t+K-1)]^T$ satisfies

$$\Phi(t) = M[0] \, \Phi(2t) + M[1] \, \Phi(2t-1).$$

(d) Show that one can compute $\Phi(t)$ at any dyadic number $t = 0.\varepsilon_1 \varepsilon_2 \cdots \varepsilon_i$ with a product of matrices:

$$\Phi(t) = M[\varepsilon_0] \times M[\varepsilon_1] \times \cdots \times M[\varepsilon_i] \times \Phi(0).$$

7.5 [2] Let us define

$$\phi_{k+1}(t) = \sqrt{2} \sum_{n=-\infty}^{+\infty} h[n] \, \phi_k(2t-n), \tag{7.275}$$

with $\phi_0 = \mathbf{1}_{[0,1]}$, and $a_k[n] = \langle \phi_k(t), \phi_k(t-n) \rangle$.

(a) Let

$$P\hat{f}(\omega)=\frac{1}{2}\left(|\hat{h}\left(\frac{\omega}{2}\right)|^2\hat{f}\left(\frac{\omega}{2}\right)+|\hat{h}\left(\frac{\omega}{2}+\pi\right)|^2\hat{f}\left(\frac{\omega}{2}+\pi\right)\right).$$

Prove that $\hat{a}_{k+1}(\omega)=P\hat{a}_k(\omega)$.

(b) Prove that if there exists ϕ such that $\lim_{k\to+\infty}\|\phi_k-\phi\|=0$, then 1 is an eigenvalue of P and $\hat{\phi}(\omega)=\prod_{p=1}^{+\infty}2^{-1/2}\hat{h}(2^{-p}\omega)$. What is the degree of freedom on ϕ_0 in order to still converge to the same limit ϕ?

(c) Implement numerically the computations of $\phi_k(t)$ for the Daubechies conjugate mirror filter with $p=6$ zeros at π. How many iterations are needed to obtain $\|\phi_k-\phi\|<10^{-4}$? Try to improve the rate of convergence by modifying ϕ_0.

7.6 [3] Let $b[n]=f(N^{-1}n)$ with $2^L=N^{-1}$ and $f\in\mathbf{V}_L$. We want to recover $a_L[n]=\langle f,\phi_{L,n}\rangle$ from $b[n]$ to compute the wavelet coefficients of f with Theorem 7.10.

(a) Let $\phi_L[n]=2^{-L/2}\phi(2^{-L}n)$. Prove that $b[n]=a_L\star\phi_L[n]$.

(b) Prove that if there exists $C>0$ such that for all $\omega\in[-\pi,\pi]$,

$$\hat{\phi}_d(\omega)=\sum_{k=-\infty}^{+\infty}\hat{\phi}(\omega+2k\pi)\geqslant C,$$

then a_L can be calculated from b with a stable filter $\phi_L^{-1}[n]$.

(c) If ϕ is a cubic spline–scaling function, compute numerically $\phi_L^{-1}[n]$. For a given numerical precision, compare the number of operations needed to compute a_L from b with the number of operations needed to compute the fast wavelet transform of a_L.

(d) Show that calculating a_L from b is equivalent to performing a change of basis in $\mathbf{V}_L$ from a Riesz interpolation basis to an orthonormal basis.

7.7 [2] *Quadrature mirror filters.* We define a multirate filter bank with four filters $h,g,\tilde{h}$, and $\tilde{g}$, which decomposes a signal $a_0[n]$

$$a_1[n]=a_0\star h[2n],\ d_1[n]=a_0\star g[2n].$$

Using the notation (7.101), we reconstruct

$$\tilde{a}_0[n]=\check{a}_1\star\tilde{h}[n]+\check{d}_1\star\tilde{g}[n].$$

(a) Prove that $\tilde{a}_0[n]=a_0[n-l]$ if

$$\hat{g}(\omega)=\hat{h}(\omega+\pi),\ \widehat{\tilde{h}}(\omega)=\hat{h}(\omega),\ \widehat{\tilde{g}}(\omega)=-\widehat{\tilde{h}}(\omega+\pi),$$

and if h satisfies the quadrature mirror condition

$$\hat{h}^2(\omega)-\hat{h}^2(\omega+\pi)=2\,\mathrm{e}^{-il\omega}.$$

(b) Show that l is necessarily odd.

(c) Verify that the Haar filter (7.46) is a quadrature mirror filter (it is the only finite impulse response solution).

7.8 [1] Let f be a function of support [0, 1] that is equal to different polynomials of degree q on the intervals $\{[\tau_k, \tau_{k+1}]\}_{0 \leq k < K}$ with $\tau_0 = 0$ and $\tau_K = 1$. Let ψ be a Daubechies wavelet with p vanishing moments. If $q < p$, compute the number of nonzero wavelet coefficients $\langle f, \psi_{j,n} \rangle$ at a fixed scale 2^j. How should we choose p to minimize this number? If $q > p$, what is the maximum number of nonzero wavelet coefficients $\langle f, \psi_{j,n} \rangle$ at a fixed scale 2^j?

7.9 [2] Let θ be a box spline of degree m obtained by $m+1$ convolutions of $\mathbf{1}_{[0,1]}$ with itself.

(a) Prove that

$$\theta(t) = \frac{1}{m!} \sum_{k=0}^{m+1} (-1)^k \binom{m+1}{k} ([t-k]_+)^m,$$

where $[x]_+ = \max(x, 0)$. *Hint:* Write $\mathbf{1}_{[0,1]} = \mathbf{1}_{[0,+\infty)} - \mathbf{1}_{(1,+\infty)}$.

(b) Let A_m and B_m be the Riesz bounds of $\{\theta(t-n)\}_{n \in \mathbb{Z}}$. With (7.9) prove that $\lim_{m \to +\infty} B_m = +\infty$. Compute numerically A_m and B_m for $m \in \{0, \ldots, 5\}$ with MATLAB.

7.10 [1] Prove that if $\{\psi_{j,n}\}_{(j,n) \in \mathbb{Z}^2}$ is an orthonormal basis of $\mathbf{L^2}(\mathbb{R})$, then for all $\omega \in \mathbb{R} - \{0\}$, $\sum_{j=-\infty}^{+\infty} |\hat{\psi}(2^j \omega)|^2 = 1$. Find an example showing that the converse is not true.

7.11 [3] Let us define

$$\hat{\psi}(\omega) = \begin{cases} 1 & \text{if } 4\pi/7 \leq |\omega| \leq \pi \text{ or } 4\pi \leq |\omega| \leq 4\pi + 4\pi/7 \\ 0 & \text{otherwise.} \end{cases}$$

Prove that $\{\psi_{j,n}\}_{(j,n) \in \mathbb{Z}^2}$ is an orthonormal basis of $\mathbf{L^2}(\mathbb{R})$. Prove that ψ is not associated to a scaling function ϕ that generates a multiresolution approximation.

7.12 [2] Express the Coiflet property (7.99) as an equivalent condition on the conjugate mirror filter $\hat{h}(e^{i\omega})$.

7.13 [1] Prove that $\psi(t)$ has p vanishing moments if and only if, for all $j > 0$, the discrete wavelets $\psi_j[n]$ defined in (7.140) have p discrete vanishing moments

$$\sum_{n=-\infty}^{+\infty} n^k \psi_j[n] = 0 \quad \text{for} \quad 0 \leq k < p.$$

7.14 [2] Let $\psi(t)$ be a compactly supported wavelet calculated with Daubechies conjugate mirror filters (h, g). Let $\psi'_{j,n}(t) = 2^{-j/2} \psi'(2^{-j}t - n)$ be the derivative wavelets.

(a) Verify that h_1 and g_1 defined by

$$\hat{h}_1(\omega) = 2\,\hat{h}(\omega)\,(\mathrm{e}^{i\omega}-1)^{-1},\ \hat{g}_1(\omega) = 2\,(\mathrm{e}^{i\omega}-1)\,\hat{g}(\omega)$$

are finite impulse response filters.

(b) Prove that the Fourier transform of $\psi'(t)$ can be written as

$$\widehat{\psi'}(\omega) = \frac{\hat{g}_1(2^{-1}\omega)}{\sqrt{2}} \prod_{p=2}^{+\infty} \frac{\hat{h}_1(2^{-p}\omega)}{\sqrt{2}}.$$

(c) Describe a fast filter bank algorithm to compute the derivative wavelet coefficients $\langle f, \psi'_{j,n}\rangle$ [108].

7.15 [3] Let $\psi(t)$ be a compactly supported wavelet calculated with Daubechies conjugate mirror filters (h, g). Let $\hat{h}^a(\omega) = |\hat{h}(\omega)|^2$. We verify that $\hat{\psi}^a(\omega) = \hat{\psi}(\omega)\,\hat{h}^a(\omega/4 - \pi/2)$ is an almost analytic wavelet.

(a) Prove that ψ^a is a complex wavelet such that $\mathrm{Re}[\psi^a] = \psi$.

(b) Compute numerically $\psi^a(\omega)$ for a Daubechies wavelet with four vanishing moments. Explain why $\psi^a(\omega) \approx 0$ for $\omega < 0$.

(c) Let $\psi^a_{j,n}(t) = 2^{-j/2}\psi^a(2^{-j}t - n)$. Using the fact that

$$\hat{\psi}^a(\omega) = \frac{\hat{g}(2^{-1}\omega)}{\sqrt{2}}\,\frac{\hat{h}(2^{-2}\omega)}{\sqrt{2}}\,\frac{|\hat{h}(2^{-2}\omega - 2^{-1}\pi)|^2}{\sqrt{2}} \prod_{k=3}^{+\infty} \frac{\hat{h}(2^{-k}\omega)}{\sqrt{2}},$$

show that we can modify the fast wavelet transform algorithm to compute the "analytic" wavelet coefficients $\langle f, \psi^a_{j,n}\rangle$ by inserting a new filter.

(d) Let ϕ be the scaling function associated to ψ. We define separable two-dimensional "analytic" wavelets by:

$$\begin{aligned} \psi^1(x) &= \psi^a(x_1)\,\phi(x_2),\ \psi^2(x) &&= \phi(x_1)\,\psi^a(x_2),\\ \psi^3(x) &= \psi^a(x_1)\,\psi^a(x_2),\ \psi^4(x) &&= \psi^a(x_1)\,\psi^a(-x_2). \end{aligned}$$

Let $\psi^k_{j,n}(x) = 2^{-j}\psi^k(2^{-j}x - n)$ for $n \in \mathbb{Z}^2$. Modify the separable wavelet filter bank algorithm from Section 7.7.3 to compute the "analytic" wavelet coefficients $\langle f, \psi^k_{j,n}\rangle$.

(e) Prove that $\{\psi^k_{j,n}\}_{1 \leq k \leq 4, j \in \mathbb{Z}, n \in \mathbb{Z}^2}$ is a frame of the space of *real* functions $f \in \mathbf{L^2}(\mathbb{R}^2)$ [108].

7.16 [2] *Multiwavelets.* We define the following two scaling functions:

$$\begin{aligned} \phi_1(t) &= \phi_1(2t) + \phi_1(2t-1)\\ \phi_2(t) &= \frac{1}{2}\Big(\phi_2(2t) + \phi_2(2t-1) - \phi_1(2t) + \phi_1(2t-1)\Big). \end{aligned}$$

(a) Compute the functions ϕ_1 and ϕ_2. Prove that $\{\phi_1(t-n), \phi_2(t-n)\}_{n\in\mathbb{Z}}$ is an orthonormal basis of a space $\mathbf{V}_0$ that will be specified.

(b) Find ψ_1 and ψ_2 with a support on [0, 1] that are orthogonal to each other and to ϕ_1 and ϕ_2. Plot these wavelets. Verify that they have two vanishing moments and that they generate an orthonormal basis of $\mathbf{L^2}(\mathbb{R})$.

7.17 [3] Let f^{repl} be the folded function defined in (7.179).

(a) Let $\alpha(t), \beta(t) \in \mathbf{L^2}(\mathbb{R})$ be two functions that are either symmetric or antisymmetric about $t = 0$. If $\langle \alpha(t), \beta(t + 2k) \rangle = 0$ and $\langle \alpha(t), \beta(2k - t) \rangle = 0$ for all $k \in \mathbb{Z}$, then prove that

$$\int_0^1 \alpha^{\text{repl}}(t)\, \beta^{\text{repl}}(t)\, dt = 0.$$

(b) Prove that if $\psi, \tilde{\psi}, \phi, \tilde{\phi}$ are either symmetric or antisymmetric with respect to $t = 1/2$ or $t = 0$, and generate biorthogonal bases of $\mathbf{L^2}(\mathbb{R})$, then the folded bases (7.181) and (7.182) are biorthogonal bases of $\mathbf{L^2}[0, 1]$. *Hint:* Use the same approach as in Theorem 7.16.

7.18 [3] A recursive filter has a Fourier transform that is a ratio of trigonometric polynomials as in (2.31).

(a) Let $p[n] = h \star \bar{h}[n]$ with $\bar{h}[n] = h[-n]$. Verify that if h is a recursive conjugate mirror filter, then $\hat{p}(\omega) + \hat{p}(\omega + \pi) = 2$ and there exists $\hat{r}(\omega) = \sum_{k=0}^{K-1} r[k]\, \mathrm{e}^{-ik\omega}$ such that

$$\hat{p}(\omega) = \frac{2|\hat{r}(\omega)|^2}{|\hat{r}(\omega)|^2 + |\hat{r}(\omega + \pi)|^2}. \tag{7.276}$$

(b) Suppose that K is even and that $r[K/2 - 1 - k] = r[K/2 + k]$. Verify that

$$\hat{p}(\omega) = \frac{|\hat{r}(\omega)|^2}{2\,|\hat{r}(\omega) + \hat{r}(\omega + \pi)|^2}. \tag{7.277}$$

(c) If $\hat{r}(\omega) = (1 + \mathrm{e}^{-i\omega})^{K-1}$ with $K = 6$, compute $\hat{h}(\omega)$ with the factorization (7.277), and verify that it is a stable filter (Exercise 3.18). Compute numerically this filter and plot the graph of the corresponding wavelet $\psi(t)$.

7.19 [2] *Balancing.* Suppose that $h, \tilde{h}$ define a pair of perfect reconstruction filters satisfying (7.124).

(a) Prove that

$$h_{new}[n] = \frac{1}{2}\Big(h[n] + h[n-1]\Big),\ \tilde{h}_{new}[n] = \frac{1}{2}\left(\tilde{h}[n] + \tilde{h}[n-1]\right)$$

defines a new pair of perfect reconstruction filters. Verify that $\hat{h}_{new}(\omega)$ and $\widehat{\tilde{h}}_{new}(\omega)$ have, respectively, one more and one less zero at π than $\hat{h}(\omega)$ and $\widehat{\tilde{h}}(\omega)$ [63].

(b) Relate this balancing operation to a lifting.

(c) The Deslauriers-Dubuc filters are $\hat{h}(\omega) = 1$ and

$$\widehat{\tilde{h}}(\omega) = \frac{1}{16}\,(-\mathrm{e}^{-3i\omega} + 9\,\mathrm{e}^{-i\omega} + 16 + 9\,\mathrm{e}^{i\omega} - \mathrm{e}^{3i\omega}).$$

Compute h_{new} and $\tilde{h}_{new}$ as well as the corresponding biorthogonal wavelets ψ_{new}, $\tilde{\psi}_{new}$, after one balancing and again after a second balancing.

7.20 [1] Compute numerically the wavelets and scaling functions associated to the predict and update lifting steps (7.264) and (7.265). Verify that you obtain the 5/3 wavelets displayed in Figure 7.15.

7.21 [1] Give the reduction of the number of operations when implementing a fast wavelet transform with 5/3 and 7/9 biorthogonal wavelets with the lifting algorithm described in Section 7.8.5, compared with a direct implementation with (7.270) and (7.271) by using the coefficients in Table 7.4.

7.22 [1] For a Deslauriers-Dubuc interpolation wavelet of degree 3, compute the dual wavelet $\tilde{\psi}$ in (7.212), which is a sum of Diracs. Verify that it has four vanishing moments.

7.23 [2] Prove that a Deslauriers-Dubuc interpolation function of degree $2p-1$ converges to a sinc function when p goes to $+\infty$.

7.24 [3] Let ϕ be an autocorrelation scaling function that reproduces polynomials of degree $p-1$ as in (7.198). Prove that if f is uniformly Lipschitz α, then under the same hypotheses as in Theorem 7.22, there exists $K > 0$ such that

$$\|f - P_{\mathbf{V}_j} f\|_\infty \leqslant K\, 2^{\alpha j}.$$

7.25 [2] Let $\phi(t)$ be an interpolation function that generates an interpolation wavelet basis of $\mathbf{C}_0(\mathbb{R})$. Construct a separable interpolation wavelet basis of the space $\mathbf{C}_0(\mathbb{R}^p)$ of uniformly continuous p-dimensional signals $f(x_1, \ldots, x_p)$. *Hint:* Construct $2^p - 1$ interpolation wavelets by appropriately translating $\phi(x_1) \cdots \phi(x_p)$.

7.26 [3] *Fractional Brownian.* Let $\psi(t)$ be a compactly supported wavelet with p vanishing moments that generates an orthonormal basis of $\mathbf{L}^2(\mathbb{R})$. The covariance of a fractional Brownian motion $B_H(t)$ is given by (6.86).

(a) Prove that $E\{|\langle B_H, \psi_{j,n}\rangle|^2\}$ is proportional to $2^{j(2H+1)}$. *Hint:* Use Exercise 6.15.

(b) Prove that the decorrelation between the same scale wavelet coefficients increases when the number p of vanishing moments of ψ increases:

$$E\{\langle B_H, \psi_{j,n}\rangle\, \langle B_H, \psi_{l,m}\rangle\} = O\Big(2^{j(2H+1)}\, |n-m|^{2(H-p)}\Big).$$

(c) In two dimensions, synthesize "approximate" fractional Brownian motion images $\tilde{B}_H$ with wavelet coefficients $\langle B_H, \psi^k_{j,n} \rangle$ that are independent Gaussian random variables, with variances proportional to $2^{j(2H+2)}$. Adjust H in order to produce textures that look like clouds in the sky.

7.27 [2] *Image mosaic.* Let $f_0[n_1, n_2]$ and $f_1[n_1, n_2]$ be two square images of N pixels. We want to merge the center of $f_0[n_1, n_2]$ for $N^{1/2}/4 \leq n_1, n_2 < 3N^{1/2}/4$ in the center of f_1. Compute numerically the wavelet coefficients of f_0 and f_1. At each scale 2^j and orientation $1 \leq k \leq 3$, replace the $2^{-2j}/4$ wavelet coefficients corresponding to the center of f_1 by the wavelet coefficients of f_0. Reconstruct an image from this manipulated wavelet representation. Explain why the image f_0 seems to be merged in f_1, without the strong boundary effects that are obtained when directly replacing the pixels of f_1 by the pixels of f_0.

7.28 [3] *Foveal vision.* A foveal image has a maximum resolution at the center, with a resolution that decreases linearly as a function of the distance to the center. Show that one can construct an approximate foveal image by keeping a constant number of nonzero wavelet coefficients at each scale 2^j. Implement this algorithm numerically.

7.29 [2] *High contrast.* We consider a color image specified by three color channels: red $r[n]$, green $g[n]$, and blue $b[n]$. The intensity image $(r+g+b)/3$ averages the variations of the three color channels. To create a high-contrast image f, for each wavelet $\psi^k_{j,n}$ we set $\langle f, \psi^k_{j,n} \rangle$ to be the coefficient among $\langle r, \psi^k_{j,n} \rangle$, $\langle g, \psi^k_{j,n} \rangle$, and $\langle b, \psi^k_{j,n} \rangle$, which has the maximum amplitude. Implement this algorithm numerically and evaluate its performance for different types of multispectral images. How does the choice of ψ affect the results?